CYCLODEXTRIN-BASED SUPRAMOLECULAR SYSTEMS OF EMERGING GUESTS WITH PHARMACEUTICAL AND ENVIRONMENTAL INTEREST

Laura Andrea Uribe Uribe

ADVERTIMENT. L'accés als continguts d'aquesta tesi doctoral i la seva utilització ha de respectar els drets de la persona autora. Pot ser utilitzada per a consulta o estudi personal, així com en activitats o materials d'investigació i docència en els termes establerts a l'art. 32 del Text Refós de la Llei de Propietat Intel·lectual (RDL 1/1996). Per altres utilitzacions es requereix l'autorització prèvia i expressa de la persona autora. En qualsevol cas, en la utilització dels seus continguts caldrà indicar de forma clara el nom i cognoms de la persona autora i el títol de la tesi doctoral. No s'autoritza la seva reproducció o altres formes d'explotació efectuades amb finalitats de lucre ni la seva comunicació pública des d'un lloc aliè al servei TDX. Tampoc s'autoritza la presentació del seu contingut en una finestra o marc aliè a TDX (framing). Aquesta reserva de drets afecta tant als continguts de la tesi com als seus resums i índexs.

ADVERTENCIA. El acceso a los contenidos de esta tesis doctoral y su utilización debe respetar los derechos de la persona autora. Puede ser utilizada para consulta o estudio personal, así como en actividades o materiales de investigación y docencia en los términos establecidos en el art. 32 del Texto Refundido de la Ley de Propiedad Intelectual (RDL 1/1996). Para otros usos se requiere la autorización previa y expresa de la persona autora. En cualquier caso, en la utilización de sus contenidos se deberá indicar de forma clara el nombre y apellidos de la persona autora y el título de la tesis doctoral. No se autoriza su reproducción u otras formas de explotación efectuadas con fines lucrativos ni su comunicación pública desde un sitio ajeno al servicio TDR. Tampoco se autoriza la presentación de su contenido en una ventana o marco ajeno a TDR (framing). Esta reserva de derechos afecta tanto al contenido de la tesis como a sus resúmenes e índices.

WARNING. Access to the contents of this doctoral thesis and its use must respect the rights of the author. It can be used for reference or private study, as well as research and learning activities or materials in the terms established by the 32nd article of the Spanish Consolidated Copyright Act (RDL 1/1996). Express and previous authorization of the author is required for any other uses. In any case, when using its content, full name of the author and title of the thesis must be clearly indicated. Reproduction or other forms of for profit use or public communication from outside TDX service is not allowed. Presentation of its content in a window or frame external to TDX (framing) is not authorized either. These rights affect both the content of the thesis and its abstracts and indexes.

UNIVERSITAT ROVIRA i VIRGILI

Cyclodextrin-based supramolecular systems of emerging guests with pharmaceutical and environmental interest

Laura Andrea Uribe Uribe

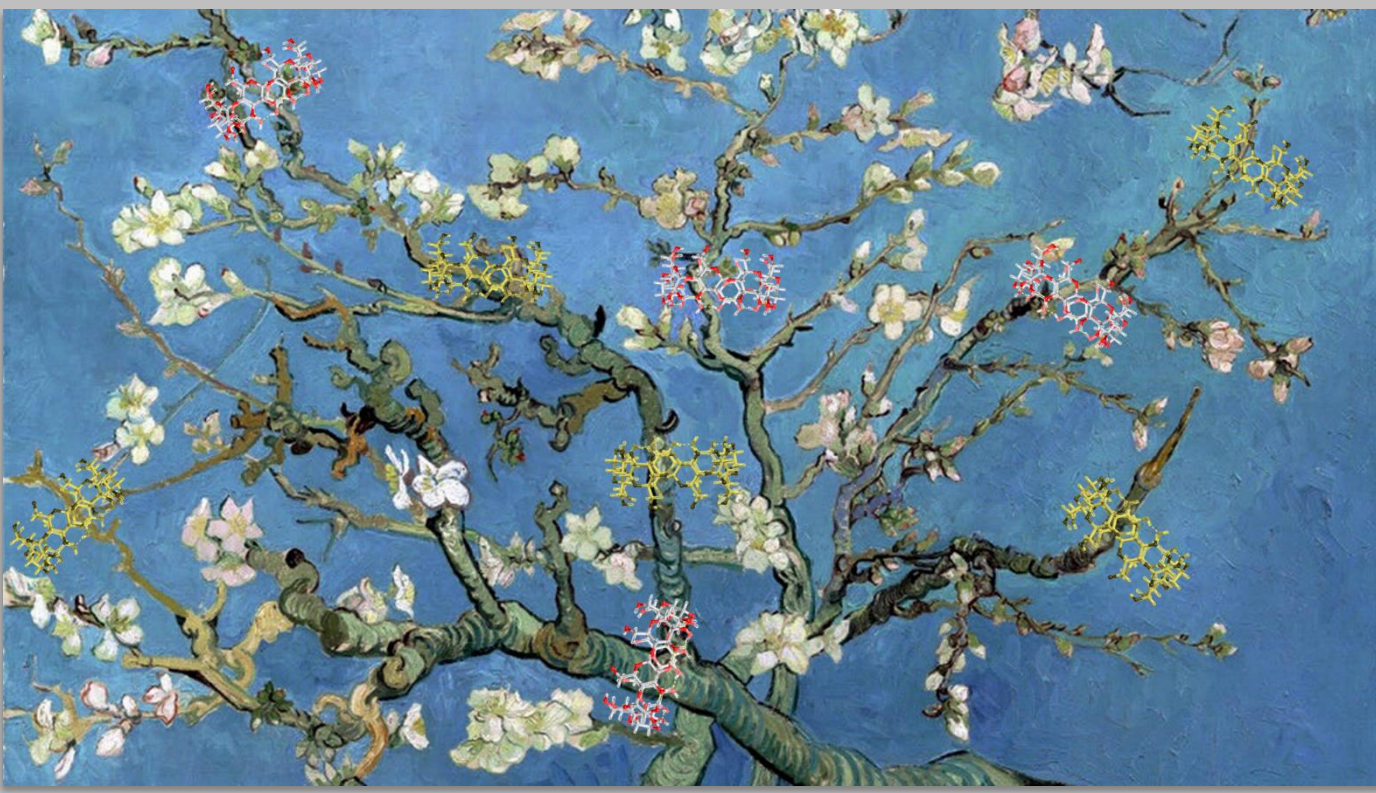

DOCTORAL THESIS

2022

UNIVERSITAT · ROVIRA · I · VIRGILI · SAPIENTIAE · LIBERI · LIBERTATI · SAPIENTES ·

Laura Andrea Uribe Uribe

CYCLODEXTRIN-BASED SUPRAMOLECULAR SYSTEMS OF EMERGING GUESTS WITH PHARMACEUTICAL AND ENVIRONMENTAL INTEREST

DOCTORAL THESIS

Supervised by Dr. Alex Fragoso Sierra

Chemical Engineering Department

UNIVERSITAT
ROVIRA i VIRGILI

Tarragona, Spain

2022

UNIVERSITAT ROVIRA I VIRGILI

Departament d'Enginyeria Química
Universitat Rovira i Virgili
Campus Sescelades,
Avda. Països Catalans, 26
43007 Tarragona
Tel: 977 55 85 79
Fax: 977 55 96 67

Dr. Alex Fragoso Sierra

CERTIFIES:

That the present study, entitled "Cyclodextrin-based supramolecular systems of emerging guests with pharmaceutical and environmental interest" presented by Laura Andrea Uribe Uribe for the award of the degree of Doctor, opting for the International Doctorate Mention, has been carried out under my supervision at the Department of Chemical Engineering of Universitat Rovira i Virgili,

Tarragona, May 9th, 2022.

Dr. Alex Fragoso Sierra

Acknowledgements

First, I want to give the biggest thank you to my supervisor **Dr. Alex Fragoso**, for his patience, support, great advice and for being a great example and a scientist role model for this newbie. Thank you, Alex, for always encouraging me to go an extra mile further, for never cutting my wings, for allowing me to be creative and bring my ideas to the table, and for helping me find the path that led me to the conclusion of this thesis.

I also want to give special thanks to all the professors and mentors along life that have been kind enough to share their knowledge with me: from my first role models at Santo Angel school in Bogotá, to all my professors from the chemical engineering department at Los Andes University in Bogotá, especially Drs. **Watson Vargas, Pablo Ortiz, Oscar Álvarez, Felipe Muñoz and Rocio Sierra**. To my master professors especially **Dr. Pascal Blondeau** who was the first one to teach me about supramolecular chemistry and whose passion in the subject was passed down to me. And my master supervisors Drs. **Ciara O'Sullivan** and **Mayreli Ortiz** for their immense guidance.

Thank you, Mayre, for always being there for me, both as my tutor and as my friend, for treating me as family, and for being the most charming person everywhere you go, without you I would not be in Spain today. Also thank you to my dear friend **Dr. Mabel Torrens del Valle** who had to bear with me, for sharing her office, for listening to me and advising me both in a scientific and human way. Mabel, keep on being the craziest and kindest person in town!

During my research stay in Aalborg I was more than lucky to count with the guidance of two professors with amazing human and scientific qualities: **Dr. Thorbjørn Terndrup Nielsen** who taught me a great deal about organic chemistry, synthesis, and useful lab tricks. TTN, thank you for helping

me find solutions wherever I felt lost and for letting me be Harald's pet sitter from time to time. Also, special thanks to **Dr. Casper Steinmann** who was kind enough to adopt this curious student as a tutor even if I had never done molecular simulations before. Thank you always for being so generous in sharing your knowledge, for your time, guidance and for your relaxed conversations, jokes, and good vibe.

Thanks to all the INTERFIBIO group members

To all my friends that I have been lucky enough to meet during this PhD journey and who have become my chosen family and support system in Tarragona: my partner in crime **Zaida Nair**, **Julio Cesar, Miriam and Sergi**, To **Eduardo**, Ivan, Xhensila, Cansu, Valerie, Lina thank you for all the laughs and humor.

Thank you to all my friends in Colombia and in the world

Finally, my deepest gratefulness goes to my parents Juan David and Maria Eugenia who let me follow my own path and have supported me every step of the way even if that meant paying the biggest price of being 8500 Km apart from each other. I know you are proud of me, but I am also extremely proud and honored to call you, my parents. Mami, thank you for teaching me that no dream is impossible, and that kindness is the most important quality in a person. Papi, thank you for teaching me the importance of critical thought, and knowledge and to have a passion in life. All the values you instilled in me, shaped me into the woman I am today. This work is yours!

List of publications

1. Supramolecular Complexes of Plant Neurotoxin Veratridine with Cyclodextrins and Their Antidote-like Effect on Neuro-2a Cell Viability- Published – Pharmaceutics 2022, 14(3), 598 doi: 10.3390/pharmaceutics140305998

2. Hydrolysis protection of different cyclodextrins to serine protease inhibitor nafamostat mesylate: proof of concept for a new administration method in drug repurposing for Covid-19 – In preparation

3. Synthesis and characterization of insoluble cyclodextrin nanosponges with variable crosslinker-size for marine toxin capturing applications – In preparation

4. Review: Cyclodextrins and toxins – In preparation

Abbreviations

^{1}HNMR: proton nuclear magnetic resonance

^{13}C-NMR: carbon nuclear magnetic resonance

ACE 2: angiotensin converting enzyme 2

ASP: amnesiac shellfish poisoning

AZP: azpiracid shellfish poisoning

BAPNA: Nα-Benzoyl-DL-Arginine-p-Nitroanilide

BISPH: 3,3',4,4'-Biphenyltetracarboxylic dianhydride

BRTX: brevetoxin

CD: cyclodextrin

CDI: 1,1-carbonyldiimidazole

CD-NS: cyclodextrin nanosponge

CE: capillary electrophoresis

CFP: ciguatera fish poisoning

D2O: deuterium oxide

DMF: dimethylformamide

DMSO: dimethyl sulfoxide

DPC: diphenyl carbonate

DS: degree of substitution

DSP: diarrhetic shellfish poisoning

ELISA: enzyme linked immunosorbent assay

FDA: food and drug administration

FESEM: field emission scanning electron microscope

FTIR: furrier transform infrared spectroscopy

HAB: harmful algal blooms

HCl: hydrochloric acid

HPCD: hydroxypropyl beta cyclodextrin

HPLC: high performance liquid chromatography

IC: inclusion complex

IRTA: Institute of Agri-food Research and Technology

ISO: 4,4'-(4,4'-Isopropylidenediphenoxy) bis (phthalic anhydride)

ITC: isothermal titration calorimetry

K_{eq}: equilibrium constant

LC-MS: liquid chromatography-mass spectroscopy

MD: molecular dynamics

MIPs: molecularly imprinted polymers

ML: machine learning

MM: molecular mechanics

MM: Molecular mechanics

MS: molecular simulations

n: stoiquiometry

NaOD: sodium deuteroxide

NM: nafamostat mesylate

NMR: nuclear magnetic resonance

NOESY: nuclear overhauser effect spectroscopy

NPD: Nieman Pick type C disease

NSP: neurotoxic shellfish poisoning

OA: okadaic acid

OXY: 4,4'-Oxydiphthalic anhydride

PCR: polymerase chain reaction

PMDA: Pyromellitic dianhydride

PSP: paralytic shellfish poisoning

PVC: polyvinyl chloride

QSARs/QPRs: Quantitative structure-activity/property relationships

ROESY: rotating-frame nuclear Overhauser effect spectroscopy

SARS-CoV-2: severe acute respiratory syndrome coronavirus 2

SBCD: sulfobutyl ether beta cyclodextrin

SPATT: solid-phase adsorption toxin tracking

SUCCI: succinyl beta cyclodextrin

TEM: transmission electron microscopy

TGA: thermogravimetric analysis

TMPRSS 2: transmembrane serine protease 2

VTD: veratridine

X_{NM}: molar fraction of nafamostat mesylate

XRD: x-ray diffraction

ΔG: Gibbs free energy change

ΔH: enthalpy change

ΔS: entropy change

α–CD: alpha cyclodextrin

β–CD: beta cyclodextrin

γ–CD: gamma cyclodextrin

Table of contents

Summary

The aim of the present thesis is to study and characterize the molecular interactions between cyclodextrins (CDs) or cyclodextrin-based materials with emerging guest molecules such as drugs or toxins for potential pharmaceutical and environmental applications.

Chapter 1 is a wide introduction to the topics that will be discussed in this thesis. It covers the general information about CDs, its applications in different industries and takes a special focus on cyclodextrin nanosponges (CD-NS) as well as the characterization techniques of CD-guest inclusion complexes in solution and using in-silico methods.

Chapter 2 covers the systematic studies of the formation of an inclusion complex between serine protease inhibitor nafamostat mesylate (NM) with different neutrally charged and anionic CDs. The mechanism of action of CDs in the drug is unveiled to be a protection against hydrolysis which depends both on the CD concentration and type. Finally, enzymatic assays confirm that the inclusion complex of NM-CD correctly inhibits the reaction of trypsin as a model enzyme thus being a proof-of-concept for further pharmaceutical research in new administration ways for NM.

Chapter 3 explores the molecular interactions of the neurotoxin veratridine (VTD) with different CDs. Subsequently, with an interest in understanding the effects of the VTD-CD inclusion complex, cell-based assays (CBAs) were performed on neuroblastoma-2a cells. Our findings reveal that the use of different amounts of CDs has an antidote-like concentration-dependent effect on the cells, significantly increasing cell viability and thus opening opportunities for novel research on applications of CDs and VTD.

Chapter 4 is dedicated to the synthesis characterization a new family of α–, β– and γ–CD-nanosponges (CD-NS) crosslinked with anhydride molecules of different lengths. The synthesized CD-NS were used in a proof-of-concept ELISA experiment as potential passive adsorption materials for the monitorization of lipid-soluble marine toxins brevetoxin and okadaic acid.

Overall, the presented thesis has contributed to expand the current knowledge on the use of CDs for pharmaceutical and environmental applications. The studies of characterization and understanding the mechanisms of CD inclusion complexes with serine protease inhibitor nafamostat mesylate and veratridine neurotoxin constitute the first reports in the literature of CD interactions with these guests. Furthermore, the synthesis and characterization of CD-NS with different anhydride crosslinkers broadens the current state of the art on CD-based polymeric materials and represents a potential novel use of CD-NS as passive adsorbers for marine toxins.

Chapter 1

Introduction - Cyclodextrins: the natural macrocycle

"*All things began in order, so shall they end, and so shall they begin again; according to the ordainer of order and mystical mathematics of the city of heaven*"

***Sir Thomas Browne -The Garden of Cyrus* (1658) ch. 5**

1.1 Supramolecular chemistry: where it all began

Supramolecular chemistry is a field defined by one of its fathers, Jean-Marie Lehn, as the study of the noncovalent intermolecular forces or "the chemistry beyond the molecule". It is an interdisciplinary field that lies at the junction of chemistry, physics, and biology areas [1]. The noncovalent interactions between molecules, such as hydrogen bonding, hydrophobic, and electrostatic causes them to organize in the process of self-assembly giving rise to structures or patterns that arise without any external direction [2] more than the molecular information already imbedded inside the atoms. The influence of nature in the concepts that lie at the core of supramolecular chemistry comes as inspiration from biological recognition processes. Moreover, as science keeps poking further into the frontier of knowledge there is growing evidence that self-assembly lies at the origin of life itself [3–5].

Studies on supramolecular chemistry are built upon the macrocyclic chemistry initiated by Cram, Lehn, and Pedersen in the 1970s who were the pioneers in the discovery and synthesis of the first macrocycles [6]: crown ethers [7], cryptands [8] and spherands [9] (Figure 1.1). As Lehn's analogy states; the key word in supramolecular chemistry is information [1]. The

macrocycles represent the building blocks to exploit the potential of that molecular information by designing selective hosts with functional characteristics which makes them useful in applications that go from drug

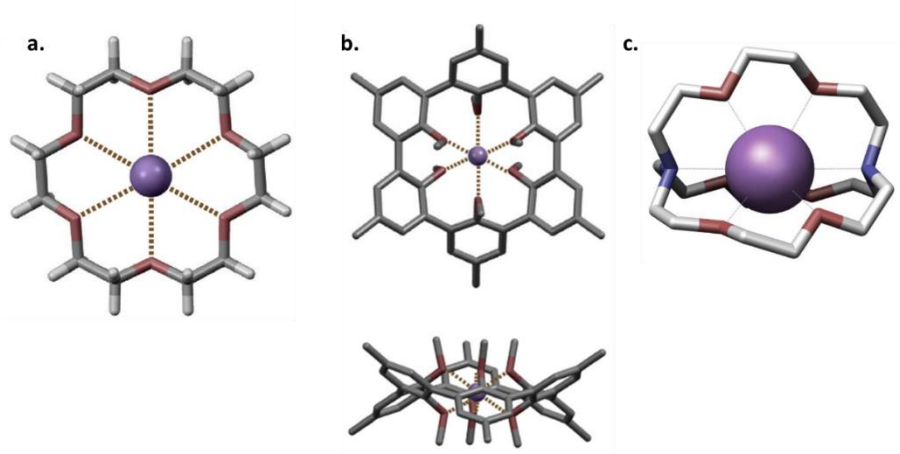

discovery to material science and sensors [10].

Figure 1.1 Crystal structures of **a.** 18-crown-6 ether **b.** spherand 5 [11] and **c.** 2.2.2 cryptand

1.2 Cyclodextrin's history in a nutshell

A particular group of non-synthetic macrocycles that have been around for a long time are cyclodextrins (CDs). CDs have been known since 1891 when Villiers [12] accidentally obtained them from a contamination of cultures with *Bacilus macerans*. Nevertheless, the discovery of the fundamentals of CD chemistry is mostly attributed to Schardinger who in 1904 was working with strains of *Bacilus macerans* which produced around 25-30% of crystalline dextrin powder from starch digestion. He could distinguish two types of dextrin products α and β by performing an iodine reaction where the α-dextrin/iodine complex would take a greenish color when dry while the

β-dextrin/iodine complex would take a reddish color when dry [13]. The systematic studies on CDs and their inclusion complexes started to boom from the 1930s by first elucidating the chemical structures of the α and β Schardinger dextrins (now known as α– and β–CDs respectively) in 1936 [14], followed by the discovery of the γ-CD around 1950 [15] and the first patent for the use of CDs in drug formulation was issued in 1953 [16]. By the 1960s CDs were prepared in a laboratory-scale and their industrial possibilities were already seen as promising. From the 1970s onward dozens of companies started to produce CDs [14]. In 1989 was founded Cyclolab Ltd, the first company focused exclusively on research and market of CDs stablished in Hungary by Dr. József Szejtli and coworkers [17]. CD scientific research has more than tripled the number of papers published since the late 1990s (~15000) [14] up to date (~52000 on Scopus with key word search cyclodextrin). In 2020 global CD market was estimated to sell more than US $260 MN and it is expected that CD sales will increase to more than US $390MN in 2027 [18].

1.3 Chemical structure: who wants a donut?

CDs are cyclic oligosaccharides formed by glucopyranose units linked by α-(1,4) glycosidic bonds. They are industrially produced by bacterial cultures of *Bacillus macerans* and other bacteria genus by the enzymatic action of cyclodextrin glucosyltransferases (CGTases) which catalyse the cleavage and successive cyclization of the linear α–1,4-linked polysaccharides [19]. In their native form they are crystalline, non-hygroscopic, substances composed of 6, 7 or 8 glucopyranose sugars (α–, β– and γ–cyclodextrin respectively) (Figure 1.1.a). The main interest in CDs comes from their capability to form host-guest inclusion complexes with a vast variety of hydrophobic molecules. This complexation ability comes from the

way how the glucopyranose units in the $^4C_1$ chair conformation are linked together, which has certain consequences for the physicochemical characteristics of CDs [20]:

On one hand, the secondary hydroxyl groups C2 and C3 are located on the wider edge of the ring while the primary hydroxyl groups C6 are located on the narrower edge. The ring thus forms a donut-like structure of a truncated cone (Figure 1.1.b) [21]. The primary and secondary hydroxyl groups make CDs water-soluble molecules. Furthermore, the C2 OH groups of one glucopyranose units can form hydrogen bonds with the C3 OH groups of the adjacent glucopyranose moiety which forms a belt of hydrogen bonds. In the case of β-CD all the glucopyranose units form hydrogen bonds with their adjacent pairs. This six-hydrogen-bond belt produces rigidity for the β-CD structure and has been thought to be the explanation of why this type of CD has the lowest solubility (Table 1.1) [14]. For the case of the α-CD, the hydrogen-bond belt is not complete since the molecule has one less glucopyranose unit than the β-CD and can only form a four hydrogen-bond belt. The γ-CD is a non-coplanar more flexible structure, which makes it the most soluble of the three native CDs [15].

On another hand, the CD cavity holds the H3 and H5 hydrogen atoms and the glycosidic oxygen bridges, which have non-bonding electron pairs pointing towards the inside of the cavity and produce a highly electron dense apolar microenvironment with the ability to hold smaller hydrophobic moieties that can fit inside [14].

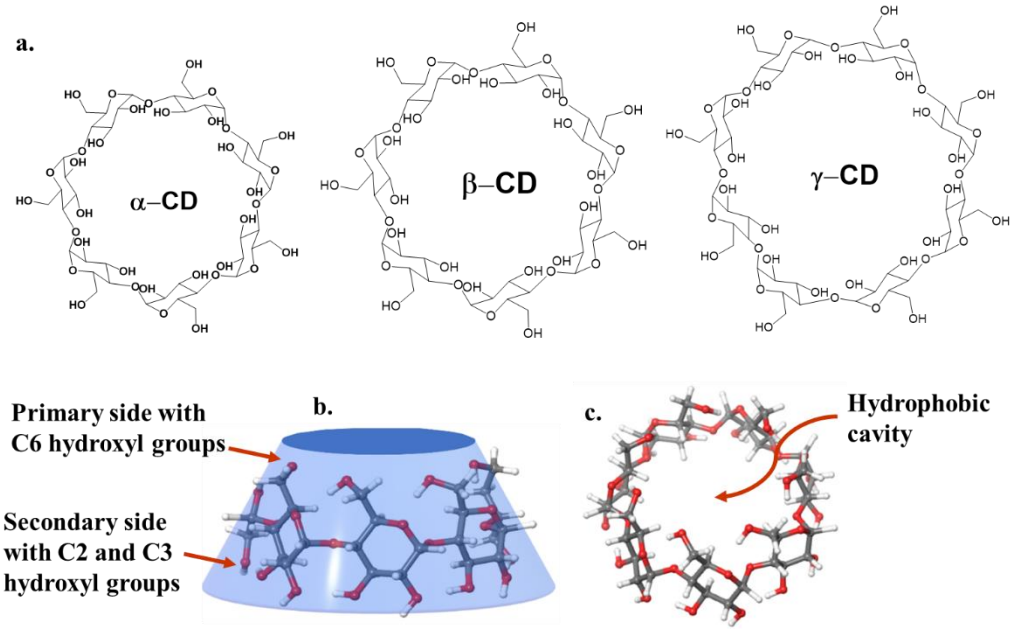

Figure 1.2 a. Molecular structure of different native CDs **b.** lateral 3D view and **c.** top 3D view of native β–CD

Since each one of the native CDs is composed of a different quantity of glucopyranose units, the cavity size of each CD varies as α-CD < β-CD < γ-CD (Table 1). Thus, different type of guest molecules can be complexed inside each CD. Non-covalent bonds are formed or broken in the formation of an inclusion complex (IC) [22,23]; being the principal driving force for the formation of the IC the release of enthalpy-rich water molecules from the cavity, which are displaced by more hydrophobic guests and leads to a lower-energy and more stable molecular configuration. This non-covalent binding occurs in a dynamic equilibrium where the binding strength will depend on the affinity between the host CD and the guest molecule [24].

Table 1.1 Characteristics of native cyclodextrin molecules.
Adapted from references [14] and [25]

Characteristic	α-Cyclodextrin	β-Cyclodextrin	γ-Cyclodextrin
Number of glucopyranose unit	6	7	8
Molecular weight g/mol	972	1135	1297
Solubility in water at 25°C (%w/v)	14.5	1.85	23.2
Outer diameter (Å)	14.6	15.4	17.5
Cavity diameter (Å)	4.7-5.3	6.0-6.5	7.5-8.3
Height of torus (Å)	7.9	7.9	7.9
Cavity volume (Å)	174	262	427
Crystal form (from water)	Hexagonal plates	Monocyclic parallelograms	Quadratic prisms

1.4 Chemically modified Cyclodextrins

Since native CDs have the potential to host a vast variety of guest molecules, in general, they are not considered as particularly selective hosts. Nevertheless, given the multiple OH groups present in the primary and secondary rims of native CDs, they can be chemically modified to enhance their molecular recognition characteristics. The degree of substitution (DS) in a CD derivative refers to the number of those hydroxyl groups that are substituted in a glucose unit. CD derivatives are normally produced by

amination, esterification, or etherification of the primary and secondary hydroxyl groups [26]. Developing CD derivatives has enhanced the field of application for these molecules for example as carriers for biologically active molecules [27], as separating agents, detergents, viscosity modifiers, etc [28].

Nevertheless, for a CD derivative to be relevant and industrially produced it needs to be non-toxic, keep their inclusion-complexation ability, have an advantage for a specific application, be synthesized in an as simple as possible manner and, finally, be economically viable. The β-CD has been the most widespread native CD for which derivatives have been developed. This is because its production has a lower cost in comparison to the α-CD and γ-CD and thus it is available in larger quantities [14]. Interestingly, β-CD is also the native CD with the lowest solubility and has the severe limitation of being nephrotoxic after parenteral administration [20]. The possibilities to synthesize new CD derivatives are countless, can go as far as the imagination of synthetic chemists (and of course the chemistry principles) allow. Although the vast majority of reported CD-derivatives won't reach mainstream use, many of the CD-derivatives can be used as intermediaries for further synthesis. Furthermore, an advantage of CD derivatives is that they can be custom designed for a particular purpose or application.

The main types of industrially relevant CD derivatives can be divided as neutral, ionizable (i.e., anionic or cationic), and CD polymers. The compounds have been developed with several types of substituents in varying positions and with different DS that enhance physicochemical properties and the inclusion complexation capacity of the natural CDs.

The most used neutral CDs are methylated (e.g., randomly methylated β-CD), hydroxy alkylated (e.g., hydroxypropyl β-CD), acylated (e.g., per-O-acetyl β-CD) and branched CDs (e.g., maltosyl β-CD) among many others [29]. Ionizable CDs form stronger complexes with polar or oppositely charged molecules. In the anionic CDs the main examples are carboxylated, sulfated, phosphated and sulfoalkylated CDs [30]. As for the cationic CDs most of the derivatives bear a nitrogen-containing moiety such as amino groups, imidazole, pyrrol, etc (i.e., trimethyl-ammonium-β–CD) [31].

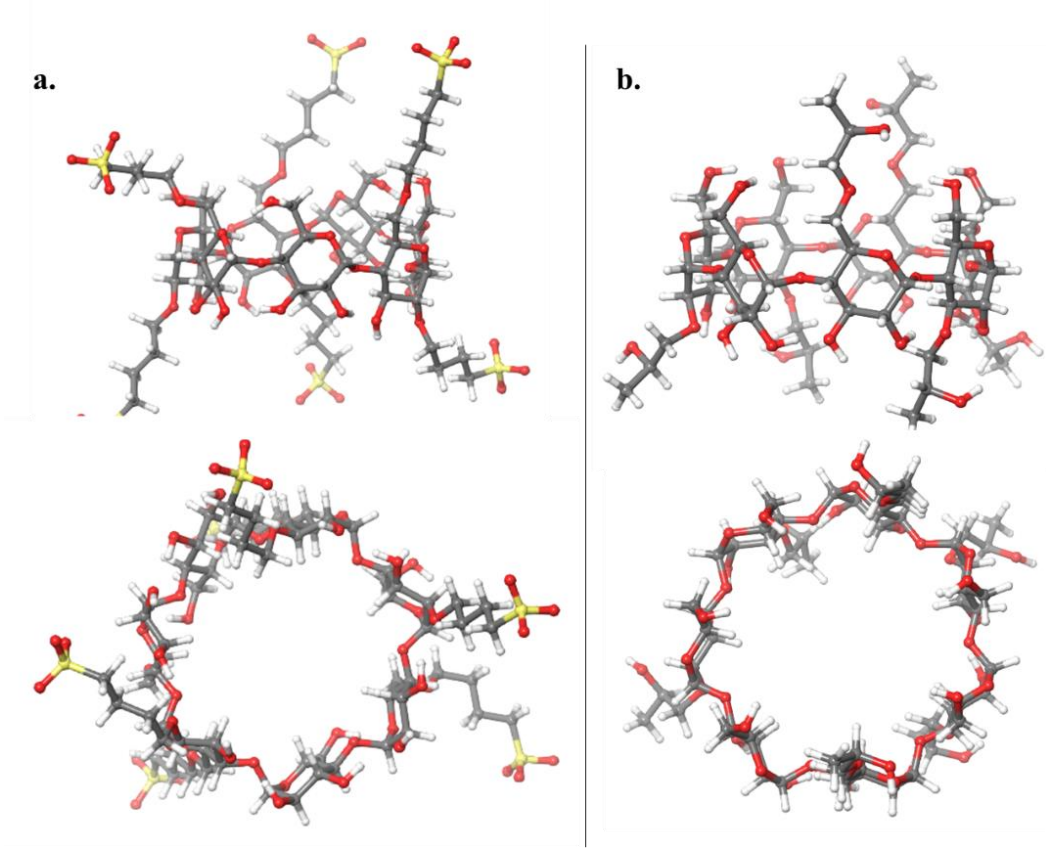

Figure 1.3 3D molecular structure (side view and top view) of CD derivatives **a.** 2-hydroxypropyl-β-CD (HPCD) and **b.** sulfobutyl ether-β-CD (SBCD)

The two most relevant derivatives for this thesis are the neutral hydroxypropyl-β-CD (HPCD) and the anionic sulfobutyl ether-β-CD (SBCD) (Figure 1.3) which are approved excipients with high solubility in water approximately 60% and 50% (w/v), respectively. Additionally, they exhibit good toxicity profiles [20,32] which makes them more suitable for pharmaceutical applications. And are approved excipients for six marketed products [33].

Another type of CD derivatives of great interest are CD polymers. This is a very extensive topic that has been well reviewed by *Tian et al* [34] and *Liu et al* [35]. Within the scope of this thesis, we will take a further look to a special class of CD polymer: CD nanosponges.

1.5 Cyclodextrin nanosponges (CD-NS)

Nanosponges are a relatively new class of nanoporous functional materials obtained by cross-linking CDs with different agents. The cross-linking reaction results in a web that has different cavities, corresponding not only to the CD hydrophobic cavity, but also to the network of cavities that are formed between the outer part of CDs and the cross-linker. This forms a material with microscopically porous/sponge-like morphology (Figures 1.4-1.7). The additional cavities of these materials, allow them to form complexes with a wider variety of guests in comparison to native CDs, since they can also host more hydrophilic guests. Additionally, the polymeric network promotes slower release kinetics of the complexed guests since the diffusion processes are difficulted. Finally, CD-NS are insoluble and easily recoverable and recycled from aqueous media [36].

1.5.1 Synthetic routes for different NS

Caldera et al [36] have classified the evolution of CD-NS to date in four big waves of research depending on their chemical composition and functionalization properties. First generation NS were classified depending on the type of cross-linker used for the synthesis as urethane/carbamate-based, carbonate-based, ester-based and ether-based. The next generations of NS consist of more functionalized versions of the previously mentioned: Second generation NS were designed as fluorescent-labelled or with an electrically charged side chains. Third generation NS are stimuli responsive NS that are able to modulate their response depending to the surrounding environment such as pH or oxidation changes. Finally, the fourth generation of NS corresponds to the molecularly imprinted CD polymers (MIPs) which are design to enhance the selectivity towards specific guest molecules. In this thesis we will focus on the main synthetic paths for CD NS.

- Cyclodextrin-Based Urethane/Carbamate Nanosponges

  These CD-NS are synthesized by cross-linking CD with diisocyanates. The synthesis is performed in DMF at 70°C and consists of reacting β–CD with hexamethylene diisocyanate and toluene-2,4-diisocyanate for 16–24 hours under nitrogen atmosphere. After purification, powder of cross-linked CD was obtained. They were firstly synthesized for water treatment applications [37]. But have also been studied for the absorption of aromatic amino acids [38] and bilirubin absorption [39].

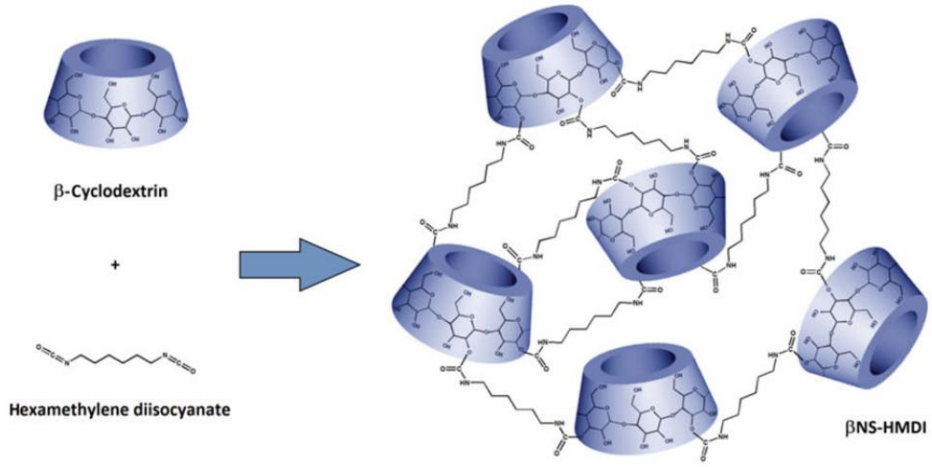

Figure 1.4 Schematic representation of the synthesis reaction of urethane β-CD nanosponge with hexamethylene diisocianate (HMDI) as crosslinker. Extracted from *Caldera et al* [36]

- Cyclodextrin-Based Carbonate Nanosponges

  These CD-NS can be synthesized by cross-linking CDs with active carbonyl compounds such as 1,1-carbonyldiimidazole (CDI), triphosgene, and diphenyl carbonate (DPC) There are different ways of performing the synthesis. Normally it is performed in DMF under reflux conditions; another alternative is to melt the cross-linker (in the case of DPC) and merge with the CD. Also, ultrasound-assisted synthesis can be performed. The reaction can take place at room temperature (e.g. CDI) or at 80-100°C (for DPC). The workup of the synthesis involves washing with water to remove unreacted reagents and purification with solvents like ethanol, acetone, or ether [40]. Carbonate-based CD-NS have been used for water decontamination from aromatic compounds such as chlorobenzene, 2,6-dichlorotoluene, and 4-chlorotoluene among others [41] as well as many drug delivery applications [42]

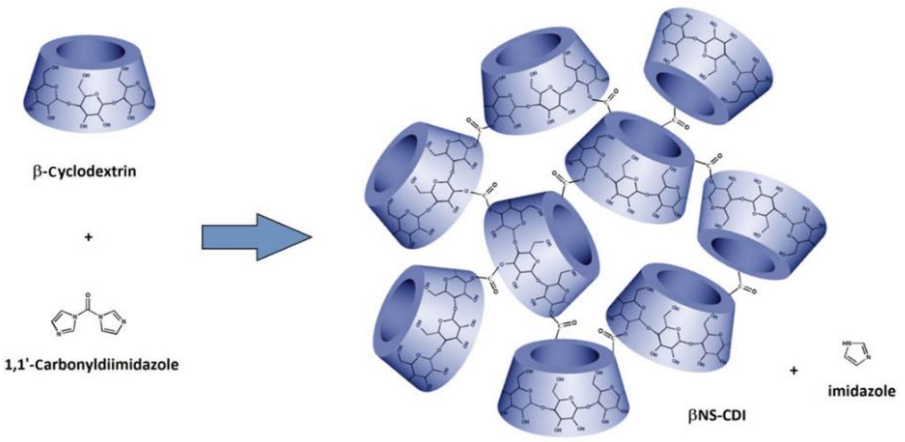

Figure 1.5 Schematic representation of the synthesis reaction carbonate β-CD nanosponge with 1,1'-carbonyldiimidazole as cross-linker agent. Extracted from *Caldera et al* [36]

- Cyclodextrin-Based Ester Nanosponges

  Ester-based NS are synthesized by cross-linking CDs with dianhydrides or polycarboxylic acids like pyromellitic dianhydride, ethylene diamine–tetraacetic acid dianhydride, and citric acid [40]. They hydrolize more easily than the previous NS. For the synthesis, the anhydride is solubilized in a polar organic solvent like DMSO or DMF with triethylamine as a catalyser. The reaction can happen at room temperature or also at 60-70°C. Application of NS The most widely studied CD-NS is in drug delivery. However, applications in the agriculture, textile, gas-storage and catalysis have also been studied.

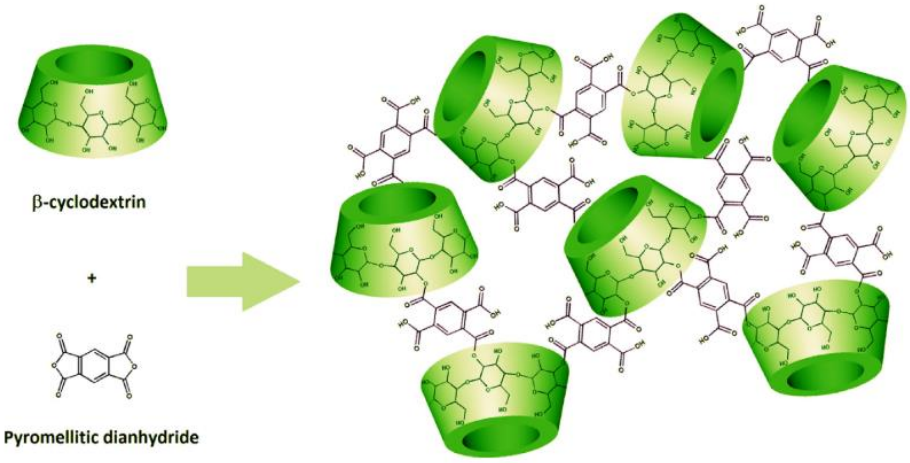

Figure 1.6 Schematic representation of the synthesis reaction ester-based β-CD nanosponge with pyromellitic dianhydride as cross-linker agent. Extracted from *Caldera et al* [36]

- Cyclodextrin-Based Ether Nanosponges

  The synthesis for this CD NS involves cross-linkers with epoxide groups such as epichlorohydrin, bisphenol-A, diglycidyl ether and ethylene glycol. Contrary to the previous synthesis, this one is performed in aqueous basic medium. Epichlorohydrin contains two reactive functional groups that can cross-link or polymerize with β-CD molecules. Ether NS have high chemical resistance and swelling properties [36]. They have been studied for drug delivery applications [43] and lately our group applied them for absorbing marine toxis [44].

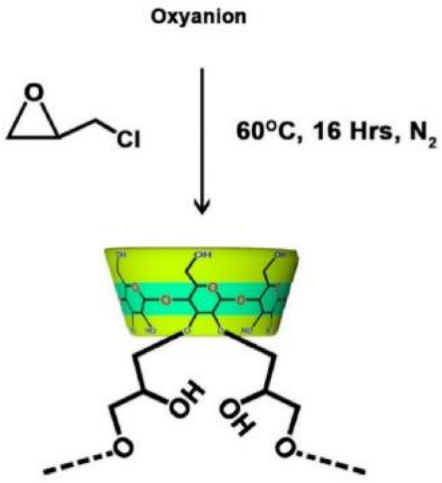

Figure 1.7 Schematic representation of the synthesis reaction ether-based β-CD nanosponge with epichlorohydrin as cross-linker agent. Extracted from *Trotta and Mele* [40]

1.6 Characterization of cyclodextrins inclusion complexes: An important choice

Studies for characterizing CD ICs are fundamental for understanding the mechanisms that hold the host-guest complex together and for channelling the potential of these molecules in many applications. The key point for evaluating the stability of an IC is to ascertain the equilibrium constant (K_{eq}) also known as formation, stability, or binding constant, since many effects or applications of the IC will depend on its strength. Many of the studies to characterize CD host-guest ICs are performed in aqueous solution. Several analytical techniques can be used to determine the K_{eq}, thermodynamic parameters such as enthalpy (ΔH), entropy (ΔS), Gibbs free energy (ΔG) and stoichiometry (n) or the molecular conformation of the IC.

A general overview of the most used analytical tools employed for the characterization of CD ICs in solution can be separated into: spectroscopic

techniques, electroanalytical techniques, separation techniques, and isothermal titration calorimetry (ITC) [45].

1.6.1 Spectroscopic methods

Spectroscopic techniques are very useful to determine the K_{eq}. Such methods rely on a variation of a property such as absorbance, NMR shift, or fluorescence intensity, upon complexation of a guest inside the CD cavity. Experiments are normally performed having a fixed guest concentration and then doing titrations by varying the concentration of CD.

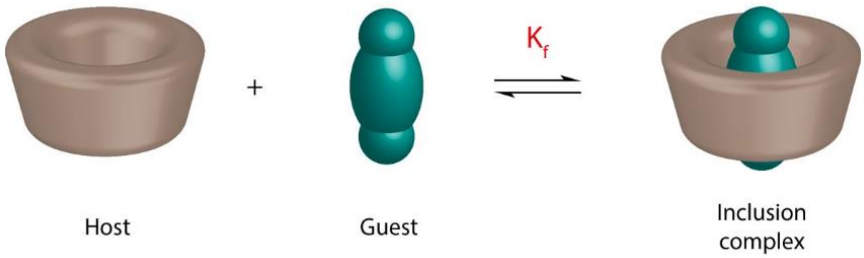

Figure 1.8 Schematic illustration of the formation of an inclusion complex between a cyclodextrin (host) and a guest. Extracted from *Kfoury et al* [46]

- UV-Vis spectroscopy

  This is a fast and economic method to study the K_{eq} by following the changes in the absorption spectra of a guest in presence of CDs. When the guest molecule that was originally in an aqueous solution is inserted into the apolar CD cavity the original UV-Vis spectrum changes for example by an increase [47,48] or a decrease [49–51] in the intensity of the absorption. A shift in the spectrum λ_{max} can also be observed which leads to the formation of isosbestic points that indicate the equilibrium between the species [52]. The K_{eq} is then calculated by using equations such as Benesi-Hildebrand [53]. From the spectral changes can also be calculated the stoichiometry of the IC by

performing continuous variation Job's Plot experiments [54]. Both Benesi-Hildebrand and Job's plot experiments will be further explained and used in the following chapters of this thesis.

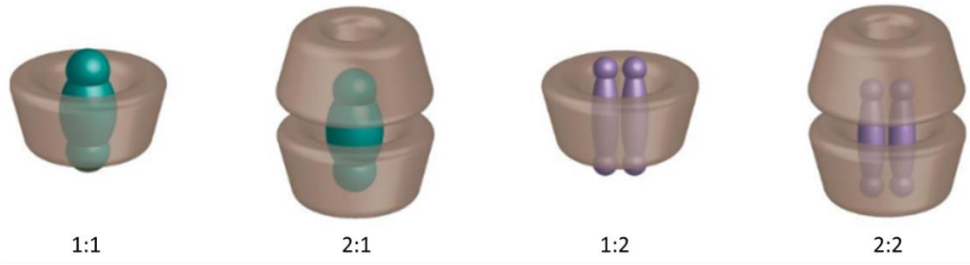

Figure 1.9 Schematic representation of the main stoichiometries of the inclusion complexes with cyclodextrins. Extracted from *Kfoury et al* [46]

- Circular dichroism spectrometry

  This is a useful technique to study ICs of chiral and non-chiral molecules with CDs. It provides a way to prove the real existence of an IC since no optical activity can be induced by each of the moieties alone, the sole responsible for a dichroic signal is the IC [55]. The inclusion of a chromophore moiety inside the CD cavity produces changes in the circular dichroism spectra which can be ascribed to the increased optical activity [56]. The most important information to be extracted from the circular dichroism spectra is the sign, the magnitude, and the wavelength of the maximum which are given by the induced Cotton effect [45]. Knowing these values, it is possible to have an insight about the degree of the guest penetration and its orientation inside the CD cavity [47].

- Fluorescence spectroscopy

  Is a highly sensitive method which becomes more useful when studying the molecular interactions between CDs and a fluorescent guest. Upon complexation with CDs, it can be noticed an increase in the fluorescence intensity. This has been attributed to the shielding from quenching when the guest lies inside the CD cavity as well as and a non-radioactive decay process [57]. Moreover, the amount of fluorescence intensity enhancement has been associated with the rigidity of the fluorophore inside the CD cavity, thus, less stable complexes produce a less intense fluorescence emission signal [58].

- Nuclear magnetic resonance (NMR) spectroscopy

  NMR experiments can give information about the K_{eq} of the inclusion complex, stoichiometry, and to allow elucidation of the molecular configuration of the IC in solution. They are regarded as one of the most complete and useful techniques to study the host-guest interactions with CDs [59].

  - Classic ^{1}H-NMR and ^{13}C-NMR experiments follow the changes in the ^{1}H proton or ^{13}C chemical shift (δ) from the free guest in comparison with the IC with CDs. The chemical shift occurs on both the guest and the CD molecules and gives information about the complex formation, as well as stoichiometry, and the geometry of the complex. To estimate the K_{eq} subsequent titrations at different CD concentration are performed [60]. The changes in the ^{1}H-NMR spectra of CDs are related with an upfield shift of the H-3 and H-5 cavity protons which is evidence of the complex formation. Depending on the extent of the chemical shift, information about the complex stability can be extracted [59]. Finally, a

partial or total inclusion of the guest in the CD cavity can be estimated by knowing if $\Delta\delta$ H3 > $\Delta\delta$ H5 (partial inclusion) or $\Delta\delta$ H3 < $\Delta\delta$ H5 (total inclusion) [61,62].

- Nuclear overhauser effect experiments are usually performed in two-dimensions 2D and allow to visualize the cross-peaks correlations between protons in the spectrum. This happens between atoms that are near each other, where the NOE phenomenon occurs, e.g., there is a transfer of the spin polarization from one population of nuclear spins to another. In CD host-guest complexes these experiments are particularly useful to understand the 3D structure of the IC by finding the cross-peaks between the guest protons and the CD cavity nuclei H-3 and H-5. The two most common experiments used to perform NOE experiments are Nuclear Overhauser Effect Spectroscopy (NOESY) and Rotational Overhauser Effect Spectroscopy (ROESY) [59].

1.6.2 Isothermal titration calorimetry (ITC)

One versatile technique to study CD complexes[1], is isothermal titration calorimetry (ITC). This is the only experimental setup that allows one to simultaneously determine thermodynamic parameters such as ΔH, ΔS, ΔG, K_{eq} and the stoichiometry of the IC. ITC measures the heat absorbed or released in solution upon a ligand binding to a CD [63]. A typical ITC experiment (Figure 1.5) consists of consecutively injecting small volumes (5-10 μL) of an aqueous solution of CD contained in a stirring syringe on a guest molecule solution contained

[1] I would personally argue ITC as the most versatile technique for studying CD ICs

in a sample cell. The reference cell is filled with the exact same buffer used to prepare the ligand and macromolecule solutions. Approximate isothermal conditions are maintained by increasing the temperature in both the reference cell and the sample cell very slowly (<0.1°C/hour). The heat changes in the sample cell upon titration causes a temperature difference (ΔT) between the reference cell and sample cell which is detected by the calorimeter [64]. The heat of the system is monitored for each injection and plotted as a function of time. Finally, an integration of the heat data as a function of the molar ratio of the two species is performed and a curve fitting makes possible to estimate all the thermodynamic values of interest.

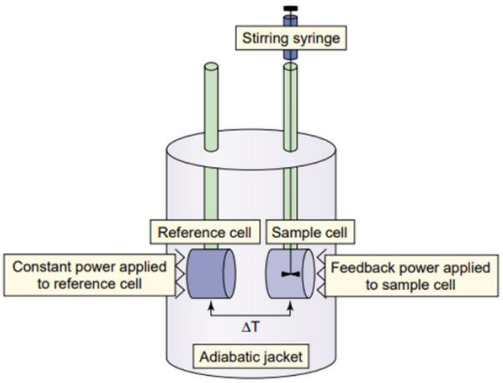

Figure 1.10 Schematic representation of the isothermal titration calorimeter. Extracted from *Holdgate et al. 2005* [64]

1.6.3 Electroanalytical techniques

Electrochemical techniques are quite effective for determining K_{eq} of ICs in solution, particularly when the guest molecule is electroactive. The interaction of CDs and guests has also been studied on electrode surfaces [65].

- Voltammetry

  This technique is very sensitive and has a low consumption of materials, which makes it useful to evaluate K_{eq} at very low concentrations of an electroactive guest. Complexation with CD brings a negative shift of the cathodic peak potential of the guest molecule as well as a decrease in the peak current intensity [66].

- Potentiometry

  Potentiometric methods are employed to determine the binding constants of acidic or basic guest molecules with CDs by following the pH changes as a function of an increasing CD concentration at a constant guest concentration. In this type of experiments, the guest moieties can be ionized or unionized in the medium, which is strongly influenced by the pH of the solution. Both forms of the guest can form ICs with the CDs which will be present together in the solution; each of them having different stability constant that will be influenced by the hydrophobicity of the ionized and unionized moieties [67].

- Electrical conductivity

  The principle of this technique takes into consideration that the conductivity of a solution containing a guest molecule will be distinctly affected by the addition of CDs. As hydrophobic guests are normally only partially soluble in water, the addition of CDs and subsequent formation of ICs will modify the solution conductivity. Similarly to other techniques, this technique can be used not only to

estimate the occurrence of the IC, but also the stoichiometry of the complex [68].

1.6.4 Separation techniques

Depending on the strength of the IC, CDs are able to selectively complexate a variety of molecules, even if they are enantiomers [56]. For this reason, CDs are being widely used as stationary phases or as mobile phase modifiers in chromatography [69], such as high-performance liquid chromatography (HPLC). CDs are also used for the separation of closely related compounds such as geometrical isomers and enantiomers by capillary electrophoresis (CE). Even though these methods are not able to provide information about the molecular structure of the IC, both HPLC and CE can be used to determine the binding constant by analyzing the molecular interactions of CD complexes [45].

- High performance liquid chromatography (HPLC)

  In HPLC CDs can be used either in the stationary part by being chemically bounded to silica gel, or they can also be studied in solution with the guest molecule in the mobile phase. The guest retention times will vary depending on the host-guest interactions with CDs [70]. On another approach, by adding the CDs to a column equilibrated with an eluent that contains the ligand molecule; the chromatogram will show visible changes such as a positive peak due to the complex formation and a negative peak which corresponds to the free ligand. This can be related to the amount of complexed guest and as a result the binding constant can be calculated by the variation of the intensity in the peaks [71]. However useful, HPLC requires large amount of materials, extensive sample preparation, a strict control of the experimental conditions, and in many cases, long separation times.

- Capillary electrophoresis (CE)

  CE is efficient for separating molecules contained in capillary tubes with an electrolytic solution by using the influence of an electric field. This separation occurs because of the difference in the mobility of ionic species and the affinity of charged or uncharged molecules in relation to a charged electrolyte. Therefore, CE has proven to be very useful to study the interactions of CDs with charged guest molecules [72].

1.6.5 Molecular simulations

Finally, in-silico methods are becoming more and more useful to estimate the binding potential between CDs and a ligand molecule. As the advance in computing power and high-performance computing infrastructure becomes more available, the development of improved calculation algorithms and more refined force-fields allows these type of techniques to become more relevant and useful for the study and characterization of CD ICs [73].

According to *Abdolmaleki et al* [74] a model can be defined as a "mathematical representation of the system (which is the physical process of interest) and an abstraction of reality". Whereas a simulation is described as "a type of model where the computer is used to imitate the behaviour of the system". Molecular modelling systems offer the advantage of manipulating and representing 3D molecular models and perform analysis such as conformational searches in the structures. They offer the capability of predicting weather CDs will potentially be good binders for an extensive library of compounds.

The main in-silico methods used to study CD-ligand interactions reported in the literature can be divided in molecular docking, molecular dynamics, quantitative structure-activity/property relationships (QSARs/QPRs),

quantum mechanics, Monte Carlo simulations and machine learning. Table 1.2 shows some examples of CD and guest molecules studied with the different simulation methods.

- Molecular docking

  Docking computation tries to predict the affinity of binding between two (or more) species. Usually, small ligand molecules are aligned and inserted e.g., docked, inside the binding cavity of a macromolecule. The resulting pose is assessed by a specific scoring function [75] which generates a binding score for each one of the poses, thus obtaining a ranking for the most suitable ligand-binder molecular conformation.

- Molecular dynamics (MD)

  MD calculates the time-dependent behaviour of a molecular system and imitates the physical motion of molecules under Newton's laws of physics, e.g., molecular mechanics (MM), and an empirical force field such as AMBER or GROMOS [76]. It is a useful method to explore the structural, dynamic, thermodynamic, and energetic conduct of CD complexes [77]. The binding free energy of the IC can be then calculated with methods such as molecular mechanics energies combined with the Poisson–Boltzmann or generalized Born and surface area continuum solvation (MM/PBSA and MM/GBSA) methods [78].

- Quantitative structure-activity/property relationships (QSARs/QPRs)

  This technique is useful for the drug design and development. In order to predict a property or activity of a drug it only requires the drug's molecular structure. The QSAR are regression models which are recompilations of a relationship between chemical structures and

biological activity within a given drug class [74]. It can also be used to calculate the binding energy and thermodynamic parameters between CDs and a guest molecule.

- Quantum mechanics (QM)

  QM offers the advantage to represent mathematically the spatial locations of all the electrons and nuclei of atoms and molecules. It is thus capable of predicting both electronic characteristics and molecular structures. In comparison, molecular mechanics (MM) methods do not involve electrons explicitly, and so, it lacks in predicting electronic properties of molecules. QM has been applied in the study of CD ICs (Table 1.2); however, it has some disadvantages; the process of energy minimization can be very time-consuming for molecules with many rotable bonds such as CDs in comparison to the fast energy minimization performed by MM [79]. Thus, for CD systems QM needs high computation power and it is also difficult to apply for solvated systems.

- Machine learning (ML)

  ML algorithms are capable of learning from input data, and make high-accuracy predictions for the classification and regression models which allows the extensive application of ML in many fields such as bioinformatics, computer vision, neuroscience, etc [80]. The application of ML for CD complexes (Table 1.2) is relatively new and is mainly focused on the pharmaceutical field. Zhao et al [81] argue that the importance of ML method is to simplify drug design and increase the efficiency of formulation research, which is especially important to early drug discovery with very scarce or expensive compounds and with complicated formulation composition.

Table 1.2 Some examples in the literature that use in-silico calculations for CD studies. Adapted from [74] and [82]

Cyclodextrin	Guest	Computational method
β-CD and four < β-CD derivatives	Luteolin [83]	Molecular docking
HPβ-CD, methyl-β-CD, Sulfobutylether β-CD	Voriconazole [84]	
β-CD	Aflatoxin [85]	
β-CD and γ-CD	Amphothericine B [86]	Molecular dynamics (MD)
α–, β-CD and γ-CD	Cumene hydroperoxide [87]	
α– and β-CD	1-alcanols, substituted phenols, substituted imidazoles [88]	
α–CD	Benzene derivatives [89]	Quantitative structure-activity/property relationships (QSARs/QPRs)
β-CD	Multiple compounds [90]	
β-CD	233 molecules [91]	
β–CD	Praziquantel [92]	Monte Carlo (MC) simulations
β-CD and methyl-β-CD	Niobocene dichloride [93]	
Sulfobutylether β-CD	Diverse organic molecules [94]	Machine learning
α-CD, β-CD, γ-CD, HPαCD, HPβCD, and HPγCD	β–lactam antibiotic [82]	

1.7 Cyclodextrin applications: One ring to rule them all

As it has been previously examined, the main quality of CDs is their inclusion complexation ability with a vast variety of either solid or gaseous compounds and in solution. The effects of the complexation of a molecule inside the CD cavity and the repercussions of the change in physicochemical characteristics have opened a door for the application of CDs in several fields such as pharmaceutical, food, cosmetic and home care, chemical industry, and bioremediation.

1.7.1 Pharmaceutical applications

There is a vast number of application of CDs in the pharmaceutical field. Perhaps one of the most explored uses of CDs in this field is as drug carriers [95] since the low absorption and the decomposition of a drug before reaching its active site is a common issue for the pharmaceutical scientists. CDs aide to solve these issues for example by enhancing the solubility and bioavailability for drugs [96] or for their stabilizing effects against degradation processes such as hydrolysis [97], oxidation [98] or photodegradation [99]. By complexation of irritating products, the gastric mucosa or the skin can be protected. Also, bad odors or flavors in drugs can be reduced [25].

Nevertheless, CDs can also be used as active drugs as has been lately reviewed by *Matencio et al* [100]. One of the most famous examples in the field of CD as an active ingredient is the Sugammadex-rocuronium IC [101]. Rocuronium bromide is a widely used anesthetic that blocks the acethylcoline in nicotinic receptors in striated muscle cells and produces neuromuscular blocking allowing the patients to remain still during surgery. Sugammadex is an FDA approved medication that forms highly stable IC with rocuronium to

remove the anestheic from the body by kidney excretion. The drug is an anionic γ–CD derivative modified with sulphanylpropanoic acid arms.

HPCD has also been used as an active drug ingredient to treat hypervitaminosis A and remove the excess of vitamin A in individuals who cannot metabolize this micronutrient [102]. It has also shown to slow the progression of the disease in patients with Nieman Pick type C disease (NPC) which is a rare metabolic disorder where there is an enhanced cholesterol accumulation in the brain and other organs that results in neurodegeneration [103]. There is research reporting CDs as a treatment or potential treatment for Parkinson's, Alzheimer's, and Huntington's disease; as well as antiviral activity reported against the influenza, HIV, Sars-Cov-2, hepatitis-C among other viruses. The main mechanism for CDs to reduce viral infection has been stablished to be the capacity to complex cholesterol which induces structural deformation in virus membranes [100].

1.7.2 Remediation applications

Using CDs and its derivatives for remediation technologies offers advantages for soil, groundwater, wastewater, and atmosphere remediation. CDs can be used to complexate a wide range of pollutant molecules that tend to accumulate in the environment such as heavy metals, industrial dyes, organic waste molecules, ionic surfactants, phenol and phenolic derivatives, Cr^{6+}, halogenated compounds, etc [104]. Since native CDs and many of the derivatives are water soluble, the strategy for using CDs in environmental remediation has been to develop insoluble CD-based materials that include cross-linked polymers and nanosponges [105], membranes, nanofibers, and functionalized systems such as polymers, silica, and organic resins [106]. A more resent and still not so explored area for bioremediation includes the complexation of marine toxins such as okadaic acid by CD polymers [44].

1.7.3 Food applications

CDs have interesting advantages for the food industry which makes their use suitable for this industry as bioactive food supplements and nutraceuticals. *Astray et al* [107] did a complete review of CD's properties and applications focused in the food industry. They are odorless, nondigestible, noncaloric, noncariogenic saccharides. They reduce the digestion of carbohydrates and lipids and have low glycemic index and decrease the glycemic index of the food. They are either non- or only partly digestible by the enzymes of the human gastrointestinal tract and can be fermented by the gut microflora. As such, they have been used as dietary fibers to control the body weight and blood lipid profile. CDs are prebiotics, improve the intestinal microflora by selective proliferation of bifidobacteria.

They have also been applied as solubilizers, stabilizers of dietary lipids, such as unsaturated fatty acids, phytosterols, vitamins, flavonoids, carotenoids, and other nutraceuticals. Additionally, CDs have been used for reducing unwanted components, such as trans-fats, allergens, mycotoxins, acrylamides, bitter compounds, as well as in smart active packaging of foods.

1.7.4 Cosmetic applications

The toiletry, personal care and fragrance industries also make use of CDs for improving the efficiency of aroma and odorant molecules, disguising unpleasant smells, enhancing the stability of essential oils and volatile compounds by controlling the losses produced by evaporation, protecting guests from degradation processes that increase product shelf-life, or transforming liquid compounds into a crystalline form. Another cosmetic application of CDs is its use in textiles that may act as deposits for cosmetic

compounds. CDs can be permanently fixed in those fabrics and release the drug once in contact with the skin [108].

1.8 Thesis objectives and contribution

As it has been described in the previous sections, cyclodextrins and their derivatives are natural macrocycles that have the potential to form inclusion complexes with innumerous guest molecules. This makes them relevant oligosaccharide molecules in many industries.

The overall objective of this thesis is to characterize the IC of CD with different guest molecules for potential new applications in the fields of pharmaceutics and bioremediation.

To achieve this general objective, we have followed more specific objectives:

- To study and characterize the IC between CDs plus some key CD derivatives with an FDA-approved drug bearing drug-repurposing potential
- To elucidate the mechanisms and effects that lie underneath the IC of CDs and the aforementioned drug molecule
- To characterize the IC between native CDs plus some key CD derivatives with a model toxin molecule
- To synthesize and characterize various CD-NS with different cross-linking and cavity sizes
- To evaluate the newly synthesized CD-NS as a potential system for the absorption of marine toxins

This thesis is thus a contribution to the CD research field by characterizing for the first time the IC between different CDs and two guest molecules: nafamostat mesylate, a drug; and veratridine, a toxin. Thus, it opens the door

for drug repurposing potential of the drug with different administration routes and states a proof-of-concept for possible antidote applications of CDs against different lipid toxins. Finally, the synthesis of a new CD-NS family with different cross-linkers attempts to enlarge the frontiers of knowledge for CD-based polymeric materials and its application for marine toxin removal.

1.9 References

1. Lehn, J.-M. Supramolecular chemistry. *Science (80-.).* **1993**, *260*, 1762–1763, doi:10.1126/science.8511582.

2. Varga, M. *Self-assembly of nanobiomaterials*; Elsevier Inc., 2016; ISBN 9780323415330.

3. Jordan, S.F.; Rammu, H.; Zheludev, I.N.; Hartley, A.M.; Maréchal, A.; Lane, N. Promotion of protocell self-assembly from mixed amphiphiles at the origin of life. *Nat. Ecol. Evol.* **2019**, *3*, 1705–1714, doi:10.1038/s41559-019-1015-y.

4. Heckl, W.M. 22 Molecular Self-Assembly and the Origin of Life. **2002**.

5. Budin, I.; Szostak, J.W. Expanding roles for diverse physical phenomena during the origin of life. *Annu. Rev. Biophys.* **2010**, *39*, 245–263, doi:10.1146/annurev.biophys.050708.133753.

6. Redd, J.T.; Steffensen, M.B.; Bradshaw, J.S.; Izatt, R.M. Organic Macrocycles. *Ref. Modul. Chem. Mol. Sci. Chem. Eng.* **2013**, doi:10.1016/B978-0-12-409547-2.05562-1.

7. Pedersen, C.J. The discovery of crown ethers. *Science (80-.).* **1988**, *241*, 536–540, doi:10.1126/science.241.4865.536.

8. Lehn, J.M. *Cryptates: Inclusion Complexes of Macropolycyclic Receptor Molecules*; International Union of Pure and Applied Chemistry, 1979; Vol. 50;.

9. Cram, D.J.; Kaneda, T.; Helgeson, R.C.; Leiin, G.M. Spherands—Ligands Whose Binding of Cations Relieves Enforced Electron-Electron Repulsions. *J. Am. Chem. Soc.* **1979**, *101*, 6752–6754.

10. Yudin, A.K. Introduction: Macrocycles. *Chem. Rev.* **2019**, *119*, 9723, doi:10.1021/acs.chemrev.9b00453.

11. Of, T.H.E.C. *The Concept of Preorganization*; Second Edi.; Elsevier, 2003; Vol. XXIV; ISBN 9780801480775.

12. Villiers, A. Sur la fermentation de le fècule par l'action du ferment butyrique. *Compt. Rend.* **1891**, *4*, 1–23.

13. Schardinger, F. Bacillus macerans, ein Aceton bildender Rottebacillus. *Zentralbl. Bakteriol. Parasintenk. Abt. 2* **1905**, *14*, 772–781.

14. Szejtli, J. Introduction and general overview of cyclodextrin chemistry. *Chem. Rev.* **1998**, *98*, 1743–1753, doi:10.1021/cr970022c.

15. Freudenberg, K.; Cramer, F.. Gamma dextrin. *Naturforsch.* **1948**, *3b*, 464.

16. Loftsson, T.; Duchêne, D. Historical Perspectives Cyclodextrins and their pharmaceutical applications. *Int. J. Pharm.* **2007**, *329*, 1–11, doi:10.1016/j.ijpharm.2006.10.044.

17. Crini, G. Review: A history of cyclodextrins. *Chem. Rev.* **2014**, *114*, 10940–10975, doi:10.1021/cr500081p.

18. Ahuja, K.; Sonal, S. Global Cyclodextrin Market Size, Share and Industry Analysis Report by Type (Alpha, Beta, Gamma) and Application (Pharmaceutical, Food & Beverage, Chemicals, Cosmetics & Personal Care), Regional Outlook, Competitive Market Share & Forecast, 2021 - 2027 Available online: https://www.gminsights.com/industry-analysis/global-cyclodextrin-market.

19. Biwer, A.; Antranikian, G.; Heinzle, E. Enzymatic production of

cyclodextrins. *Appl. Microbiol. Biotechnol.* **2002**, *59*, 609–617, doi:10.1007/s00253-002-1057-x.

20. Stella, V.J.; he, Q. Cyclodextrins. *Toxicol. Pathol.* **2008**, *36*, 30–42, doi:10.1177/0192623307310945.

21. Cramer, F. Über Einschlußverbindungen, V. Mitteil.: Basenkatalyse durch innermolekulare Hohlräume. *Chem. Ber.* **1953**, *86*, 1576–1581, doi:10.1002/cber.19530861217.

22. Cramer, F.; Henglein, F.M. Über Einschlußverbindungen, XII. Verbindungen von α-Cyclodextrin mit Gasen. *Chem. Ber.* **1957**, *90*, 2572–2575, doi:10.1002/cber.19570901123.

23. Duchêne, D.; Bochot, A. Thirty years with cyclodextrins., doi:10.1016/j.ijpharm.2016.07.030.

24. Waldvogel, S. *Book Review Cyclodextrins and Their Complexes: Chemistry, Analytical Methods, Applications (Helena Dodziuk, Ed.)*; 2007; Vol. 2007; ISBN 9783527312801.

25. Del Valle, E.M.M. Cyclodextrins and their uses: A review. *Process Biochem.* **2004**, *39*, 1033–1046, doi:10.1016/S0032-9592(03)00258-9.

26. Řezanka, M. Synthesis of substituted cyclodextrins. *Environ. Chem. Lett.* **2019**, *17*, 49–63, doi:10.1007/S10311-018-0779-7.

27. Liao, R.; Lv, P.; Wang, Q.; Zheng, J.; Feng, B.; Yang, B. Cyclodextrin-based biological stimuli-responsive carriers for smart and precision medicine. *Biomater. Sci.* **2017**, *5*, 1736–1745, doi:10.1039/c7bm00443e.

28. Szejtli, J. Past, present, and future of cyclodextrin research. *Pure Appl. Chem.* **2004**, *76*, 1825–1845, doi:10.1351/pac200476101825.

29. Szente, L.; Szejtli, J. Highly soluble cyclodextrin derivatives: chemistry, properties, and trends in development. *Adv. Drug Deliv. Rev.* **1999**, *36*, 17–

28.

30. Mavridis, I.M.; Yannakopoulou, K. Mini review Anionic cyclodextrins as versatile hosts for pharmaceutical nanotechnology: Synthesis, drug delivery, enantioselectivity, contrast agents for MRI. **2015**, doi:10.1016/j.ijpharm.2015.06.004.

31. Yannakopoulou, K. Cationic cyclodextrins: Cell penetrating agents and other diverse applications. *J. Drug Deliv. Sci. Technol.* **2012**, *22*, 243–249, doi:10.1016/S1773-2247(12)50035-3.

32. Arima, H.; Motoyama, K.; Irie, T. Recent Findings on Safety Profiles of Cyclodextrins, Cyclodextrin Conjugates, and Polypseudorotaxanes. *Cyclodextrins Pharm. Cosmet. Biomed. Curr. Futur. Ind. Appl.* **2011**, 91–122, doi:10.1002/9780470926819.ch5.

33. Kurkov, S. V.; Loftsson, T. Cyclodextrins. *Int. J. Pharm.* **2013**, *453*, 167–180, doi:10.1016/j.ijpharm.2012.06.055.

34. Tian, B.; Liu, J. The classification and application of cyclodextrin polymers: a review. *New J. Chem.* **2020**, *44*, 9137–9148, doi:10.1039/c9nj05844c.

35. Liu, Z.; Ye, L.; Xi, J.; Wang, J.; Feng, Z. guo Cyclodextrin polymers: Structure, synthesis, and use as drug carriers. *Prog. Polym. Sci.* **2021**, *118*, 101408, doi:10.1016/j.progpolymsci.2021.101408.

36. Caldera, F.; Tannous, M.; Cavalli, R.; Zanetti, M.; Trotta, F. Evolution of Cyclodextrin Nanosponges. **2017**, doi:10.1016/j.ijpharm.2017.06.072.

37. Li, D.; Ma, M. Nanosponges for water purification. *Clean Prod. Process.* **2000**, *2*, 0112–0116, doi:10.1007/s100980000061.

38. Tang, S.; Kong, L.; Ou, J.; Liu, Y.; Li, X.; Zou, H. Application of cross-linked β-cyclodextrin polymer for adsorption of aromatic amino acids. *J. Mol. Recognit.* **2006**, *19*, 39–48, doi:10.1002/jmr.756.

39. Yang, Y.; Long, Y.; Cao, Q.; Li, K.; Liu, F. Molecularly imprinted polymer using β-cyclodextrin as functional monomer for the efficient recognition of bilirubin. *Anal. Chim. Acta* **2008**, *606*, 92–97, doi:10.1016/J.ACA.2007.10.044.

40. Trotta, F.; M.A. *Nanosponges: Synthesis and applications*; Trotta, F., Ed.; 1377; ISBN 9783527340996.

41. Trotta, F.; Cavalli, R. Characterization and Applications of New Hyper-Cross-Linked Cyclodextrins. *Compos. Interfaces* **2009**, *16*, 39–48, doi:10.1163/156855408X379388.

42. Trotta, F. Cyclodextrin Nanosponges and their Applications. *Cyclodextrins Pharm. Cosmet. Biomed. Curr. Futur. Ind. Appl.* **2011**, 323–342, doi:10.1002/9780470926819.ch17.

43. Ahmed, R.Z.; Patil, G.; Zaheer, Z. Drug Development and Industrial Pharmacy Nanosponges-a completely new nano-horizon: pharmaceutical applications and recent advances. **2012**, doi:10.3109/03639045.2012.694610.

44. Campàs, M.; Rambla-Alegre, M.; Wirén, C.; Alcaraz, C.; Rey, M.; Safont, A.; Diogène, J.; Torréns, M.; Fragoso, A. Cyclodextrin polymers as passive sampling materials for lipophilic marine toxins in Prorocentrum lima cultures and a Dinophysis sacculus bloom in the NW Mediterranean Sea. *Chemosphere* **2021**, *285*, doi:10.1016/j.chemosphere.2021.131464.

45. Mura, P. Analytical techniques for characterization of cyclodextrin complexes in the solid state: A review. *J. Pharm. Biomed. Anal.* **2015**, *113*, 226–238, doi:10.1016/j.jpba.2015.01.058.

46. Kfoury, M.; Landy, D.; Ruellan, S.; Auezova, L.; Greige-Gerges, H.; Fourmentin, S. Determination of formation constants and structural characterization of cyclodextrin inclusion complexes with two phenolic

isomers: carvacrol and thymol. *Beilstein J. Org. Chem* **2016**, *12*, 29–42, doi:10.3762/bjoc.12.5.

47. Calabrò, M.L.; Tommasini, S.; Donato, P.; Stancanelli, R.; Raneri, D.; Catania, S.; Costa, C.; Villari, V.; Ficarra, P.; Ficarra, R. The rutin/β-cyclodextrin interactions in fully aqueous solution: Spectroscopic studies and biological assays. *J. Pharm. Biomed. Anal.* **2005**, *36*, 1019–1027, doi:10.1016/j.jpba.2004.09.018.

48. Miyake, K.; Irie, T.; Arima, H.; Hirayama, F.; Uekama, K.; Hirano, M.; Okamoto, Y. Characterization of itraconazole/2-hydroxypropyl-β-cyclodextrin inclusion complex in aqueous propylene glycol solution. *Int. J. Pharm.* **1999**, *179*, 237–245, doi:10.1016/S0378-5173(98)00393-7.

49. Zerrouk, N.; Ginès Dorado, J.M.; Arnaud, P.; Chemtob, C. Physical characteristics of inclusion compounds of 5-ASA in α and β cyclodextrins. *Int. J. Pharm.* **1998**, *171*, 19–29, doi:10.1016/S0378-5173(98)00165-3.

50. Van Hees, T.; Piel, G.; De Hassonville, S.H.; Evrard, B.; Delattre, L. Determination of the free/included piroxicam ratio in cyclodextrin complexes: Comparison between UV spectrophotometry and differential scanning calorimetry. *Eur. J. Pharm. Sci.* **2002**, *15*, 347–353, doi:10.1016/S0928-0987(02)00018-0.

51. Uekama, K.; Hirayama, F.; Otaguiri, M.; Otaguiri, Y.; Ikeda, K. Inclusion complexation of B-cyclodextrin with some sulfonamides in aqueous solution. *Chem. Pharm. Bull.* **1978**, *26*, 1162–1167.

52. Tablet, C.; Matei, I.; Hillebr, M. The Determination of the Stoichiometry of Cyclodextrin Inclusion Complexes by Spectral Methods: Possibilities and Limitations. *Stoichiom. Res. - Importance Quant. Biomed.* **2012**, doi:10.5772/34287.

53. Benesi, A.; Hildebrand, J.H. Spectrophotometry of Iodine with Aromatic

Hydrocarbons A Spectrophotometric Investigation of the Interaction of Iodine with Aromatic Hydrocarbons. **1949**.

54. Job, P. Recherches sur la formation de complexes mineraux en solution et sur leur stabilite. *Ann. Chim.* **1928**, *Vol. 9*, 113–203.

55. Landy, D.; Fourmentin, S.; Salome, M.; Surpateanu, G. Analytical Improvement in Measuring Formation Constants of Inclusion Complexes between β-Cyclodextrin and Phenolic Compounds. *J. Incl. Phenom. Macrocycl. Chem.* **2000**, *38*, 187–198.

56. Marconi, G.; Mezzina, E.; Manet, I.; Manoli, F.; Zambelli, B.; Monti, S. Stereoselective interaction of ketoprofen enantiomers with β-cyclodextrin: Ground state binding and photochemistry. *Photochem. Photobiol. Sci.* **2011**, *10*, 48–59, doi:10.1039/c0pp00262c.

57. Madrid, J.M.; Villafruela, M.; Serrano, R.; Mendicuti, F. Experimental thermodynamics and molecular mechanics calculations of inclusion complexes of 9-methyl anthracenoate and 1-methyl pyrenoate with β-cyclodextrin. *J. Phys. Chem. B* **1999**, *103*, 4847–4853, doi:10.1021/jp9838240.

58. Ventrella, A.; Verrone, R.; Longobardi, F.; Agostiano, A.; Lippolis, V.; Pascale, M.; Maragos, C.M.; Appell, M.; Catucci, L. Interactions between cyclodextrins and fluorescent T-2 and HT-2 toxin derivatives: a physico-chemical study., doi:10.1007/s10847-012-0130-z.

59. Schneider, H.-J.; Hacket, F.; Rüdiger, V.; Ikeda, H. NMR Studies of Cyclodextrins and Cyclodextrin Complexes. *Chem. Rev.* **1998**, *98*, 1755–1785.

60. Fielding, L. Determination of association constants (Ka) from solution NMR data. *Tetrahedron* **2000**, *56*, 6151–6170, doi:10.1016/S0040-4020(00)00492-0.

61. Rekharsky, M.; Goldberg, R.N.; Schwarz, F.P.; B., T.Y.; Ross, P.D.; Yamashoji, Y.; Inoue, Y. Thermodynamic and Nuclear Magnetic Resonance Study of the Interactions of alpha- and beta-Cyclodextrin with Model Substances: Phenethylamine, Ephedrines, and Related Substances. *J. Am. Chem. Soc.* **1995**, *117*, 8830–8840, doi:https://doi.org/10.1021/ja00139a017.

62. Greatbanks, D.; Pickford, R. Cyclodextrins as chiral complexing agents in water, and their application to optical purity measurements. *Magn. Reson. Chem.* **1987**, *25*, 208–215, doi:10.1002/mrc.1260250306.

63. Wiseman, T.; Williston, S.; Brandts, J.F.; Lin, L.N. Rapid measurement of binding constants and heats of binding using a new titration calorimeter. *Anal. Biochem.* **1989**, *179*, 131–137, doi:10.1016/0003-2697(89)90213-3.

64. Holdgate, G.A.; Ward, W.H.J. Measurements of binding thermodynamics in drug discovery. *Drug Discov. Today* **2005**, *10*, 1543–1550, doi:10.1016/S1359-6446(05)03610-X.

65. Radi, A.-E.; Eissa, S. Electrochemistry of cyclodextrin inclusion complexes of pharmaceutical compounds. *Open Chem. Biomed. Methods J.* **2010**, *3*, 74–85.

66. Radi, A.E.; Eissa, S. Voltammetric and spectrophotometric study on the complexation of glibenclamide with β-cyclodextrin. *J. Incl. Phenom. Macrocycl. Chem.* **2010**, *68*, 417–421, doi:10.1007/s10847-010-9801-9.

67. Kopecký, F.; Vojteková, M.; Kaclík, P.; Demko, M.; Bieliková, Z. Bupivacaine hydrochloride complexation with some α- and β-cyclodextrins studied by potentiometry with membrane electrodes. *J. Pharm. Pharmacol.* **2010**, *56*, 581–587, doi:10.1211/0022357023295.

68. Gao, Y.A.; Li, Z.H.; Du, J.M.; Han, B.X.; Li, G.Z.; Hou, W.G.; Shen, D.; Zheng, L.Q.; Zhang, G.Y. Preparation and characterization of inclusion complexes of β-cyclodextrin with ionic liquid. *Chem. - A Eur. J.* **2005**, *11*,

5875–5880, doi:10.1002/chem.200500120.

69. Deng, Y.; Maruyama, W.; Yamamura, H.; Kawai, M.; Dostert, P.; Naoi, M. *Mechanism of Enantioseparation of Salsolinols, Endogenous Neurotoxins in Human Brain, with Ion-Pair Chromatography Using-Cyclodextrin as a Mobile Phase Additive*; 1996;

70. Fujimura, K.; Ueda, T.; Kitagawa, M.; Takayanagi, H.; Ando, T. Reversed-Phase Retention Behavior of Aromatic Compounds Involving β-Cyclodextrin Inclusion Complex Formation in the Mobile Phase. *Anal. Chem.* **1986**, *58*, 2668–2674, doi:10.1021/ac00126a020.

71. Hummel, J.P.; Dreyer, W.J. Measurement of protein-binding phenomena by gel filtration. *Biochim. Biophys..4cta*, **1962**, *63*, 530–532.

72. Steinbock, B.; Vichaikul, P.P.; Steinbock, O. *Nonlinear analysis of dynamic binding in affinity capillary electrophoresis demonstrated for inclusion complexes of b-cyclodextrin*; 2001;

73. Quevedo, M.A.; Zoppi, A. Current trends in molecular modeling methods applied to the study of cyclodextrin complexes. *J. Incl. Phenom. Macrocycl. Chem.* **2018**, *90*, 1–14, doi:10.1007/s10847-017-0763-z.

74. Abdolmaleki, A.; Ghasemi, F.; Jahan, |; Ghasemi, B. Computer-aided drug design to explore cyclodextrin therapeutics and biomedical applications. *Chem Biol Drug Des* **2017**, *89*, 257–268, doi:10.1111/cbdd.12825.

75. Pantsar, T.; Poso, A. Binding affinity via docking: Fact and fiction. *Molecules* **2018**, *23*, 1899, doi:10.3390/molecules23081899.

76. Wang, W.; Donini, O.; Reyes, C.M.; Kollman, P.A. Biomolecular simulations: Recent developments in force fields, simulations of enzyme catalysis, protein-ligand, protein-protein, and protein-nucleic acid noncovalent interactions. *Annu. Rev. Biophys. Biomol. Struct.* **2001**, *30*, 211–243, doi:10.1146/annurev.biophys.30.1.211.

77. Mazurek, A.H.; Szeleszczuk, Ł.; Gubica, T. Molecular Sciences Application of Molecular Dynamics Simulations in the Analysis of Cyclodextrin Complexes. **2021**, doi:10.3390/ijms22179422.

78. Genheden, S.; Ryde, U. The MM/PBSA and MM/GBSA methods to estimate ligand-binding affinities. *Expert Opin. Drug Discov.* **2015**, *10*, 449–461, doi:10.1517/17460441.2015.1032936.

79. Liu, L.; Guo, Q.X. Use of quantum chemical methods to study cyclodextrin chemistry. *J. Incl. Phenom.* **2004**, *50*, 95–103, doi:10.1007/s10847-003-8847-3.

80. Jordan, M.I.; Mitchell, T.M. Machine learning: Trends, perspectives, and prospects. **2015**, *349*.

81. Zhao, Q.; Ye, Z.; Su, Y.; Ouyang, D. Predicting complexation performance between cyclodextrins and guest molecules by integrated machine learning and molecular modeling techniques. *Acta Pharm. Sin. B* **2019**, *9*, 1241–1252, doi:10.1016/j.apsb.2019.04.004.

82. Mizera, M.; Lewandowska, K.; Miklaszewski, A.; Cielecka-Piontek, J. Machine Learning Approach for Determining the Formation of β-Lactam Antibiotic Complexes with Cyclodextrins Using Multispectral Analysis. *Mol. 2019, Vol. 24, Page 743* **2019**, *24*, 743, doi:10.3390/MOLECULES24040743.

83. Liu, B.; Li, W.; Zhao, J.; Liu, Y.; Zhu, X.; Liang, G. Physicochemical characterisation of the supramolecular structure of luteolin/cyclodextrin inclusion complex. **2013**, doi:10.1016/j.foodchem.2013.03.097.

84. Suvarna, P.; Chaudhari, P.; Birangal, S.; Mallela, L.S.; Roy, S.; Koteshwara, A.; Aranjani, J.M.; Lewis, S.A. Voriconazole–Cyclodextrin Supramolecular Ternary Complex-Loaded Ocular Films for Management of Fungal Keratitis. *Mol. Pharm.* **2022**, *19*, 258–273, doi:10.1021/acs.molpharmaceut.1c00746.

85. Ramírez-Galicia, G.; Garduño-Juárez, R.; Vargas, M.G. Effect of water molecules on the fluorescence enhancement of Aflatoxin B1 mediated by Aflatoxin B1:b-cyclodextrin complexes. A theoretical study. **2007**, doi:10.1039/b614107b.

86. He, J.; Chipot, C.; Shao, X.; Cai, W. Cyclodextrin-Mediated Recruitment and Delivery of Amphotericin B. *J. Phys. Chem. C* **2013**, *117*, 11750–11756, doi:10.1021/jp3128324.

87. Jiao, A.; Zhou, X.; Xu, X.; Jin, Z. Molecular dynamics simulations of cyclodextrin-cumene hydroperoxide complexes in water. *Comput. Theor. Chem.* **2013**, *1013*, 1–6, doi:10.1016/J.COMPTC.2013.02.023.

88. El-Barghouthi, M.I.; Jaime, C.; Al-Sakhen, N.A.; Issa, A.A.; Abdoh, A.A.; Al Omari, M.M.; Badwan, A.A.; Zughul, M.B.; Naor, J. Molecular dynamics simulations and MM-PBSA calculations of the cyclodextrin inclusion complexes with 1-alkanols, para-substituted phenols and substituted imidazoles. **2008**, doi:10.1016/j.theochem.2007.12.005.

89. Ghasemi, J.B.; Salahinejad, • M; Rofouei, • M K; Mousazadeh, • M H Docking and 3D-QSAR study of stability constants of benzene derivatives as environmental pollutants with a-cyclodextrin., doi:10.1007/s10847-011-0078-4.

90. Pérez-Garrido, A.; Helguera, A.M.; Cordeiro, M.N.D.S.; Escudero, A.G. QSPR modelling with the topological substructural molecular design approach: β-cyclodextrin complexation. *J. Pharm. Sci.* **2009**, *98*, 4557–4576, doi:10.1002/JPS.21747.

91. Pérez-Garrido, A.; Morales Helguera, A.; Abellán Guillén, A.; Natália, M.; Cordeiro, D.S.; Garrido Escudero, A. Convenient QSAR model for predicting the complexation of structurally diverse compounds with b-cyclodextrins. **2008**, doi:10.1016/j.bmc.2008.11.040.

92. Mota, G.V.S.; De Oliveira, C.X.; Neto, A.M.J.C.; Costa, F.L.P. Inclusion complexation of praziquantel and β-cyclodextrin, combined molecular mechanic and monte carlo simulation. *J. Comput. Theor. Nanosci.* **2012**, *9*, 1090–1095, doi:10.1166/JCTN.2012.2148.

93. Pereira, C.C.L.; Nolasco, M.; Braga, S.S.; Almeida Paz, F.A.; Ribeiro-Claro, P.; Pillinger, M.; Gonçalves, I.S. A combined theoretical-experimental study of the inclusion of niobocene dichloride in native and permethylated β-cyclodextrins. *Organometallics* **2007**, *26*, 4220–4228, doi:10.1021/OM7003749/SUPPL_FILE/OM7003749-FILE012.PDF.

94. Merzlikine, A.; Abramov, Y.A.; Kowsz, S.J.; Thomas, V.H.; Mano, T. Development of machine learning models of β-cyclodextrin and sulfobutylether-β-cyclodextrin complexation free energies. *Int. J. Pharm.* **2011**, *418*, 207–216, doi:10.1016/J.IJPHARM.2011.03.065.

95. Conceicao, J.; Adeoye, O.; Cabral-Marques, H.M.; Lobo, J.M.S. Cyclodextrins as Drug Carriers in Pharmaceutical Technology: The State of the Art. *Curr. Pharm. Des.* **2017**, *24*, 1405–1433, doi:10.2174/1381612824666171218125431.

96. Miyake, K.; Arima, H.; Hirayama, F.; Yamamoto, M.; Horikawa, T.; Sumiyoshi, H.; Noda, S.; Uekama, K. Improvement of solubility and oral bioavailability of rutin by complexation with 2-hydroxypropyl-β-cyclodextrin. *Pharm. Dev. Technol.* **2000**, *5*, 399–407, doi:10.1081/PDT-100100556.

97. Matsubara, K.; Ando, Y.; Tetsumi, I.; Uekama, K. Protection Afforded by Maltosyl-β-cyclodextrin Against α-Chymotrypsin-Catalyzed Hydrolysis of a Luteinizing Hormone-Releasing Hormone Agonist, Buserelin Acetate. *Pharm. Res.* **1997**, *14*, 1401–1405, doi:doi.org/10.1023/A:1012120705408.

98. Loftsson, T.; Fridhriksdottir, H.; Olafsdottir, B.J.; Gudhmundsson, O. Solubilization and stabilization of drugs through cyclodextrin complexation.

Acta Pharm. Nord. **1991**, *3*, 215–217.

99. Wang, Z.; Landy, D.; Sizun, C.; Cézard, C.; Solgadi, A.; Przybylski, C.; de Chaisemartin, L.; Herfindal, L.; Barratt, G.; Legrand, F.X. Cyclodextrin complexation studies as the first step for repurposing of chlorpromazine. *Int. J. Pharm.* **2020**, *584*, 119391, doi:10.1016/j.ijpharm.2020.119391.

100. Matencio, A.; Caldera, F.; Cecone, C.; Manuel López-Nicolás, J.; Trotta, F. Cyclic Oligosaccharides as Active Drugs, an Updated Review. *Pharmaceuticals* **2020**, *13*, doi:10.3390/ph13100281.

101. Plosker, G.L.; Gauthier, S. Sugammadex. A review of its use in anesthetic practice. *Drugs* **2009**, *69*, 919–942.

102. Carpenter, T.O.; Pettifor, J.M.; Russell, R.M.; Pitha, J.; Mobarhan, S.; Ossip, M.S.; Wainer, S.; Anast, C.S. *Severe hypervitaminosis A in siblings' Evidence of variable tolerance to retinol intake*; 1987;

103. Liu, B.; Turley, S.D.; Burns, D.K.; Miller, A.M.; Repa, J.J.; Dietschy, J.M. *Reversal of defective lysosomal transport in NPC disease ameliorates liver dysfunction and neurodegeneration in the npc1 / mouse*; 2009;

104. Landy, D.; Mallard, I.; Ponchel, A.; Monflier, E.; Fourmentin, S. Remediation technologies using cyclodextrins: An overview. *Environ. Chem. Lett.* **2012**, *10*, 225–237, doi:10.1007/s10311-011-0351-1.

105. Morin-Crini, N.; Winterton, P.; Fourmentin, S.; Wilson, L.D.; Fenyvesi, É.; Crini, G. Water-insoluble β-cyclodextrin–epichlorohydrin polymers for removal of pollutants from aqueous solutions by sorption processes using batch studies: A review of inclusion mechanisms. *Prog. Polym. Sci.* **2018**, *78*, 1–23, doi:10.1016/j.progpolymsci.2017.07.004.

106. Crini, G.; Fourmentin, S.; Fenyvesi, É.; Torri, G.; Fourmentin, M.; Morin-Crini, N. Cyclodextrins, from molecules to applications. **2018**, *16*, 1361–1375, doi:10.1007/s10311-018-0763-2.

107. Astray, G.; Gonzalez-Barreiro, C.; Mejuto, J.C.; Rial-Otero, R.; Simal-Gándara, J. A review on the use of cyclodextrins in foods. *Food Hydrocoll.* **2009**, *23*, 1631–1640, doi:10.1016/j.foodhyd.2009.01.001.

108. Buschmann, H.-J.; Knittel, D.; Schollmeyer, E. *New Textile Applications of Cyclodextrins*; 2001; Vol. 40;.

Chapter 2

Hydrolysis protection of cyclodextrins to serine protease inhibitor nafamostat mesylate: proof of concept for a new administration method in drug repurposing for Covid-19

2.1 Introduction

Covid-19 pandemic has become a major global health emergency since 2020 and although to date vaccines are available to prevent it, there are remaining obstacles such as vaccine allocation in many countries and vaccine hesitancy [1] which make it still valuable to find more treatments to fight SARS-CoV-2, the virus responsible for the disease. In addition, as the virus keeps mutating into new variants [2,3] many people are still developing the disease, for that reason there is an ongoing number of research and clinical trials to find potential treatments [4]. SARS-Cov-2 viral entry into the cells is mediated by its spike (S) protein which binds to the ACE 2 cell receptor on the surface of target cells [5]. The S protein priming is done by the TMPRSS2 serine protease which allows the union of both the cell and viral membrane. In this sense, the use of serine protease inhibitors that can potentially hinder the TMPRSS2 activity to block viral entry into the cell are good candidates for developing treatments for Covid-19 [6].

Nafamostat mesylate (NM) is an FDA-approved serine protease inhibitor used in the treatment of acute pancreatitis and disseminated intravascular coagulation [7] [8] (Figure 2.1). The activity of several serine protease inhibitors such as camostat mesylate, gabexate mesylate and nafamostat mesylate have been tested in vitro against SARS-Cov-2. Recent research has proven the ability of NM to block more efficiently the SARS-Cov-2 infection of human lung cells respect to other serine protease inhibitors [9].

Furthermore, NM presented higher antiviral activity in comparison to camostat mesylate which makes it a promising drug for developing a new treatment against SARS-CoV-2 [9]. To date, there are four ongoing clinical trials to study the efficacy of NM to treat Covid-19 infection, and the method of administration of the drug is via continuous intravenous infusion [10]. However, NM is an ester drug that presents extensive hydrolysis in vivo since the enzymes responsible for the hydrolysis can be found in many places of the human body, being the main hydrolysis sites the blood and tissue such as liver or kidney [11].

We hypothesize that the use of cyclodextrins (CDs) could potentially protect NM from hydrolysis, possibly providing new administration alternatives for the drug besides the intravenous or by being an improvement for the intravenous formulation. As described in this thesis introduction, CDs are cyclic oligosaccharides formed by 6, 7 or 8 glucopyranose units (α, β,or γ–cyclodextrin respectively) with a cone-like shape that gives them supramolecular properties (Figure 2.1). CDs are very hydrophilic on their exterior while their inner cavity is an apolar microenvironment where hydrophobic moieties with the right size for the cavity can be encapsulated. They act forming non-covalent host-guest complexes with a great number of lipophilic molecules [12]. Native CDs can be chemically modified to produce different derivatives which can be non-anionic, cationic, anionic CDs, polymers, etc. These modifications can enhance the stability and selectivity of the formed host-guest ICs [13]. CDs affect the physicochemical properties of the guest molecules for example increasing their solubility, protecting them from degradation such as oxidation [14], visible or UV light[15], hiding flavours or odours [16], controlling the administration and release of drugs [17] and also protection against hydrolysis [18].

Sulfobutyl ether β-cyclodextrin (SBCD), commercially known as Captisol® is an anionic cyclodextrin with very high solubility in water and non-nephrotoxicity. It is an FDA approved excipient that is currently used in at least 4 commercial products as a drug carrier [19,20]. It has potential for pharmaceutical applications since anionic CDs can form stronger interactions with charged drug molecules, this adds up to the hydrophobic forces inside their cavity thus producing higher stability constants between the CD and the drug [21].

In this work we present for the first time the study of the complexation between the native β-CD and its derivatives hydroxypropyl β-CD (HPCD), a neutrally charged derivative, as well as the anionic derivatives sulfobutylether β-CD (SBCD) and succinyl β-CD (SUCCI), with the drug NM. We performed UV-Vis spectroscopic studies to calculate the stability constant of the all the inclusion complexes (ICs). Furthermore, ^{1}HNMR and 2D ROESY spectroscopy experiments confirmed the insertion of NM inside the CDs cavity. Docking and molecular dynamic simulations of the ICs showed the most stable molecular configuration. Drug hydrolysis kinetics in the presence of all the CDs were carried out to study the hydrolysis protection mechanism of CDs. Finally, we performed enzymatic assays to study the inhibition of the NM-CD complex versus NM using trypsin as a model serine protease in lieu of TMPRSS2 the serine protease that allows the fusion of SARS-Cov-2 and human cells membranes.

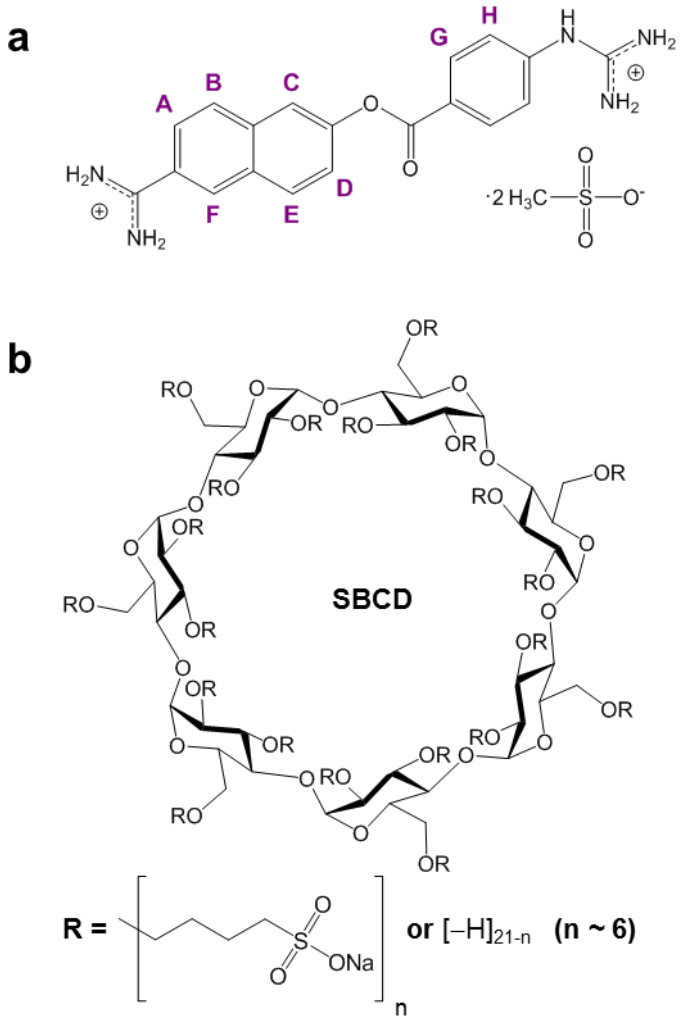

Figure 2.1. Molecular structures of NM showing atom labelling (a) and SBCD (b).

2.2 Materials and methods

Isothermal titration calorimetry was performed using a Microcal VP-ITC isothermal titration calorimeter (Microcal Inc., Northampton, MA). Absorption spectra data was collected using a Pharmacia Ultraspec 3000pro UV–Vis spectrophotometer using Hellma® 10 mm pathlength quartz cells. Nuclear magnetic resonance experiments were performed using a Varian NMR System 400. Particle size estimation was performed with a Malvern Panalytical Z-Sizer Nano. Milli-Q® 18.2 MΩ/cm water and analytical grade chemicals were used without further purification. Sulfobutyl β-cyclodextrin (SBCD) and Hydroxypropyl β-cyclodextrin (HPCD), were kindly gifted by Cyclolab Ltd (Hungary). Succinyl β-cyclodextrin >95% (SUCCI) as purchased from Sigma Aldrich/Merck. Nafamostat mesylate >98% was bought from TCI Chemicals Japan and used as received. Nα-Benzoyl-DL-Arginine-p-Nitroanilide (BAPNA) and bovine pancreatic trypsin (EC 232-650-8, ≥10000 units/mg) were purchased from Merck. pH 8 TRIS buffer was purchased at Merck and adjusted to pH 7.8 using 1 M hydrochloric acid solution. Deuterium oxide (D2O water) 99.9% atom was purchased from Sigma-Aldrich

Isothermal titration calorimetry (ITC)

Isothermal titration calorimetry was performed at 25°C and atmospheric pressure using a Microcal VP-ITC isothermal titration calorimeter (Microcal Inc., Northampton, MA). The ITC was calibrated electronically. The data were acquired by computer software provided by Calorimetry Sciences Corp and analyzed using the one-site model. NM-SBCD binding experiments were performed by injecting 10 µL aliquots with 240 s of separation of a SBCD solution (4 mM) into the sample cell containing NM solution (200 mM). All experiments were performed with constant stirring (200 rpm) driven by a

stepping motor coupled to the isothermal titration calorimeter. 20 mM pH 7.8 TRIS buffer was used to prepare the solutions and all the solutions were degassed before the titration experiment. We worked with concentrations bellow the critical aggregation concentration (cac) of the SBCD [22] to ensure that the measured enthalpy change corresponds to the complex formation without contributions from a simultaneous dissolution of the SBCD aggregates. In control experiments, 10 µL aliquots of a SBCD solution (4 mM) were injected into the sample cell containing pH 7.8 TRIS buffer without the serine protease inhibitor NM.

UV-Vis spectroscopic study

UV-spectroscopic titration experiments were executed to quantitatively study the equilibrium constant of the host-guest complex formed between the SBCD and NM by measuring the variation of absorbance at a fixed NM concentration in the presence of increasing concentrations of SBCD.

For the stock solutions, we prepared NM 0.741 mM and a mixture of NM+SBCD 0.741 mM + 7.41 mM, respectively. For the titrations, using a 1400 µL absorption cuvette, 1000 µL of a 14.5 μM NM solution was prepared from the stock in pH 7.8 TRIS buffer. After measuring the initial NM UV-absorbance, we added subsequent aliquots of NM+SBCD stock solution measuring each absorbance at increasing CD concentration.

Job Plot Experiments

Stock solutions containing equimolar concentrations of SBCD, and NM were prepared at a concentration of 0.741 mM. Afterwards, we prepared samples by mixing different volumes of SBCD with the NM in a way that the

total concentration of [SBCD]+[NM] remained constant and the molar fraction of the guest, X_{NM} varied from 0-1. Finally, we measured the absorbance of each sample for both sets of experiments.

H-NMR and ROESY experiments

^{1}H-NMR and 2D ^{1}H-^{1}H ROESY spectra were recorded in D_2O at 400 MHz in Varian NMR System 400 at 298 K using a 1:1 NM:CD molar ratio for each cyclodextrin (β-CD, HPCD, SUCCI or SBCD). All signals were referenced to internal HDO (4.79 ppm). The ROESY spectra were acquired with a mixing time of 400 ms and a relaxation delay of 1.8 s. Proton resonances of NM, the pure CDs and the inclusion complexes were assigned with the aid of standard COSY and HSQC experiments on the same solutions.

Molecular docking experiments

Structure preparation

Preparation of the structure and analysis were carried out with Maestro v 9.1, (Schrödinger LLC, New York, NY, 2010). The 3D structure of β-CD was retrieved from the Protein Data Bank. The SBCD isomer degree of substitution (DS) 6 was built with the Maestro Builder module. The glucopyranose units 1 and 5 (counted from n=1 in Figure 1) have a double substitution of the SBE side chains at C2 + C6 and C3 + C6 respectively. As for glucopyranose units 2 and 7 both have mono-substitutions of the SBE side chains at C6. We performed a Conformational Search in Maestro to find the energy minimized structure for the built SBCD isomer using a OPLS 3 force field [23] and water as solvent. For the NM ligand, the structure was retrieved from the Cambridge Crystallographic Data Centre (ID: HAMJAK, deposition number 2107852) and used for the docking studies [24].

Docking Studies

Docking of NM ligand inside the SBCD was done with Glide [25,26] to obtain free energies of binding. A grid for the host was generated using the center of mass of the SBCD to define the box where to dock the NM. For all docking simulations, rigid docking was applied, and Glide XP was used with the Extra Precision mode [27] which uses explicit water molecules for the docking to better emulate the displacement of high energy waters from the lipophilic cavities thus obtaining a more reliable docking score [28].

The SBCD used for the experimental part was a gift from Cyclolab Ltd. and has an average degree of substitution (DS) of 6 sulfobutyl ether chains, randomly substituted in the β-CD hydroxyl groups. The actual molecular configuration of the molecule is unknown and other groups have reported the building of isomers for in-silico docking tests [29,30].

Molecular Dynamics Experiments

We obtained free energies of binding for the inclusion complexes of NM and the β-CD and HPCDs using the molecular mechanics (MM) generalized Born (GB) and surface area (SA) continuum solvation model (MM/GBSA) [34] available in the AMBER program package [35]. The starting structures were obtained by manually placing the NM ligand inside the cavity of the β-CD and HPCD. Free energies of binding with SUCCI and SBCDs were not performed due to a lack of suitable parameters. The NM ligand was parametrized with the general amber force field (GAFF) [36]. The CDs were parametrized with the GLYCAM-06 force field [37]. The entire inclusion complex was solvated in a cubic box of TIP3P water [38]. The side of the box was at least 14 Å away from the inclusion complex. We first minimize the system with the conjugate gradient method for 1000 steps followed by slowly heating the system with

NVT from a temperature of T= 0 K to T= 300 K using Langevin dynamics [39] with a collision frequency of 2 ps^{-1}. This was followed by equilibrating the pressure in the NPT ensemble using a Berendsen barostat [40] keeping the pressure at 1 atm. After equilibration, a 100 ns production run was performed to obtain a trajectory and on completion of the simulation, the free energies of binding were computed using the MM/GBSA model.

Hydrolysis protection experiments

The kinetic experiments were designed to understand the effect of various amounts of SBCD in the hydrolysis of NM at different temperatures ranging from 30-45°C.

We prepared stock solutions0.74 mM of NM and 25 mM of SBCD. For the kinetic experiments, we monitored the spectral change in the NM UV-absorbance for 4 hours every 60 min and then after 24 hours. Using six 1400 μL absorption cuvettes, we prepared 1000 μL of a 148 mM NM solution for each cuvette in pH 7.8 TRIS buffer. After measuring the initial NM UV-absorbance, we added to five cuvettes different increasing amounts of the SBCD stock solution (0.5X SBCD, 1X SBCD, 2 X SBCD, 3X SBCD, and 4X SBCD), while one of the cuvettes was used as a control without SBCD. The experiments were performed in duplicate.

Enzymatic assay of bovine pancreatic trypsin inhibition by nafamostat mesylate

The continuous spectrophotometric rate determination method was used to study the inhibition of NM-SBCD complex in the reaction of trypsin digestion of Nα-Benzoyl-DL-Arginine-p-Nitroanilide hydrochloride (BAPNA) as a substrate at pH 7.8 (Equation 2.1). All enzymatic assays were performed at 25°C, and the absorbance of released p-nitroaniline was measured at 405 nm.

Tris buffer pH 8 was adjusted to pH 7.8 using HCl. 0.1% (w/v) BAPNA solution was prepared in Milli-Q® water, the solution was gently heated not exceeding 65°C to prevent chemical decomposition of the substrate. Immediately before use, a solution of 0.27mg/mL trypsin solution was prepared in cold (4°C) 1 mM HCl. 1 mM HCl solution was used as blank [31]. We prepared a stock 0.01 mM NM solution, a stock solution 0.1 mM of each CD and a stock containing a 1:10 NM:CD mixture of the complex e.g., 0.01 mM NM + 0.1 mM CD.

Enzymatic assays were performed (Table 2.1), by varying the NM concentrations from from 40 nM NM until 180 nM and ten times higher in the case of the SBCD from 400 nM NM until 1800 nM. For the inclusion complex solution, we respected the same concentrations and ratios as in the free moieties solutions.

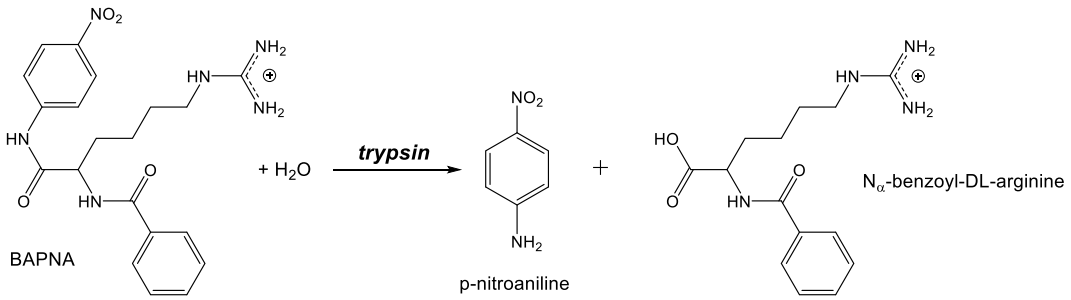

(1)

Table 1. *Preparation of the solutions for the enzymatic assay experiments*
Q corresponds to the amount of 4, 5, 6, 10, 14, 18 µL*

Enzymatic assay / **Solutions (µL)**	**a. Blank HCl assay**	**b. Uninhibited assay**	**c. NM solution assay**	**d. SBCD assay**	**e. SBCD-NM inclusion complex assay**
Tris buffer pH 7.8	600	600	600 - *Q**	600 - Q*	600 - Q*
HCl 1 mM	50	-	-	-	-
Trypsin in 1 mM HCl	-	50	50	50	50
NM in Tripsin pH 7.8	-	-	***Q****	-	-
SBCD solution	-	-	-	***Q****	-
SBCD + NM Inclusion complex	-	-	-	-	***Q****
BAPNA	350	350	350	350	350
Total volume	1000	1000	1000	1000	1000

2.3 Results and Discussion

UV-Vis spectroscopic study and stoichiometry determination

We performed UV-Vis spectroscopy titration experiments as an additional method to determine the equilibrium constant of the NM-SBCD host-guest complex. We measured the absorbance variation of the NM in the presence of different SBCD concentrations by consequently adding aliquots from a stock SBCD+NM solution.

It has been previously reported in the literature the importance of having a fixed guest concentration throughout these experiments to ensure that the spectral variations are due to the actual complexation of the guest inside the cyclodextrin cavity and not to dilution effects [32]. For this reason, the preparation of the stock solution of SBCD+NM was done from the NM stock in pH 7.8 Tris buffer and then directly dissolving the SBCD powder to obtain a concentration ten times bigger than the NM stock.

The results show that the initial UV absorbance of NM subsequently decreases when SBCD aliquots are added to the solution (Figure 1). This indicates the incorporation of the NM molecule inside de CD cavity. A dynamic equilibrium is formed between the NM and the SBCD which is also shown in the spectral observation with the formation of an isosbestic point at 273 nm [33].

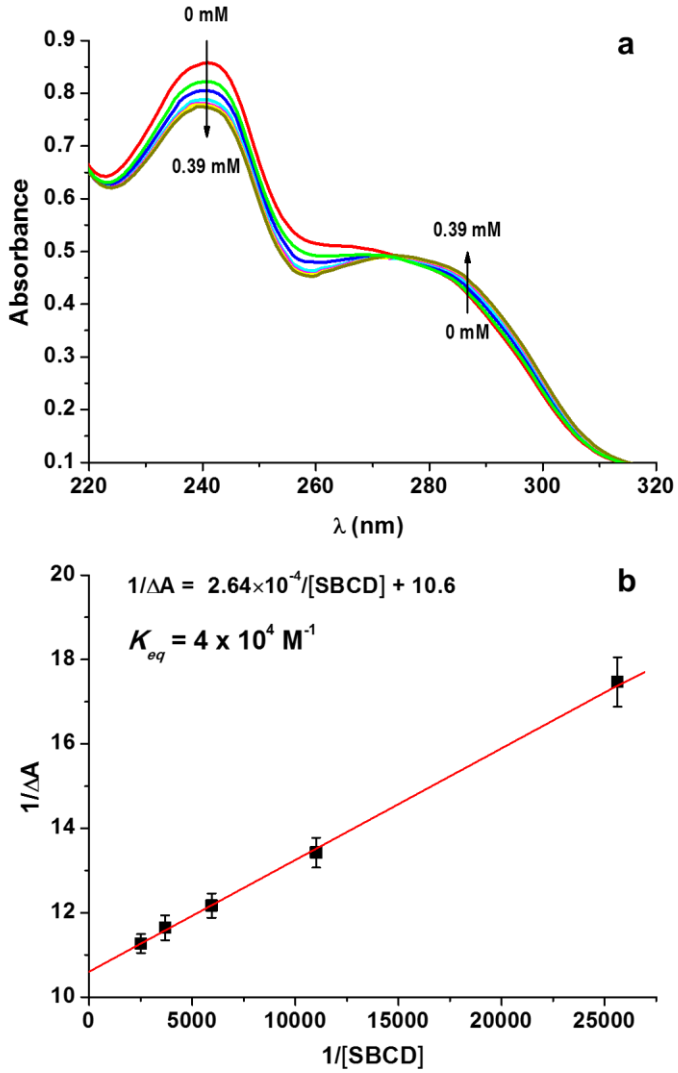

Figure 1 (a) *UV-Vis absorption spectra of NM in presence of increasing concentrations of SBCD* ***(b)*** *Linear regression for the K_{eq} calculation of the inclusion complex NM-SBCD*

In order to determine the stoichiometry of the complex, we performed the continuous variation method (Job's method). We plotted the variation of the absorbance of the guest in presence of the host $\Delta A * X_{NM}$ versus the molar

fraction of NM (X_{NM}). SBCD Job's plot shows a maximum deviation X_{NM} = 0.5 indicating the formation of a 1:1 complex CD:NM (Figure 2).

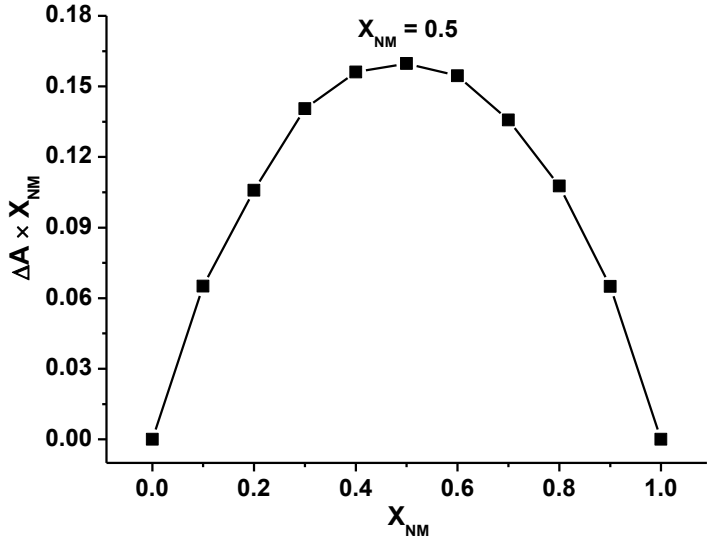

Figure 2. *Job plot for the NM- SBCD inclusion complex*

To calculate the equilibrium constants (K_{eq}), we linearized the absorbance data variation at the peak value spectra at 242 nm. Given that the stoichiometry of the complex was confirmed to be 1:1, we did a linear fit of the data by using the Benesi-Hildebrand (Equation 2) where the values of K_{eq} for the three systems were calculated by dividing the intercept by the slope of the linear regression. We obtained a strong binding value for the drug and anionic SBCD of $4x10^4$ M^{-1}.

$$\frac{1}{\Delta A} = \frac{1}{\Delta\varepsilon\,[NAFA]_0[CD]_0\,K_{eq}} + \frac{1}{\Delta\varepsilon[CD]_0} \qquad (2)$$

Isothermal titration calorimetry (ITC)

Isothermal titration calorimetry was performed at 25°C and atmospheric pressure using a Microcal VP-ITC isothermal titration calorimeter (Microcal Inc., Northampton, MA).

ITC allows to directly measure the differential heat of binding released or taken during the interaction of a binder and a ligand. From the obtained thermogram it is possible to characterize the stoichiometry of the complex N, the equilibrium constant K_{eq} and the enthalpy change ΔH. Additionally, the entropy change ΔS and Gibbs free energy ΔG can be deducted from the equation (Equation 3) [34].

$$\Delta G = RTlnK_{eq} = \Delta H - T\Delta S \quad (3)$$

The differential heat obtained in the ITC experiment depends on a dimensionless parameter c value that determines the shape of the binding isotherm [35]. The c value relates the total macromolecule concentration (in this case the CDs), relative to the ligand concentration and relative to the equilibrium constant Equation 4.

$$c = [CD]K_{eq} \quad (4)$$

The host-guest system that we study between the SBCD and the NM guest has a low affinity, if we compare it with systems with very high affinity constants such as interactions with ligands and proteins or enzymes, as can be seen from the obtained isotherms (Figure 3a) where the shape does not corresponds to a sigmoidal curve. c values between $1 < c < 1000$ are a good range for accurately estimating all the thermodynamic parameters [35]. Given that the c value depends on the concentration of the ligand and the binder, it is ideal that systems with lower K_{eq} work with higher concentrations to make sure that the

c value is located between the appropriate range. Nevertheless, in the case of working with systems that involve CDs it is important to have in mind that self-aggregation phenomenon start to occur at critical concentrations of 2% m/v for the SBCD [22,36] and this can lead to mistakes in the measurements of the differential heat of binding. This means that instead of measuring the differential heat that corresponds to the formation of a host-guest inclusion complex, the experimental value corresponds to the differential heat for the CDs aggregation. For our system, it was thus important to find a balance between the SBCD concentration and the obtained isotherm curve. We obtained a c value of 0.44 for our system. Nevertheless, this type of isotherm obtained in our experiment (Figure 3) is not uncommon for systems involving CDs [34][37][38]. Moreover, the obtained results for the K_{eq} were previously verified and are in complete agreement with the ones obtained in the spectroscopic studies and the stoichiometry of the complex had been determined to be 1:1 with the job plot experiment as previously discussed. A K_{eq} value of *3839 +/- 329* M^{-1} obtained with the ITC shows that the IC formed between the NM and the SBCD is stable. This K_{eq} value is also higher in comparison to the native □-CD and the derivative hydroxypropyl □-CD of 1100+/-68 M^{-1} and 800 +/-100 M^{-1} respectively. The free binding energy ΔG -20.46 kJ/mol also indicates a spontaneous process in the IC formation [39].

The thermodynamic parameters obtained are a result of the energy contributions that come from the expulsion of water molecules contained inside the SBCD cavity when the NM is complexed and the main driving forces in the binding process are hydrophobic and van der Waals interactions [39]. A large exothermic heat effect is given by the negative ΔH values which shows that van der Waals forces stabilize the IC in comparison to an also negative but much smaller ΔS values obtained, which represent the

hydrophobic interactions. Thus, we can say that the SBCD-NM IC is mostly enthalpy-driven but also presents entropic contributions.

Additionally, the sulfobutyl arms chemically attached through ether bonds to the native b-CD elongate the cavity and give an anionic character to the cyclodextrin. This could represent an additional favourable driving force (besides the already mentioned van der Waals and hydrophobic) to the IC since the sulfonic groups can form Coulomb interactions with the amino groups present in the SBCD.

Table 2. Stability constants (K_{eq}), standard changes of enthalpy (DH°), Gibbs binding energy (DG°) and entropy change (DS°) for the formation of complexes from the VTD guest with three CD hosts (g-CD, SBCD and b-CD) in aqueous TRIS buffer solution pH 6 and 298.2K

	K_{eq} [M^{-1}]	**DH° (kJ/mol)**	**DG° (kJ/mol)**	**DS° (kJ/mol)**
SBCD	3839± 329	-29.265± 4.76	-20.46± 0.2	-0.351± 0.19

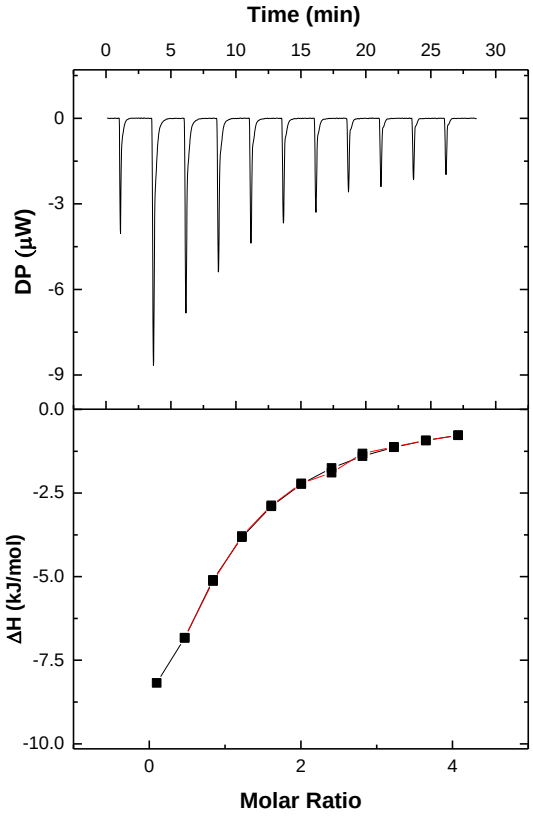

Figure 3. Isothermal titration calorimetry data obtained for the binding interaction of [200 mM] Nafamostat Mesylate with [4 mM] SBCD. The upper graph shows the variation of heat released upon injection of 10mL of each CD. The lower graph corresponds to the binding curve obtained from the integrated heat data.

H-NMR and ROESY experiments

Figure 5a shows the ^{1}H-NMR spectra of the aromatic protons of NM and its inclusion complex SBCD. As a general trend, all peaks of the NM:SBCD complex are strongly deshielded (displaced to higher frequencies) with respect to free NM, indicating inclusion in the CD cavity. The highest displacements correspond to protons C and D of the naphthalene group, and G and H of the benzene ring.

2D ^{1}H-^{1}H rotational Overhauser enhancement experiments (ROESY) provide information on the through-space proximity (typically 3-4 Å) of host protons and the guest parts. The appearance of cross-peaks is indicative of supramolecular complexation, and their intensities are proportional to the proximity of the protons involved.

Figure 5b presents the ROESY spectrum of the NM:SBCD inclusion complex in D_2O. It shows strong cross-peaks between protons G and H of NM, corresponding to the 4-guanidinobenzoic acid moiety, and H-3, H-5 and the OCH_2 group of SBCD. Another strong set of peaks is observed between these protons of SBCD and protons C and D of the naphthalene group of NM. These are the protons closer to the ester group and thus indicates that NM enters the cavity through the benzene ring. No interactions with the other sulfobutyl methylene groups were observed.

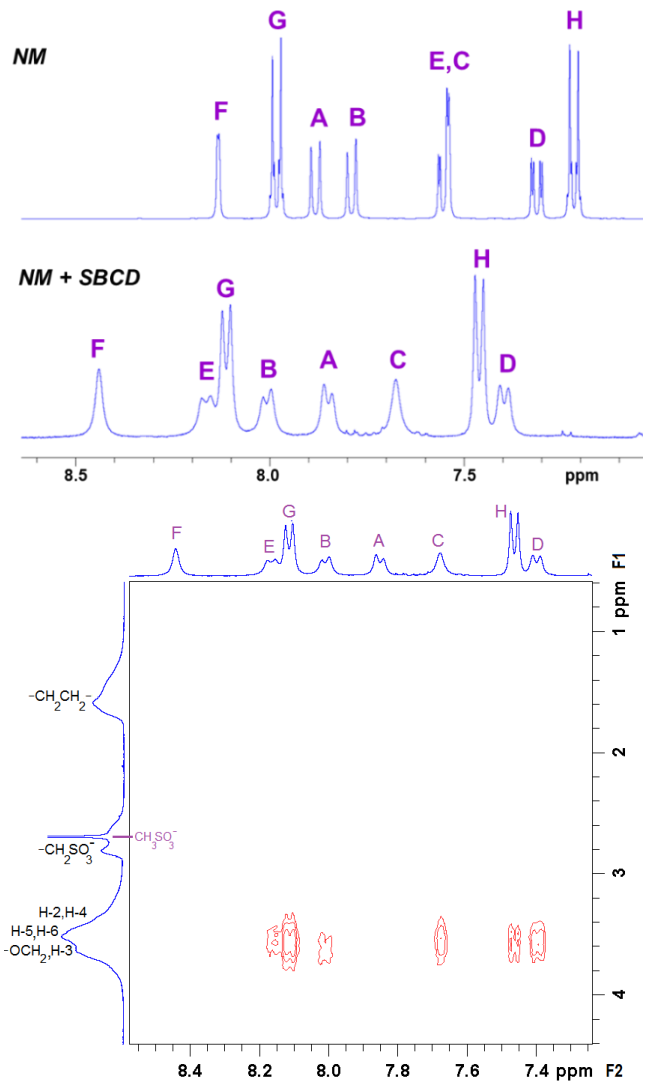

Figure 5. a) Aromatic region of the ^{1}H-NMR spectra (D_2O, 500 MHz, 298 K) of NM and NM:SBCD inclusion complex. b) 2D-ROESY NMR spectrum of NM:SBCD showing intermolecular cross-peaks. See Figure 1 for atom labelling.

Molecular simulations

We obtained a docking score value of -19.7 kJ/mol. From the results we can conclude that the SBCD is a potential binder for the NM molecule since there is an inclusion of the drug inside the lipophilic cavity of the SBCD. We can

say that this result is in agreement with the experimental results obtained with the UV-Vis spectroscopy and ITC where the K_{eq} obtained showed there is a good affinity between the SBCD and the NM. And the negative docking score value also indicates the process is spontaneous and more energetically favorable for the formation of the IC. From the 3D structure we can see that the best pose for the SBCD-NM complex (Figure 5 a & b) is one where the naphthalene part of the NM molecule is introduced inside the SBCD cavity. And the elongation of the cavity by the sulfobutyl arms creates extra space to better fit the rest of the NM molecule. Also, the nitrogen atoms of the NM potentially interact with the $SO3^-$ groups of the SBCD further stabilizing the NM molecule and the IC. The docking results are also in agreement with the 2D ROESY NMR experiments.

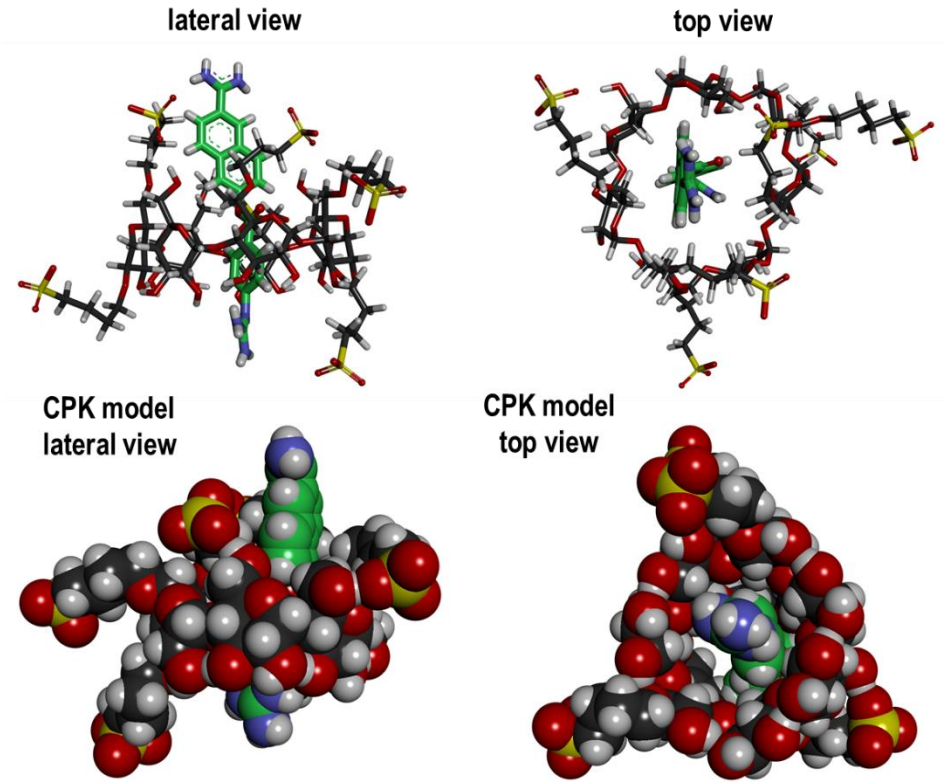

Figure 5. Three-dimensional energy minimized structures obtained by molecular docking of the inclusion complex between NM and SBCD. The C atoms of NM have been highlighted in green.

Hydrolysis kinetic experiments

In our kinetic experiments, we monitored the UV-absorbance of NM under three different variables: temperature, time, and the SBCD concentration. The UV-spectra obtained show a subsequent decrease in the l_{283nm} peak (Figure 6) that corresponds to the 4-guanidinobenzoate moiety. This is due to the hydrolysis of the ester group that binds together the naphthalene and 4-guanidinobenzoic acid moieties of NM, which produces the loss of the

conjugation of the pi orbitals between the 4-guanidinobenzoate and the ester group.

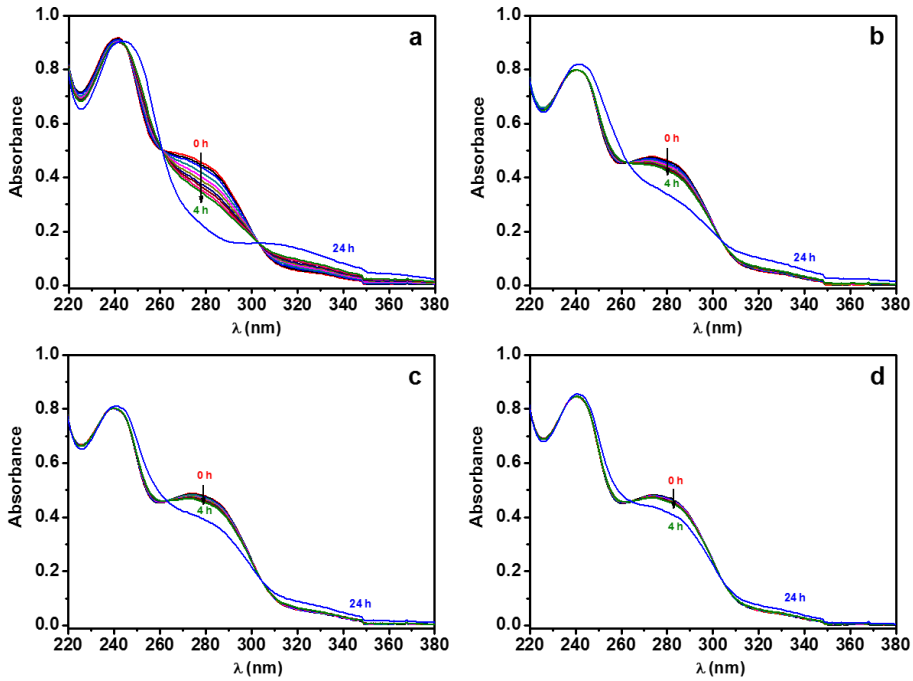

Figure 6. Different UV-Vis spectra of NM at 37°C and pH 7.8 showing the drug hydrolysis recorded at different times **(a)** without the addition of SBCD **(b)** 0.5X SBCD **(c)** 1X SBCD **(d)** 2X SBCD **(e)** 3X SBCD **(f)** 4X SBCD

To quantify these results, we calculated the drug hydrolysis percentage in respect to the absorbance value at the λ_{283nm} for the spectra corresponding to the NM without any addition of SBCD after 24hrs, where the drug was completely hydrolysed (Figure 7). By adding increasing amounts of SBCD the hydrolysis of NM is remarkably diminished and there is a concentration-dependent protective effect through time of the SBCD on the NM drug. Even with the lowest amount of 0.5X SBCD there is a hydrolysis-protection effect, decreasing the drug hydrolysis up to 82% after 4 hours and 40% after 24hrs. Moreover, for the highest

concentrations of 3X and 4X SBCD we obtained fairly similar results with the hydrolysis percentage decreasing up to 95% after 4 hours and up to 80% after 24 hours. These results are explained by the direct effect that SBCD has on the kinetics of the NM hydrolysis reaction (Figure 8) where higher concentrations of SBCD decrease the kinetic rate constant of the reaction (Table 3). The reaction fits a first order kinetic equation (Equation 5)

$$\ln[A] = -\kappa t + \ln[A]_0 \quad (5)$$

Where k is the kinetic rate constant that corresponds to the slope of the line, A is the absorbance value and t corresponds to the reaction time. By diminishing the hydrolysis rate, SBCD enhances the drug stability. The hydrolysis experiments were also performed at different temperatures obtaining similar results as for 37°C (See supplementary information).

The mechanism of the protective effect is explained by our previously discussed results that prove the insertion of the NM inside the SBCD cavity forming an inclusion complex with a high equilibrium constant.

Table 3. *Kinetic rate constant k for the first order kinetics of the hydrolysis reaction of NM in presence of different concentrations of SBCD*

SBCD	**0X**	**0.5X**	**1X**	**2X**	**3X**	**4X**
k	0.05452	0.02692	0.01681	0.0097	0.00672	0.00682

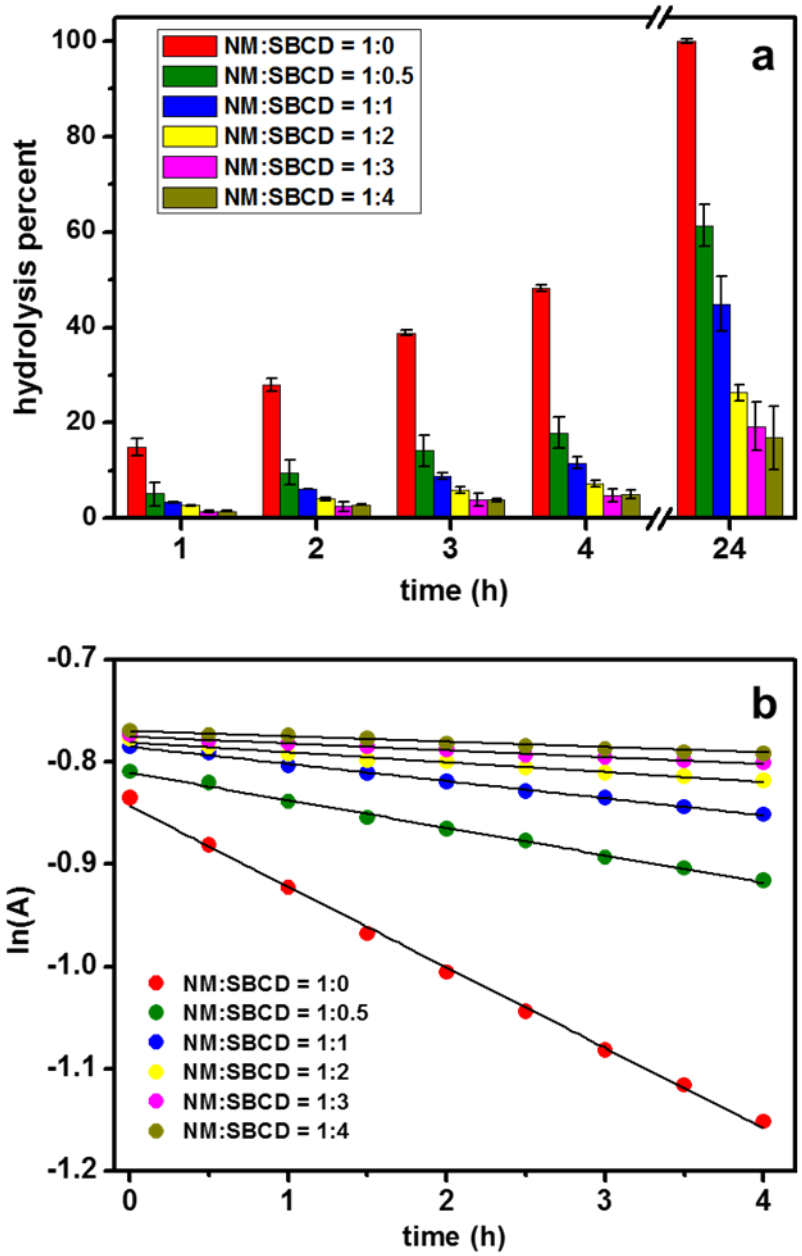

Figure 7. (a) Hydrolysis percentage and (b) ln(A) vs. time plot for the hydrolysis of NM (37°C, pH 7.8) in the absence and presence of SBCD at different molar ratios.

Effect of NM-CD complexation on trypsin inhibition by nafamostat mesylate

As we were able to prove with the previous results, NM forms inclusion complexes with the anionic SBCD. In order to further study the complex behavior, and its potential use in drug release and drug design for the Covid-19 or other diseases, it was important to check the appropriate release of NM from the SBCD cavity. We developed an enzymatic assay experiment using trypsin as a model serine protease in lieu of the SARS-Cov-2 TMPRSS2, since the last one is not commercially available. It has been demonstrated that trypsin is actually able to protolyze both SARS-CoV arginine R662 [40] and SARS-CoV-2 S1/S2 [41] active sites, and initiate the virus-cell fusion. For this reason, we consider our enzymatic assay a suitable proof-of-concept for the inhibition of TMPRSS2 by NM-SBCD inclusion complex.

The inhibition of trypsin enzyme was first compared using NM at different concentrations to inhibit the enzymatic reaction and afterwards the same enzymatic reactions were performed in the presence of the inclusion complexes of NM-SBCD at different concentrations. For both experiments, the concentrations of NM and NM+CD were varied from 40nM -180 nM NM. For the case of the inclusion complex, the NM:CD ratio was maintained in 1:10 for each concentration. These concentrations are in accordance with the ones presented in the literature to be sufficient to inhibit viral entry into cells both in vitro [42] and in an in vivo treatment for critically ill Covid-19 patients where the intravenous concentration of NM was maintained between 30-240 nM [43].

Since NM is a serine protease inhibitor, the results show an expected increase in the trypsin inhibition at increasing NM concentrations (Figure 9).

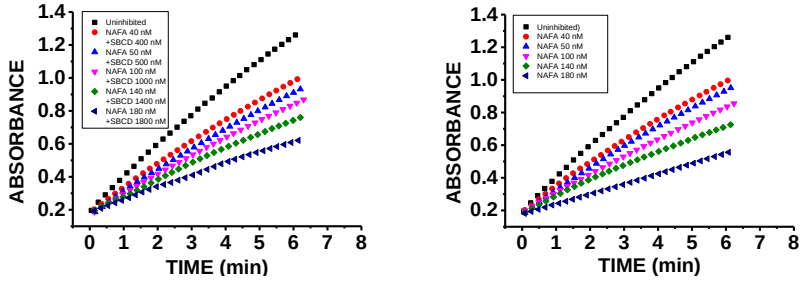

(a) **(b)**

Figure 9. Enzymatic assay for Trypsin inhibition by **(a)** Nafamostat Mesylate and SBCD inclusion complex at different concentrations and **(b)** Nafamostat Mesylate at different concentrations without SBCD

Moreover, the enzymatic assay carried out in the presence of the inclusion complex of NM-SBCD shows the same tendency, indicating that the NM is correctly released from the SBCD cavity in the presence of the serine protease enzyme. As studied by Ramjee et al, the mechanism of inhibition of NM has an initial noncovalent binding of NM with trypsin followed by the attack of the trypsin's serinyl nucleophile on the NM carbonyl group producing an acylation of the enzyme and cleaving the NM molecule in two products so that there is a covalent attachment of the 4-guanidinobenzoic acid product of NM to the serine protease [44]. NM release from the CDs cavity occurs possibly in a competitive way due to the higher affinity of NM to covalently react with the serine protease enzyme, thus displacing the equilibria of the complex and forcing the drug to abandon the CD cavity and binding to the enzyme's active site [45]. Additionally, we have proved that it is the naphthalene part of the NM the one that is more likely incorporated inside the SBCD cavity and the 4-guanidinobenzoate part lies outside the cavity stabilized by the sulfobutyl arms and thus this part of the molecule could be more available to react with the enzyme. Control experiments were performed using only the SBCD at the same concentrations as in the inclusion complex experiment and we observed

the enzymatic reaction also proceeded but with some inhibition at higher concentrations of SBCD but not at the same rate as with the NM or the NM-SBCD IC (see supplementary information).

2.4 Conclusions

In conclusion, we have successfully proved the formation of an inclusion complex between the serine protease inhibitor NM and the anionic b-cyclodextrin derivative SBCD. The equilibrium constant was estimated to be 3839± 329 M^{-1} both with ITC and UV-spectroscopic techniques. This K_{eq} is higher than the ones previously reported by our group with b-CD and the derivative hydroxypropyl b-CD. H NMR and ROESY experiments confirmed the incorporation of NM in the SBCD cavity and the most stable orientation of the NM molecule inside the host was elucidated performing docking experiments. NM hydrolysis kinetic in the presence of SBCD confirmed the protection mechanism against hydrolysis in a concentration-dependent manner. Finally, enzymatic assays showed that the inclusion complex of NM-SBCD correctly inhibits the reaction of trypsin as a model enzyme thus gaining a next step in further pharmaceutical research for new administration ways for NM. To the best of our knowledge this is the first study of the interactions between NM drug and SBCD and opens the door to further study the pharmaceutical applications of this supramolecular system. Further in vitro studies of the NM-CD complex should be done in order to assess the correct blocking of the SARS-CoV-2 viral entry inside cells.

2.5 References

1. Contreras, S.; Olivera-Nappa, Á.; Priesemann, V. Rethinking COVID-19 vaccine allocation: it is time to care about our neighbours. *Lancet Reg. Heal. - Eur.* **2022**, *12*, 1–2, doi:10.1016/j.lanepe.2021.100277.

2. Hebbani, A.V.; Pulakuntla, S.; Pannuru, P.; Aramgam, S.; Badri, K.R.; Reddy, V.D. COVID-19: comprehensive review on mutations and current vaccines. *Arch. Microbiol.* **2022**, *204*, 1–17, doi:10.1007/s00203-021-02606-x.

3. Wang, R.; Chen, J.; Gao, K.; Wei, G.W. Vaccine-escape and fast-growing mutations in the United Kingdom, the United States, Singapore, Spain, India, and other COVID-19-devastated countries. *Genomics* **2021**, *113*, 2158–2170, doi:10.1016/j.ygeno.2021.05.006.

4. Search of: Covid19 - List Results - ClinicalTrials.gov Available online: https://clinicaltrials.gov/ct2/results?cond=Covid19&term=&cntry=&state=&city=&dist= (accessed on Sep 22, 2020).

5. Shang, J.; Ye, G.; Shi, K.; Wan, Y.; Luo, C.; Aihara, H.; Geng, Q.; Auerbach, A.; Li, F. Structural basis of receptor recognition by SARS-CoV-2. *Nature* **2020**, *581*, doi:10.1038/s41586-020-2179-y.

6. Hoffmann, M.; Kleine-Weber, H.; Schroeder, S.; Mü, M.A.; Drosten, C.; Pö, S. SARS-CoV-2 Cell Entry Depends on ACE2 and TMPRSS2 and Is Blocked by a Clinically Proven Protease Inhibitor. *Cell* **2020**, *181*, 271-280.e8, doi:10.1016/j.cell.2020.02.052.

7. IWAKI, M.; INO, Y.; MOTOYOSHI, A.; OZEKI, M.; SATO, T.; KURUMI, M.; AOYAMA, T. Pharmacological studies of FUT-175, nafamostat mesilate. V. Effects on the pancreatic enzymes and experimental acute pancreatitis in rats. *Jpn. J. Pharmacol.* **1986**, *41*, 155–162, doi:10.1254/jjp.41.155.

8. Akizawa, T.; Koshikawa, S.; Ota, K.; Kazama, M.; Mimura, N.; Hirasawa, Y. Nafamostat Mesilate: A Regional Anticoagulant for

Hemodialysis in Patients at High Risk for Bleeding. *Nephron* **1993**, *64*, 376–381, doi:10.1159/000187357.

9. Hoffmann, M.; Schroeder, S.; Kleine-Weber, H.; Müller, M.A.; Drosten, C.; Pöhlmann, S. Nafamostat Mesylate Blocks Activation of SARS-CoV-2: New Treatment Option for COVID-19. **2020**, doi:10.1128/AAC.00754-20.

10. Search of: nafamostat | Covid19 - List Results - ClinicalTrials.gov Available online: https://clinicaltrials.gov/ct2/results?cond=Covid19&term=nafamostat+&cntry=&state=&city=&dist= (accessed on Sep 22, 2020).

11. Yan-Guang CAO; Yuan-Cheng CHEN; Kun HAO; Ming ZHANG; Xiao-Quan LIU An in Vivo Approach for Globally Estimating the Drug Flow between Blood and Tissue for Nafamostat Mesilate: the Main Hydrolysis Site Determination in Human Available online: https://www.jstage.jst.go.jp/article/bpb/31/11/31_11_1985/_pdf/-char/ja (accessed on Jun 21, 2021).

12. Del Valle, E.M.M. Cyclodextrins and their uses: A review. *Process Biochem.* **2004**, *39*, 1033–1046, doi:10.1016/S0032-9592(03)00258-9.

13. Szente, L.; Szejtli, J. Highly soluble cyclodextrin derivatives: chemistry, properties, and trends in development. *Adv. Drug Deliv. Rev.* **1999**, *36*, 17–28.

14. Kfoury, M.; Landy, D.; Ruellan, S.; Auezova, L.; Greige-Gerges, H.; Fourmentin, S. Determination of formation constants and structural characterization of cyclodextrin inclusion complexes with two phenolic isomers: carvacrol and thymol. *Beilstein J. Org. Chem* **2016**, *12*, 29–42, doi:10.3762/bjoc.12.5.

15. Brewster, M.E.; Loftsson, T.; Estes, K.S.; Lin, J.L.; Fridriksdóttir, H.; Bodor, N. Effect of various cyclodextrins on solution stability and dissolution rate of doxorubicin hydrochloride. *Int. J. Pharm.* **1992**, *79*, 289–299, doi:10.1016/0378-5173(92)90121-H.

16. Astray, G.; Gonzalez-Barreiro, C.; Mejuto, J.C.; Rial-Otero, R.; Simal-Gándara, J. A review on the use of cyclodextrins in foods. *Food Hydrocoll.* **2009**, *23*, 1631–1640, doi:10.1016/j.foodhyd.2009.01.001.

17. Loftsson, T.; Duchêne, D. Historical Perspectives Cyclodextrins and their pharmaceutical applications. *Int. J. Pharm.* **2007**, *329*, 1–11, doi:10.1016/j.ijpharm.2006.10.044.

18. Iglesias, E. Ester Hydrolysis and Enol Nitrosation Reactions of Ethyl Cyclohexanone-2-carboxylate Inhibited by-Cyclodextrin. **2000**, doi:10.1021/jo0007231.

19. Loftsson, T.; Duchêne, D. Historical Perspectives Cyclodextrins and their pharmaceutical applications. *Int. J. Pharm.* **2007**, *329*, 1–11, doi:10.1016/j.ijpharm.2006.10.044.

20. Stella, V.J.; Rajewski, R.A. Sulfobutylether-β-cyclodextrin. **2020**, doi:10.1016/j.ijpharm.2020.119396.

21. Mavridis, I.M.; Yannakopoulou, K. Mini review Anionic cyclodextrins as versatile hosts for pharmaceutical nanotechnology: Synthesis, drug delivery, enantioselectivity, contrast agents for MRI. **2015**, doi:10.1016/j.ijpharm.2015.06.004.

22. Do, T.T.; Van Hooghten, R.; Van den Mooter, G. A study of the aggregation of cyclodextrins: Determination of the critical aggregation concentration, size of aggregates and thermodynamics using

isodesmic and K2–K models. *Int. J. Pharm.* **2017**, *521*, 318–326, doi:10.1016/j.ijpharm.2017.02.037.

23. Harder, E.; Damm, W.; Maple, J.; Wu, C.; Reboul, M.; Yu Xiang, J.; Wang, L.; Lupyan, D.; K. Dahlgren, M.; L. Knight, J.; et al. OPLS3: A Force Field Providing Broad Coverage of Drug-like Small Molecules and Proteins. *J. Chem. Theory Comput.* **2015**, *12*, 281–296, doi:10.1021/acs.jctc.5b00864.

24. Fujii, I. Crystal structure of nafamostat dimesylate. *Acta Crystallogr. Sect. E Crystallogr. Commun.* **2021**, *77*, 999–1002, doi:10.1107/S2056989021009245.

25. A. Friesner, R.; L. Banks, J.; B. Murphy, R.; A. Halgren, T.; J. Klicic, J.; T. Mainz, D.; P. Repasky, M.; H. Knoll, E.; Shelley, M.; K. Perry, J.; et al. Glide: A New Approach for Rapid, Accurate Docking and Scoring. 1. Method and Assessment of Docking Accuracy. *J. Med. Chem.* **2004**, *47*, 1739–1749, doi:10.1021/jm0306430.

26. A. Halgren, T.; B. Murphy, R.; A. Friesner, R.; S. Beard, H.; L. Frye, L.; Thomas Pollard, W.; L. Banks, J. Glide: A New Approach for Rapid, Accurate Docking and Scoring. 2. Enrichment Factors in Database Screening. *J. Med. Chem.* **2004**, *47*, 1750–1759, doi:10.1021/jm030644s.

27. A. Friesner, R.; B. Murphy, R.; P. Repasky, M.; L. Frye, L.; R. Greenwood, J.; A. Halgren, T.; C. Sanschagrin, P.; T. Mainz, D. Extra Precision Glide: Docking and Scoring Incorporating a Model of Hydrophobic Enclosure for Protein−Ligand Complexes. *J. Med. Chem.* **2006**, *49*, 6177–6196, doi:10.1021/jm051256o.

28. Pantsar, T.; Poso, A. Binding affinity via docking: Fact and fiction.

Molecules **2018**, *23*, 1899, doi:10.3390/molecules23081899.

29. Jain, A.S.; Date, A.A.; Pissurlenkar, R.R.S.; Coutinho, E.C.; Nagarsenker, M.S. Sulfobutyl Ether7 β-Cyclodextrin (SBE7 β-CD) Carbamazepine Complex: Preparation, Characterization, Molecular Modeling, and Evaluation of In Vivo Anti-epileptic Activity. *AAPS PharmSciTech* **2011**, *12*, 1163–1175, doi:10.1208/s12249-011-9685-z.

30. Shityakov, S.; Puskás, I.; Pápai, K.; Salvador, E.; Roewer, N.; Förster, C.; Broscheit, J.A. Sevoflurane-sulfobutylether-β-cyclodextrin complex: Preparation, characterization, cellular toxicity, molecular modeling and blood-brain barrier transport studies. *Molecules* **2015**, *20*, 10264–10279, doi:10.3390/molecules200610264.

31. Enzymatic Assay of Aprotinin | Sigma-Aldrich Available online: https://www.sigmaaldrich.com/technical-documents/protocols/biology/enzymatic-assay-of-aprotinin.html (accessed on Sep 24, 2020).

32. Landy, D.; Fourmentin, S.; Salome, M.; Surpateanu, G. Analytical Improvement in Measuring Formation Constants of Inclusion Complexes between β-Cyclodextrin and Phenolic Compounds. *J. Incl. Phenom. Macrocycl. Chem.* **2000**, *38*, 187–198.

33. Tablet, C.; Matei, I.; Hillebr, M. The Determination of the Stoichiometry of Cyclodextrin Inclusion Complexes by Spectral Methods: Possibilities and Limitations. *Stoichiom. Res. - Importance Quant. Biomed.* **2012**, doi:10.5772/34287.

34. Waldvogel, S. *Book Review Cyclodextrins and Their Complexes: Chemistry, Analytical Methods, Applications (Helena Dodziuk, Ed.)*; 2007; Vol. 2007; ISBN 9783527312801.

35. Wiseman, T.; Williston, S.; Brandts, J.F.; Lin, L.N. Rapid measurement of binding constants and heats of binding using a new titration calorimeter. *Anal. Biochem.* **1989**, *179*, 131–137, doi:10.1016/0003-2697(89)90213-3.

36. Loftsson, T.; Saokham, P.; Sá Couto, A.R. Self-association of cyclodextrins and cyclodextrin complexes in aqueous solutions. *Int. J. Pharm.* **2019**, *560*, 228–234, doi:10.1016/j.ijpharm.2019.02.004.

37. Zheng, P.J.; Wang, C.; Hu, X.; Tam, K.C.; Li, L. Supramolecular complexes of azocellulose and α-cyclodextrin: Isothermal titration calorimetric and spectroscopic studies. *Macromolecules* **2005**, *38*, 2859–2864, doi:10.1021/ma0483241.

38. Sun, D.Z.; Li, L.; Qiu, X.M.; Liu, F.; Yin, B.L. Isothermal titration calorimetry and 1H NMR studies on host-guest interaction of paeonol and two of its isomers with β-cyclodextrin. *Int. J. Pharm.* **2006**, *316*, 7–13, doi:10.1016/j.ijpharm.2006.02.020.

39. Bouchemal, K.; Mazzaferro, S. How to conduct and interpret ITC experiments accurately for cyclodextrin-guest interactions. *Drug Discov. Today* **2012**, *17*, 623–629, doi:10.1016/j.drudis.2012.01.023.

40. Simmons, G.; Bertram, S.; Glowacka, I.; Steffen, I.; Chaipan, C.; Agudelo, J.; Lu, K.; Rennekamp, A.J.; Hofmann, H.; Bates, P.; et al. Different host cell proteases activate the SARS-coronavirus spike-protein for cell-cell and virus-cell fusion. **2011**, doi:10.1016/j.virol.2011.02.020.

41. Jaimes, J.A.; Millet, J.K.; Whittaker, G.R. Proteolytic Cleavage of the SARS-CoV-2 Spike Protein and the Role of the Novel S1/S2 Site., doi:10.1016/j.isci.2020.101212.

42. Yamamoto, M.; Kiso, M.; Sakai-Tagawa, Y.; Iwatsuki-Horimoto, K.; Imai, M.; Takeda, M.; Kinoshita, N.; Ohmagari, N.; Gohda, J.; Semba, K.; et al. The Anticoagulant Nafamostat Potently Inhibits SARS-CoV-2 S Protein-Mediated Fusion in a Cell Fusion Assay System and Viral Infection In Vitro in a Cell-Type-Dependent Manner. *Viruses* **2020**, *12*, 629, doi:10.3390/v12060629.

43. Doi, K.; Ikeda, M.; Hayase, N.; Moriya, K.; Morimura, N.; Maehara, H.; Tagami, S.; Fukushima, K.; Misawa, N.; Inoue, Y.; et al. Nafamostat mesylate treatment in combination with favipiravir for patients critically ill with Covid-19: a case series. *Crit. Care* **2020**, *24*, 392, doi:10.1186/s13054-020-03078-z.

44. Ramjee, M.K.; Henderson, I.M.J.; Mcloughlin, S.B.; Padova, A. *The Kinetic and Structural Characterization of the Reaction of Nafamostat with Bovine Pancreatic Trypsin*; 2000; Vol. 98;.

45. Stella, V.J.; he, Q. Cyclodextrins. *Toxicol. Pathol.* **2008**, *36*, 30–42, doi:10.1177/0192623307310945.

Chapter 3

Supramolecular Complexes of Plant Neurotoxin Veratridine with Cyclodextrins and their Antidote-Like Effect on Neuro-2a Cell Viability[1]

3.1. Introduction

Veratridine (VTD) is a lipid-soluble alkaloid neurotoxin derived from *Veratrum* plants, which belong to the lily family. It has been used in the past as a drug against arterial hypertension although its pharmacological use was stopped due to secondary effects of intoxication. Nowadays, VTD is used as a research tool given that it acts by targeting the voltage-gated sodium channels (VGSCs) of cell membranes, thus producing a persistent Na^+ current and increasing intracellular Na^+ concentration [1]. An important use of VTD in research is enhancing the specificity of neuroblastoma (Neuro-2a) cell-based assays (CBAs) used for the detection, evaluation of toxicity and study of mechanisms of VGSC toxins [2]. VGSCs transmit action potentials in neurons, skeletal muscles, and cardiac cells. Unsurprisingly, the alteration in VGSC caused by VTD produces symptoms such as intense retching, bradycardia, hypotension, arrhythmia, loss of consciousness, and seizure. The treatment for VTD poisoning is mainly focused on relieving the symptoms using drugs such as atropine, dopamine, and diazepam [3,4]. Additionally, activated charcoal is used to remove the unabsorbed excess of alkaloids [5]. Nevertheless, there is currently no specific antidote that targets the toxin molecule itself.

On the other hand, cyclodextrins (CDs) are cyclic oligosaccharides formed by 6, 7 or 8 glucopyranose units (α, β or γ-cyclodextrin, respectively) forming a truncated cone-like shape that gives them the ability to form host-guest inclusion complexes (ICs). CDs possess a hydrophilic exterior because

of the hydroxyl groups that lie in their outer rims. In their inner cavity, the C-H and ether-bond glycosidic oxygens generate an apolar microenvironment where hydrophobic moieties with the right size for the cavity can be encapsulated. Thus, CDs form non-covalent host-guest complexes with a great number of lipophilic molecules [6]. Native CDs can be chemically modified to produce different derivatives such as cationic or anionic CDs, bridged CDs, polymers, etc. These modifications can enhance the stability and selectivity of the formed host-guest ICs [7]. The encapsulation of guests inside the CD cavities changes the physicochemical properties of the guest molecules resulting, for example, in an increase in their solubility [8], protection from oxidation [9], visible or UV light degradation [10], hiding flavors or odors [11], and controlling the administration and release of drugs. Their applications include biotechnology [12], environmental [13] and pharmaceutical industries [14], among many others.

A promising and ever-growing application for CDs is as supramolecular antidotes against toxins. There is research regarding the complexation of CDs with several mycotoxins like alternariol [15], ochratoxin A [16], aflatoxins [17], citrinin [18,19] and zearalenone [20], as well as with some neurotoxins like the rodenticide tetramethylenedisulfotetramine [21] and the insecticide paraoxon [22]. Nevertheless, there is still a lot of room for studying the interactions and applications of CDs with many other neurotoxin molecules that target the VGSC. For example, those that are produced by plants and animals such as VTD, aconitine, grayanotoxins and batrachotoxin, which are small lipid-soluble toxins; or marine toxins produced by algae such as okadaic acid, ciguatoxin and brevetoxin which are cyclic polyethers [23].

In this work, we studied for the first time the complexation between native β and γ-cyclodextrin (β–CD and γ-CD) and the anionic derivative

sulfobutyl β-cyclodextrin (SBCD) with the neurotoxin VTD (Fig. 1). We performed isothermal titration calorimetry (ITC) studies of the interaction of with β-CD, γ-CD and SBCD to estimate thermodynamic parameters and the stability constant of the complex in the different CDs. Furthermore, we characterized and confirmed the insertion of VTD inside the CDs cavity using 1D and 2D nuclear magnetic resonance (NMR). A docking and molecular dynamic study confirmed the best CD binders and the most energy stable configuration for the inclusion complex. Finally, with an interest in understanding the effects of the VTD-CDs inclusion complexes, we evaluated their toxicity with a cell-based assay (CBA) on Neuro-2a cells.

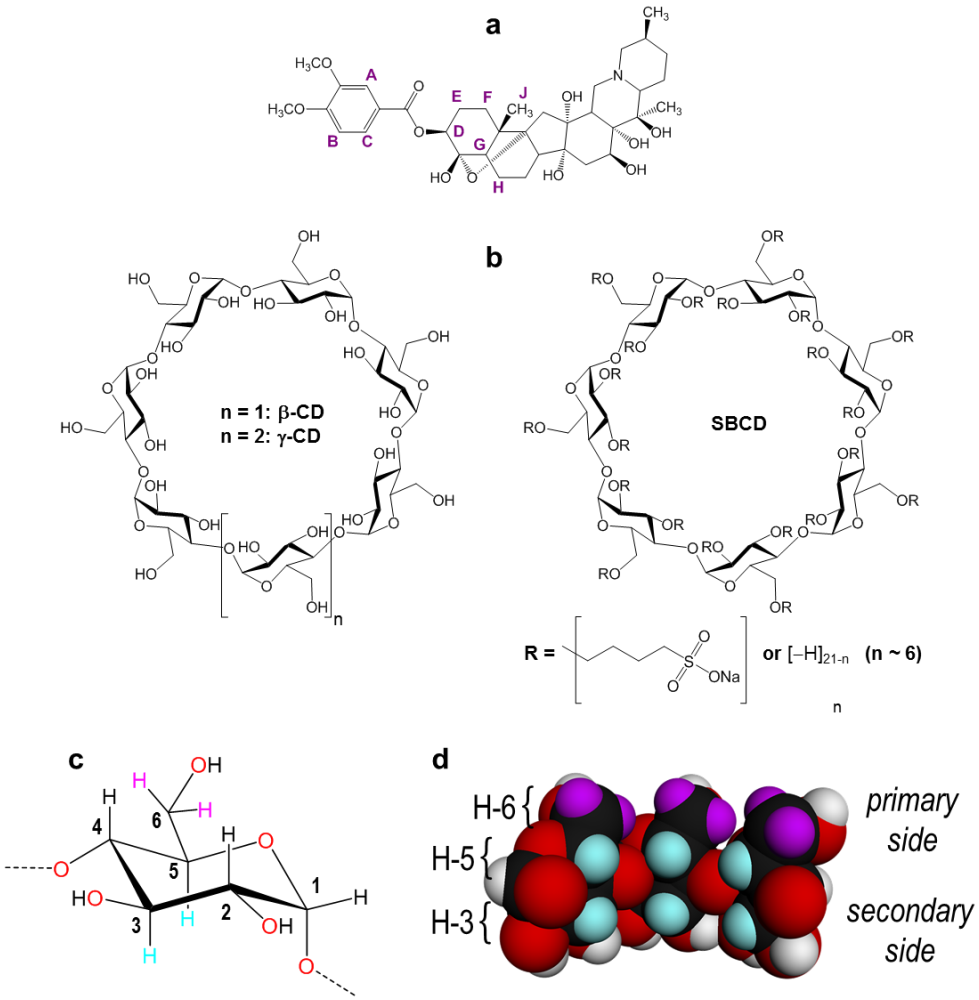

Figure 3.1. (**a**) Structure of VTD showing atom labelling. (**b**) Structure of the cyclodextrin hosts used in this work. (c) Atom labelling of the glucopyranose ring. (d) Cross-section view from inside the β-CD cavity showing the H-3 and H-5 rims (cyan) and the H-6 atoms located on the border of the primary side (violet).

3.2. Materials and Methods

All reagents used were of analytical grade and used without further purification. β-CD and γ-CD were obtained from Wacker Chemie AG (Germany). Sulfobutyl β-cyclodextrin was a gift from Cyclolab Ltd. (Hungary). Veratridine (>90% HPLC), D_2O (99.99% D) and DCl (35%, 99.9% D) were purchased from Sigma Aldrich. pH 6 buffer was prepared using Tris base from Sigma Aldrich and the pH was adjusted using 1 M HCl. At this pH concentrated stock solutions of VTD could be prepared without solubility limitations. The Neuro-2a cell line was obtained from American Tissue Culture Collection (ATCC), batch CCL131.

3.2.1. Isothermal Titration Calorimetry

ITC was performed using a Microcal VP-ITC isothermal titration calorimeter (Microcal Inc., Northampton, MA) at 298.2 K and atmospheric pressure. The instrument was calibrated electronically. The data were acquired with a computer software provided by Calorimetry Sciences Corp and analyzed using the one-site model. VTD/CD binding experiments were performed by injecting 10 µL aliquots with 240 s of separation of a CD solution (4 mM) into the sample cell containing VTD solution (200 µM). All experiments were performed with constant stirring (200 rpm) driven by a stepping motor coupled to the isothermal titration calorimeter. 20 mM pH 6 Tris buffer was used to prepare the solutions and all the solutions were degassed before the titration experiment. The CD concentrations for the experiment were chosen in order to work bellow the critical aggregation concentration (cac) of each CD [24,25] to ensure that the measured enthalpy change represents the complex formation without contributions from a simultaneous dissolution of the CD aggregates. In control experiments, 10 µL

aliquots of a CD solution (4 mM) were injected into the sample cell containing Tris buffer without the VTD toxin.

3.2.2. NMR Spectroscopy

^{1}H-NMR and 2D ^{1}H-^{1}H ROESY spectra were recorded in D_2O containing DCl 0.1% (v/v) at 400 MHz in Varian NMR System 400 at 298 K using a 1:1 VTD:CD molar ratio for each cyclodextrin (β-CD, γ-CD or SBCD). All signals were referenced to internal HDO (4.79 ppm). The ROESY spectra were acquired with a mixing time of 400 ms and a relaxation delay of 1.8 s. Proton resonances of VTD, the pure CDs and the inclusion complexes were assigned with the aid of standard COSY and HSQC experiments on the same solutions.

3.2.3. Molecular Simulation

3.2.3.1 Structure Preparation

Preparation of the structure and analysis were carried out with Maestro v 9.1, (Schrödinger LLC, New York, NY, 2010). The 3D structures of β-CD and γ-CD were retrieved from the Protein Data Bank. SBCD used has an average degree of substitution of ~6 sulfobutyl ether chains, as determined by ^{1}H-NMR, which are randomly substituted in the β-CD hydroxyl groups. The actual molecular configuration of the molecule is unknown and other groups have reported the building of isomers for in-silico docking tests [26,27]. The SBCD isomer used here was built with the Maestro Builder module. The glucopyranose units 1 and 5 (counted from n = 1 in Figure 1b) have a double substitution of the SBE side chains at C-2 + C-6 and C-3 + C-6 respectively. As for glucopyranose units 2 and 7, both have mono-substitutions of the SBE side chains at C-6. We performed a Conformational Search in Maestro to find the energy minimized structure for the built SBCD isomer using a OPLS 3

force field [28] and water as solvent. For the VTD ligand, the structure was retrieved from the Cambridge Crystallographic Data Centre (ID: BUWMIP, deposition number 1117590) and used for the docking studies [29] .

3.2.3.2. Docking Studies

We used docking of VTD into the three CDs with Glide [30,31] to obtain free energies of binding. A grid for each host was generated with the center of mass of each CD used to define the box where to dock the VTD. For all docking simulations, rigid docking was applied and Glide XP was used with the Extra Precision mode [32] which uses explicit water molecules for the docking. This simulates better the displacement of high energy waters from the lipophilic cavities thus obtaining more reliable docking scores [33].

3.2.3.3. Molecular Dynamics Experiments

We obtained free energies of binding for the inclusion complexes of VTD and the CDs using the molecular mechanics (MM) generalized Born (GB) and surface area (SA) continuum solvation model (MM/GBSA) [34] available in the AMBER program package [35]. The starting structures were obtained by manually placing the VTD ligand inside the cavity of the β-CD and γ-CD. Free energies of binding with SBCDs were not performed due to a lack of suitable parameters. The VTD ligand was parametrized with the general amber force field (GAFF) [36]. The CDs were parametrized with the GLYCAM-06 force field [37]. The entire inclusion complex was solvated in a cubic box of TIP3P water [38]. The side of the box was at least 14 Å away from the inclusion complex. We first minimize the system with the conjugate gradient method for 1000 steps followed by slowly heating the system with NVT from a temperature of T= 0 K to T= 300 K using Langevin dynamics [39] with a collision frequency of 2 ps^{-1}. This was followed by equilibrating

the pressure in the NPT ensemble using a Berendsen barostat [40] keeping the pressure at 1 atm. After equilibration, a 100 ns production run was performed to obtain a trajectory and on completion of the simulation, the free energies of binding were computed using the MM/GBSA model.

3.2.4. Neuro-2a Cell Viability Experiments

Neuro-2a cells (ATCC, CCL131) were maintained in 10% fetal bovine serum (FBS) RPMI medium (Sigma-Aldrich, St. Louis, MO, USA) at 310 K in a 5% CO_2 humidified atmosphere (Binder, Tuttlingen, Germany) [41]. For the experiments, cells were cultured in a 96-well microplate in 5% FBS RPMI medium at an approximate density of 34,000 cells per well for 24 h. A stock solution of VTD (1 mM) was prepared in MilliQ® water and adjusted to pH 2 for solubilization. Stock solutions of CDs (50 mM β-CD, 200 mM γ-CD and 200 mM SBCD) were prepared in PBS. Prior to exposure to VTD and CDs, a half of the microplate was treated with 0.4 mM ouabain (OB, Sigma-Aldrich). Then, 10 μL of VTD and 10 μL of CDs at different concentrations were added into the wells with and without the OB treatment (as a control to evaluate CDs toxicity) and incubated for 24 h. Each well had a final pH value of 6. Cell viability was assessed in triplicate experiments using the colorimetric [3-(4,5-dimethylthiazol-2-yl)-2,5-diphenyltetrazolium] MTT assay [42]. Absorbance values were read at 570 nm using an automated multi-well scanning spectrophotometer (Biotek, Synergy HT, Winooski, VT, USA). The cell viability values were normalized with respect to the viability of the control without OB treatment.

3.3. Results and Discussion

3.3.1. Isothermal Titration Calorimetry (ITC)

Calorimetric titrations were carried out in order to verify the formation of host-guest complexes between VTD and CDs. Figure 3.2 shows the heat evolved and curve fitting of the enthalpy of complex formation for the three studied systems and Table 1 the thermodynamic parameters obtained.

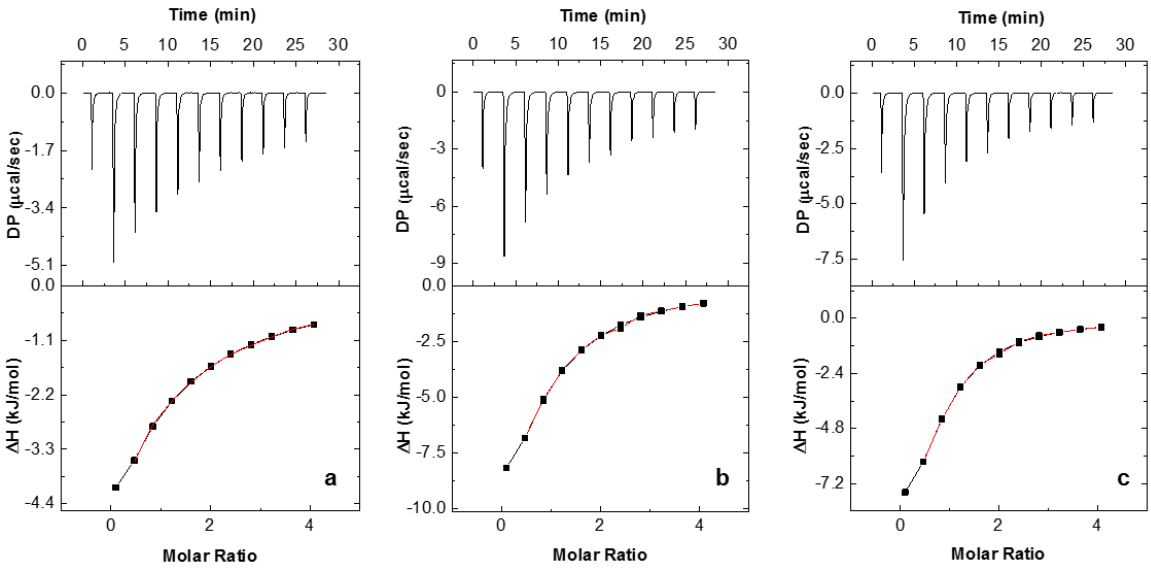

Figure 3.2. Isothermal titration calorimetry data obtained for the binding interaction of VTD with: (**a**) β-CD, (**b**) γ-CD and (**c**) SBCD. The upper graphs show the variation of heat released upon injection of 10 µL of each CD. The lower graphs correspond to the binding curve obtained from the integrated heat data. Conditions: [VTD] = 0.2 mM, [CD] = 4 mM, T = 298.2 K.

ITC allows one to directly measure the differential heat of binding released or absorbed during the interaction of a binder and a ligand. From the obtained thermogram (Figure 3.2.) it is possible to characterize the

stoichiometry of the complex (*n*), the equilibrium constant (K_{eq}), the enthalpy (ΔH) and entropy (ΔS) changes, which are related to the Gibbs free energy (ΔG) by equation (1) [43].

$$\Delta G = RTlnK_{eq} = \Delta H - T\Delta S \quad (1)$$

The differential heat measured in ITC depends on a dimensionless parameter (*c*) that determines the shape of the binding isotherm and relates the total host concentration (in this case the CDs) with the equilibrium constant according to equation 2 [22].

$$c = n[CD]K_{eq} \quad (2)$$

Table 3.1. Stability constants (K_{eq}), standard enthalpy changes ($\Delta H°$), Gibbs's binding energy ($\Delta G°$) and entropy changes ($\Delta S°$) for the formation of VTD complexes with three CD hosts (γ–CD, SBCD and β–CD) in Tris buffer solution pH 6 at 298.2 K.

	n	***K_{eq}*** **(M^{-1})**	***ΔH°*** **(kJ/mol)**	***ΔG°*** **(kJ/mol)**	***ΔS°*** **(kJ/mol)**
β–CD	0.7 ± 0.2	1500 ± 70	n.d.	-18.1 ± 0.1	n.d.
γ–CD	0.95 ± 0.03	7200 ± 100	-16.7 ± 0.2	-22.1 ± 0.1	0.21 ± 0.01
SBCD	0.94 ± 0.02	8200 ± 60	-14.5 ± 0.1	-22.4 ± 0.1	0.31 ± 0.01

n.d.: could not be determined accurately

Values of *c* between $1 < c < 1000$ are considered to be a good range for accurately estimating the thermodynamic parameters. Ideally, for systems with K_{eq} values in the order of those commonly observed for CD complexes (10^2-10^4 mol^{-1}) relatively high concentrations should be used in the experiment to guarantee that the *c* value lies between the appropriate range. However, when working with systems that involve CDs it is important to have in mind that aggregation starts to occur at critical concentrations above 1-2% (m/v) for

β-CD, γ-CD and SBCD [25,44]. This can lead to incorrect measurement of the differential heat of binding since part of the heat is consumed in the aggregation process. This compromise between the CD concentrations and *c* values could be easily attained in the case of the γ-CD and SBCD due to their high solubility.

As can be seen from Table 3.1., the formation of inclusion complexes with γ-CD and SBCD is mainly enthalpy-driven since $|\Delta H| > |\mathrm{T}\Delta S|$ [45]. The thermodynamic parameters obtained for CD complexes are a result of the contributions of the release of water molecules contained inside the CD cavities driven by the occurrence of van der Waals and hydrophobic interactions between the host and the guest [46]. The large exothermic effect seen in the negative enthalpy values of γ-CD and SBCD indicate that their interaction with VTD is mostly driven by van der Waal forces than by hydrophobic interactions [45], as observed in other CD complexes [43] [47][48].

On the other hand, γ-CD and SBCD have K_{eq} values of 7200 M^{-1} and 8200 M^{-1}, respectively, in comparison with 1500 M^{-1} for β-CD (Table 3.1), indicating that the two first CDs form more stable inclusion complexes with the VTD toxin. This can be attributed to the larger cavity size in the case of the γ–CD with respect to β–CD where the VTD guest can potentially fit better. In the case of the anionic SBCD derivative, the diameter of the cavity is the same as β–CD, but the cavity is enlarged due to the sulfobutyl arms chemically attached through ether bonds. This longer cavity also helps to accommodate the VTD toxin. Since the pK_a of VTD is 9.5 [49], at pH 6 the molecule is protonated and electrostatic interactions between the $-SO_3^-$ groups and the NH^+ group of VTD also help to stabilize the inclusion complex resulting in a higher K_{eq} for VTD-SBCD than in the case of the VTD-γ-CD. Finally, the

β–CD has the lowest affinity for the VTD toxin. This is expected, since a weaker inclusion complex is formed due to the smaller cavity size where the VTD toxin can fit only partially, resulting in the smaller value for the K_{eq}.

3.3.2. NMR Experiments

VTD is the 3,4-dimethoxybenzoate ester of a 6-ring steroidal structure. The molecule thus features two well-distinguished parts that should interact in different ways with the CD hosts. The strong overlapping of some steroid protons with those of the CD hosts in the ^{1}H-NMR spectra prevented an accurate analysis of the effect of VTD on H-3 and H-5, which point towards the cavity and are usually the most affected by guest inclusion (Figure 3.3). However, analysis of the aromatic part of the spectra gave some hints on the possible inclusion geometry. Figure 4.3 (left) shows the ^{1}H-NMR spectra of the aromatic protons of VTD and their inclusion complexes with the three studied CDs. In all cases, the peaks of the VTD-CD complexes are shifted with respect to free VTD, indicating inclusion of the aromatic moiety in the CD cavities. In the case of β–CD and SBCD, all proton signals are shielded, with proton C showing the highest displacement (~0.3 ppm). The shift to lower frequencies of protons A and B was higher for SBCD (0.04 and 0.13 ppm, respectively) than for β-CD (0.02 and 0.06 ppm, respectively), suggesting a stronger interaction of the aromatic moiety with the anionic host and consistent with the ITC results. In the case of γ–CD, the aromatic resonances were less affected by the inclusion. Interestingly, protons A and B are slightly shifted to higher frequencies with respect to VTD, suggesting that these protons are close to oxygen atoms outside the cavity of the host [50,51]. This is an indication that the steroid part is deeply included in the cavity of γ-CD due to its larger size with the 3,4-dimethoxybenzoate group protruding from the primary side.

2D ^{1}H-^{1}H rotational Overhauser enhancement experiments (ROESY) are very useful tools to study the solution geometry of inclusion complexes with CDs. They provide information on the through-space proximity (typically 3-4 Å) of host protons and the guest parts involved in the supramolecular complexation in the form of cross-peaks with intensity proportional to the proximity of the protons involved. Figures 3.4, 3.5 and 3.6 show the ROESY spectra of the studied 1:1 VTD inclusion complexes in D_2O.

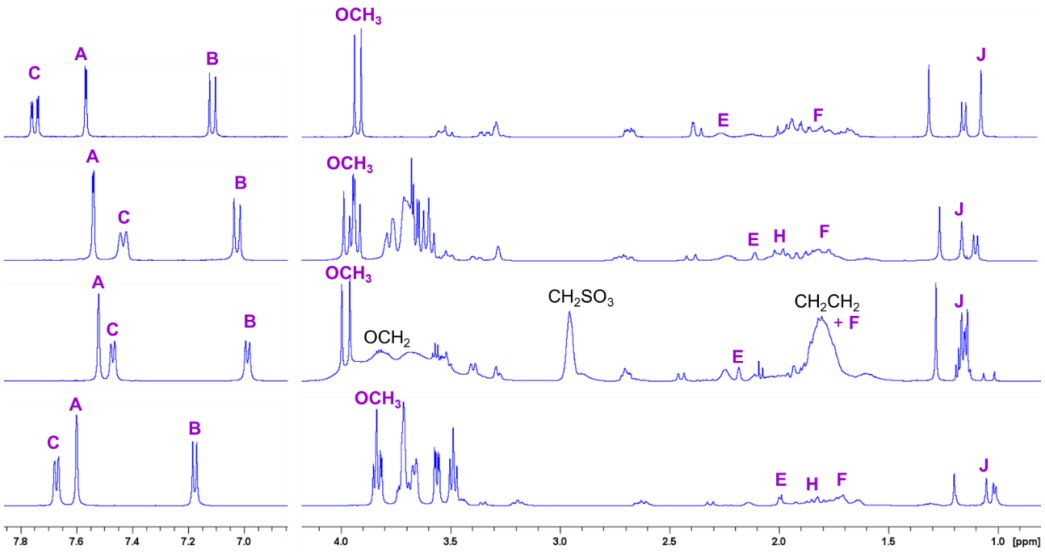

Figure 3.3. High frequency (left) and low frequency (right) regions of the ^{1}H-NMR spectra (0.1% DCl in D_2O, 500 MHz, 298 K) of: (**a**) VTD, (**b**) VTD:β-CD, (**c**) VTD:SBCD and (**d**) VTD:γ-CD. VTD protons are indicated in violet and SBCD spacer protons in black. For the assignment of other cyclodextrin protons please see Figures 4.4, 4.5 and 4.6.

The ROESY spectrum of the VTD:β-CD inclusion complex (Figure 3.4) shows cross-peaks between the aromatic protons and H-5. This indicates that VTD enters the cavity though the wider secondary side with the aromatic ring residing close to the primary side. This is further confirmed by the presence of strong cross-peaks between protons E, F, and H, and methyl group

J of VTD and H-3. Protons E and F also show weaker cross-peaks with H-5. These protons correspond to the steroid ring closer to the 3,4-dimethoxybenzoate group, indicating that this part of the VTD molecule also enters the cavity.

In the case of the VTD:SBCD inclusion complex (Figure 3.5), the ROESY spectrum shows a similar cross-peak pattern to VTD:β-CD and thus indicate a comparable inclusion geometry. Besides the steroid/H-3 and the aromatic/H-5 cross-peaks, the spectrum reveals spatial vicinity between the aromatic protons and the OCH_2 protons of the sulfobutyl group located on the primary side [52], although we could not detect cross-peaks with the VTD methoxy groups due to signal overlap. No interactions with the other sulfobutyl methylene groups were observed.

The ROESY spectrum of VTD:γ-CD also reveals an inclusion geometry in which the aromatic ring sits farther to the primary side of the γ-CD cavity as compared with β-CD. In this case, the aromatic protons show weaker interactions with H-5 but stronger with the H-6 protons that lie on the border of the cavity. This is in agreement with the signal displacements observed on the 1D ^{1}H-NMR spectrum. Protons E, H and F also show cross-peaks with H-3 and H-5 confirming the inclusion of the steroid part and a deeper penetration in the cavity. Interestingly, methyl group J also shows a strong signal with both H-3 and H-5, in contrast to β-CD in which this group lies closer to H-3. The differences in the relative position of the VTD guest in the β-CD and γ-CD cavity is mainly due to the larger size of γ-CD, that accommodates better the bulky steroidal part.

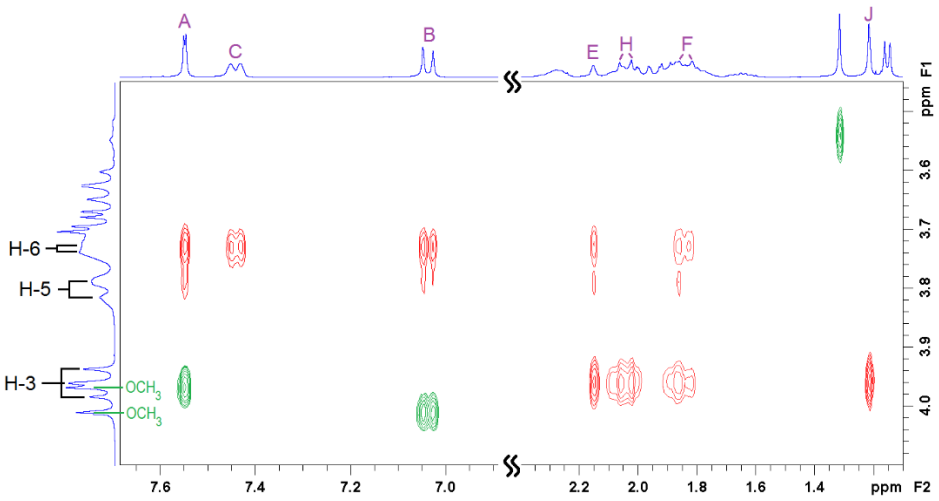

Figure 3.4. 2D-ROESY NMR spectrum of the 1:1 VTD:β-CD inclusion complex showing intermolecular (red) and intramolecular (green) cross-peaks. See Figures 4.1a and 4.1c for atom labelling.

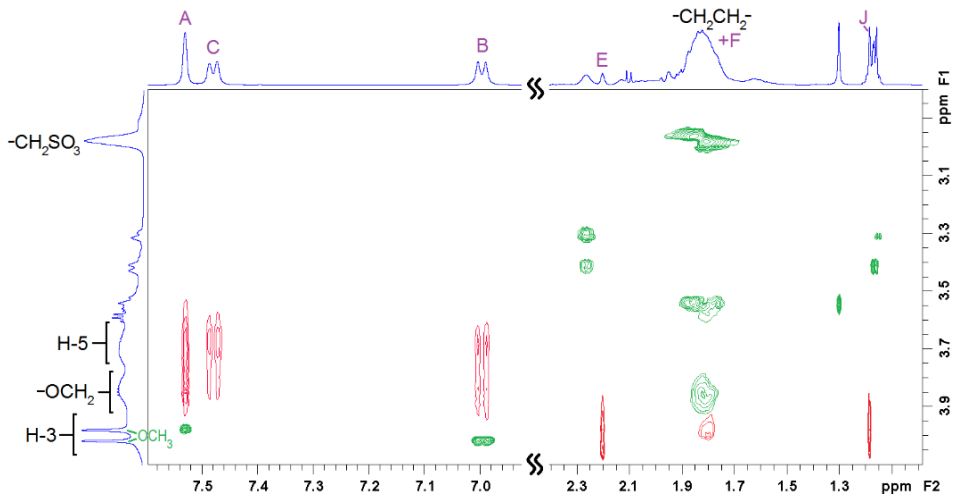

Figure 3.5. 2D-ROESY NMR spectrum of the 1:1 VTD:SBCD inclusion complex showing intermolecular (red) and intramolecular (green) cross-peaks. See Figures 4.1a and 4.1c for atom labelling.

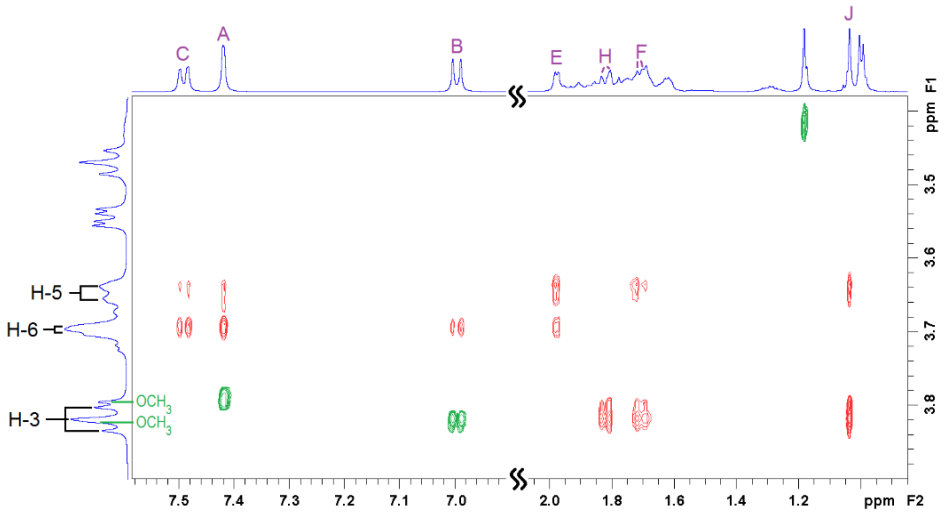

Figure 3.6. 2D-ROESY NMR spectrum of the 1:1 VTD:γ-CD inclusion complex showing intermolecular (red) and intramolecular (green) cross-peaks. See Figures 4.1a and 4.1c for atom labelling.

3.3.3. Molecular Simulations

Molecular docking is a widely used tool that aids to understand the geometries and interactions involved in the formation of inclusion complexes and often complements the experimental results [53]. From the simulation results presented in Table 4.2 we observe that all three CDs are predicted to be potential binders for the VTD. From docking, we obtain -25.9 kJ/mol, -26.7 kJ/mol and -5.6 kJ/mol for SBCD, γ-CD and β-CD, respectively. These results are in agreement with the experimental results obtained by ITC where SBCD and γ-CD are stronger binders for VTD in comparison with β-CD. From the 3D structures we can see that the best pose for the VTD:β-CD complex (Figure 3.7a) is one where the VTD molecule is not completely introduced inside the β-CD cavity. The aromatic ring is located inside the cavity and most of the steroid part of the molecule lies outside the cavity. In the case of SBCD (Figure

3.7b), although it is a β-CD derivative, the host has an elongated cavity because of the presence of the sulfobutyl ether arms that create more space for the guest, resulting in more penetration of VTD. Additionally, its anionic character may help to further stabilize the inclusion complex by electrostatic interactions with the protonated nitrogen atom present in the steroid part. On the other hand, the best pose of the VTD complex with the larger γ-CD host (Figure 3.7c) shows that the guest is deeply introduced inside the cavity and the aromatic ring actually protrudes from the primary side. This results in a sort of pseudorotaxane structure in which the host cavity mainly interacts with the steroid part. As can be seen, the docking results are in good agreement with the 2D ROESY NMR experiments, confirming the validity of this tool to understand inclusion complexation in cyclodextrins.

Docking studies involve several simplifications; the simulations are not dynamic, and normally they do not use an explicit solvent [33]. It is a good tool to quickly estimate the best binding pose for an inclusion complex [54] but should be complemented with more thorough methods such as MD which in fact uses explicit water molecules and considers a dynamic component of the inclusion complexes. Hence, the docking simulations were complemented with a molecular dynamics approach (trajectory videos available in the Supplementary information). The free energies of VTD binding with β-CD and γ-CD obtained with MM/GBSA [34] were -1.6 ± 1.3 kJ/mol and -18 ± 3 kJ/mol, respectively. An interesting result was seen in the MD of the γ-CD complex, where at the start of the trajectory simulation VTD was in fact not docked inside of the γ-CD cavity. As the simulation time elapsed, it could be seen how the molecule became incorporated inside the cavity, confirming again that this is the most energy stable configuration for the molecules in solution. The computed MM/GBSA $\Delta G°$ values also match both with the

docking scores and the ITC data, confirming that γ-CD is a much better binder than β-CD. The underestimation of ΔG° for the β-CD complex (-1.6 ± 1.3 kJ/mol) is most likely due to the geometry of the inclusion complex in which most of the steroid part of VTD is outside the cavity and not complexed inside the cavity and thus exposed to the solvent (see Figure 4.7a).

Table 3.2. Gibbs binding energy (ΔG°) values obtained by ITC and molecular dynamics (MD) and docking scores for the formation of inclusion complexes between VTD and the studied CD hosts.

	K_{eq} (M^{-1})	$\Delta G°$ (kJ/mol) ITC	$\Delta G°$ (kJ/mol) MD	*Docking Score* (kJ/mol)
β–CD	1500 ± 70	-18.1 ± 0.1	-1.6 ± 1.3	-5.6
SBCD	8200 ± 60	-22.4 ± 0.1	n.d.	-25.9
γ–CD	7200 ± 100	-22.1 ± 0.1	-18 ± 3	-26.7

n.d.: not determined. SBCD molecule not available in the literature for MD studies.

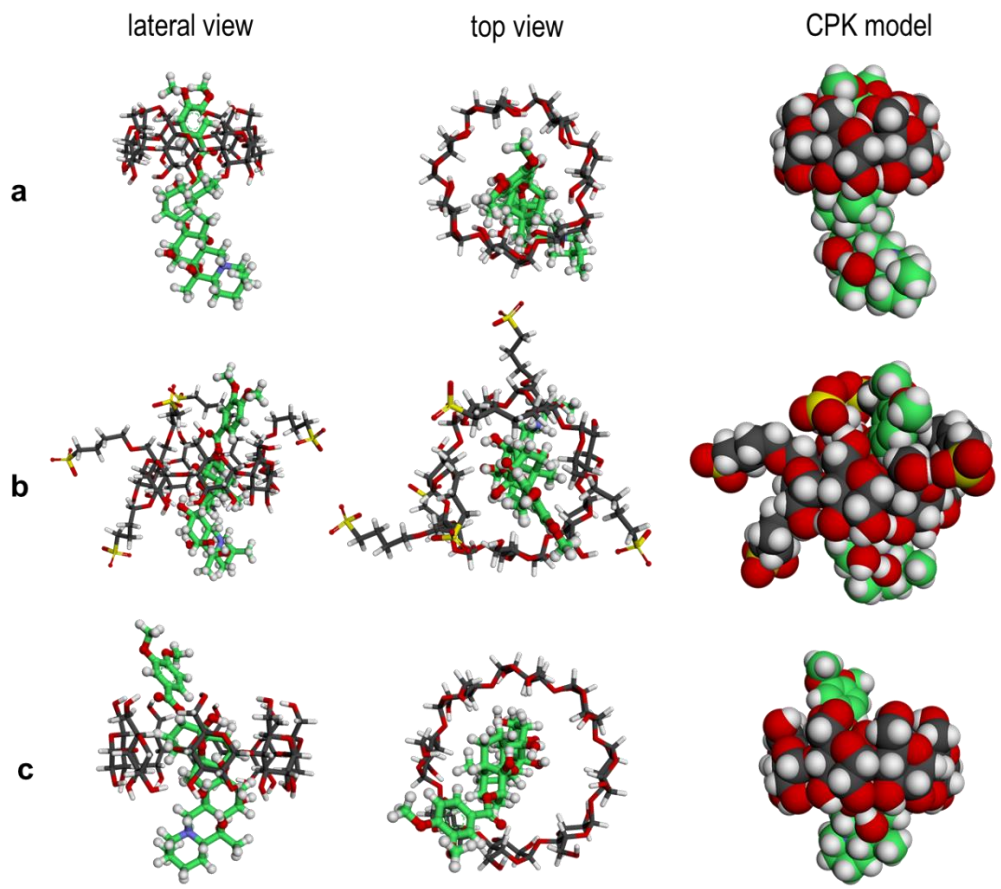

Figure 3.7. Three-dimensional energy minimized structures obtained by molecular docking of the inclusion complex between VTD and (**a**) β-CD, (**b**) SBCD and (**c**) γ-CD. The C atoms of VTD have been highlighted in green.

3.3.4. Cytotoxicity Evaluation

The VTD toxicity on Neuro-2a cells was evaluated with a CBA [55]. In this CBA, ouabain (OB), a toxic cardiac glycoside that inhibits the Na^+/K^+ pump [56], is added for the specific and sensitive detection of VTD since it prevents cells from counteracting the increasing sodium intracellular concentrations produced by VTD exposure [41,57]. The exposure to OB

sensitizes the cells and usually results in a slight decrease of the cell viability (Figure 4.8).

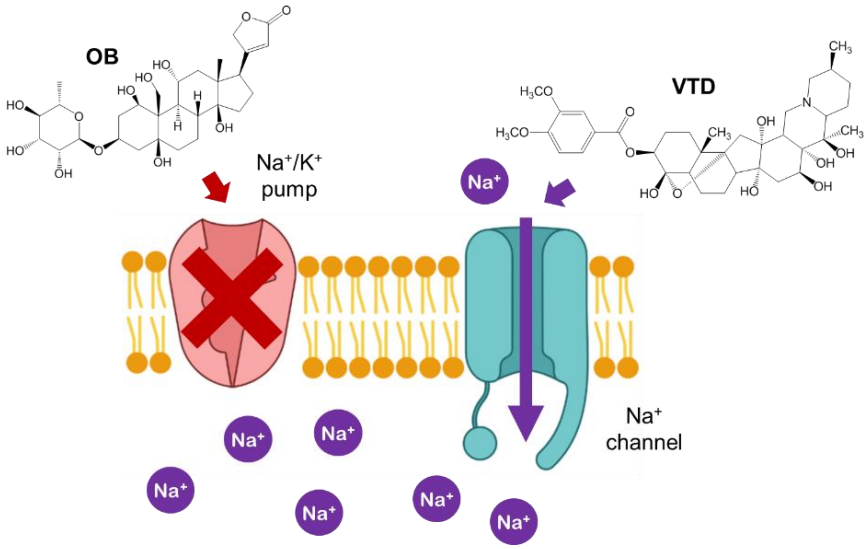

Figure 3.8. Structure of OB and effect of VTD and OB in the Na^+ cell transport.

In our experiments, the pre-treatment of the Neuro-2a cells with 0.4 mM OB resulted in around 30-40% decrease in cell viability (Figure 3.9). The effect of CDs on the Neuro-2a cells was simultaneously evaluated. Cells were exposed to different CDs concentrations up to 50 mM in the case of β-CD (higher concentrations could not be tested because of the low solubility of this CD) and up to 200 mM for γ-CD and SBCD. Cell viabilities around 60-70% were obtained in the absence (0 mM CD) and in the presence of all CDs and at all studied concentrations, demonstrating that CDs are harmless to Neuro-2a cells. On the other hand, this experiment also suggests that the CDs do not form host-guest complexes with OB. This is not surprising, since OB is the glycoside of a pentahydroxylated steroid and thus a highly polar and hydrophilic molecule with little or no affinity for the CDs.

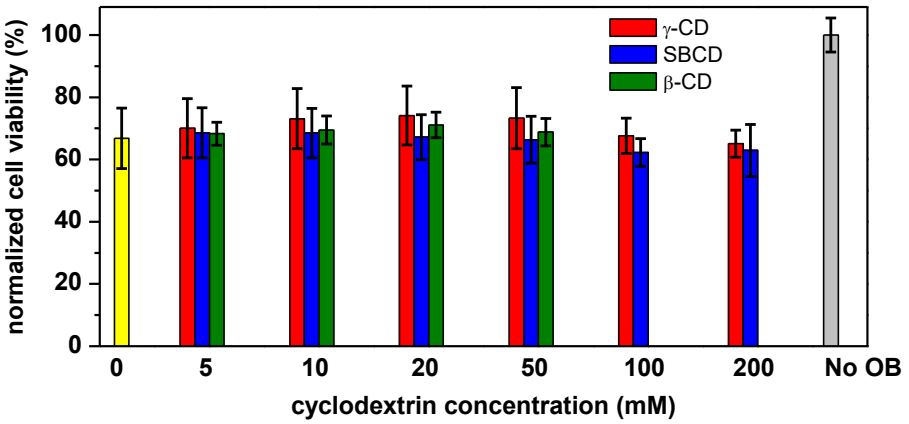

Figure 3.9. Normalized cell viability of Neuro-2a cells pre-treated with 0.4 mM ouabain (OB) in the absence (yellow) and in the presence of γ-CD (red), SBCD (blue) and β-CD (green) at different concentrations. The control in absence of OB is the grey bar.

Neuro-2a cells were then exposed to different VTD and CDs concentrations, in the presence of OB, to test if the formation of inclusion complexes between VTD and the studied CDs resulted in an inhibition of VTD toxicity. In the absence of CDs, the addition of 1 and 0.25 mM VTD caused around 100% cell mortality (0% cell viability) (Figure 3.10). For 1 mM VTD, cell viabilities increased with increasing CD concentrations for γ-CD and SBCD, reaching around 100% of the cell viability and protecting the Neuro-2a cells from the VTD toxicity. (Figure 3.10a). However, β-CD was unable to protect the Neuro-2a cells at this VTD concentration. These results agree with the higher stability constants determined for the γ-CD and SBCD complexes than for β-CD. The results also show that the cell culture medium is not affecting the ability of CDs to complex VTD and highlight the selectivity of the CDs for VTD and not towards other molecules present in the medium.

Experiments were then performed using 0.25 mM VTD. In this case, all CDs were able to neutralize the toxic effect of VTD totally or partially, again in a concentration-dependent matter (Figure 3.10b). As expected, lower CDs concentrations are needed to inhibit the VTD toxicity. In the case of β-CD, even though a higher concentration (compared to γ-CD and SBCD) is required to inhibit the VTD toxicity, 70% cell viability recovery is achieved at the highest tested β-CD concentration of 50 mM. Therefore, the three studied CDs have antidote-like characteristics, which depend on the type of CD as well as on VTD and CD concentrations.

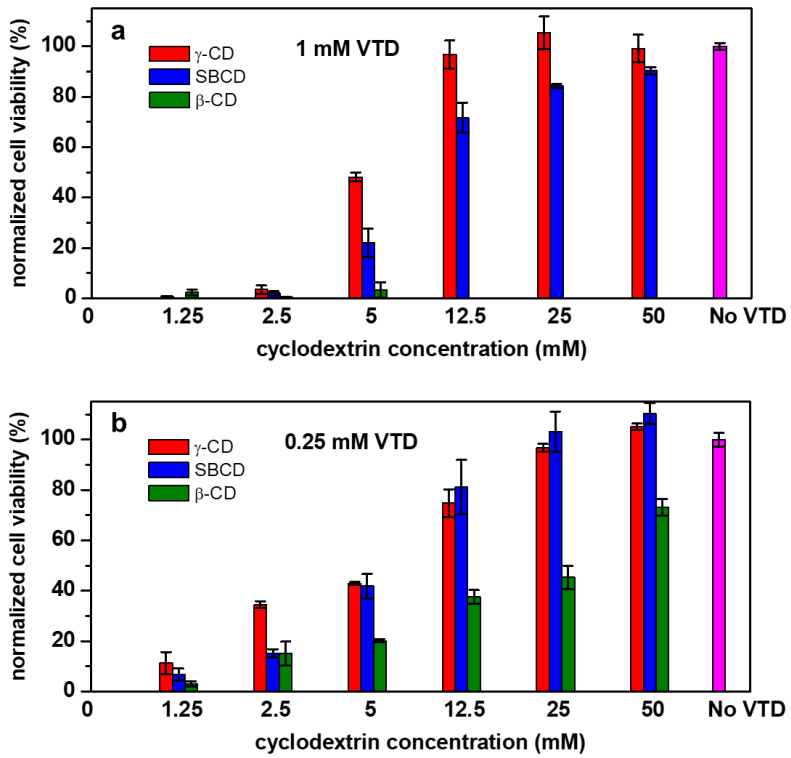

Figure 3.10. Normalized cell viability of Neuro-2a cells pre-treated with 0.4 mM ouabain (OB) after the incubation with (a) 1 mM and (b) 0.25 mM VTD in the absence (0 mM) and in the presence of γ-CD (red), SBCD (blue) and β-CD (green) at different concentrations. The control in absence of VTD is the magenta bar.

4.4. Conclusions

We have successfully proved the formation of inclusion complexes between the alkaloid neurotoxin VTD and native β-CD and γ-CD as well as the anionic β-CD derivative SBCD. The equilibrium constants were estimated to be 1500 M^{-1}, 7200 M^{-1} and 8200 M^{-1} for β-CD, γ-CD and SBCD, respectively, making the γ-CD and the anionic SBCD the most stable hosts. ^{1}H-NMR and ^{1}H-^{1}H ROESY experiments confirmed the incorporation of VTD in each of the CDs cavities and the most stable orientation of the molecule inside the CDs was elucidated by performing docking and molecular dynamics simulations. In-vitro studies showed that the three studied CDs have antidote-like effects against the VTD toxicity, protecting Neuro-2a cell viability at a different extent depending on the CD type as well as the CD and VTD concentrations. To the best of our knowledge, this is the first study of the interactions between VTD neurotoxin and CDs and opens the door to further study the role of CDs with other lipid toxins.

4.5. References

1. Wang, S.-Y.; Wang, G.K. Voltage-gated sodium channels as primary targets of diverse lipid-soluble neurotoxins. *Cell. Signal.* **2003**, *15*, 151–159, doi:https://doi.org/10.1016/S0898-6568(02)00085-2.

2. Caillaud, A.; Eixarch, H.; de la Iglesia, P.; Rodriguez, M.; Dominguez, L.; Andree, K.B.; Diogène, J. Towards the standardisation of the neuroblastoma (neuro-2a) cell-based assay for ciguatoxin-like toxicity detection in fish: Application to fish caught in the Canary Islands. *Food Addit. Contam. - Part A Chem. Anal. Control. Expo. Risk Assess.* **2012**, *29*, 1000–1010, doi:10.1080/19440049.2012.660707.

3. Mcdonough, J.H.; Jaax, N.K.; Crowley, R.A.; Mays, M.Z.; Modrow, H.E. Atropine and / or Diazepam Therapy Protects against Soman-Induced Neural and Cardiac Pathology ' The chemical warfare nerve agent soman (pi- nacolyl methylphosphonofluoridate) is a po- tent anticholinesterase organophosphonate. **1989**, 256–276.

4. Erecinfska, M.; Nelson, D.; Silver, I.A. Interactions of benztropine, atropine and ketamine with veratridine-activated sodium channels: effects on membrane depolarization, K+-efflux and neutrotransmitter amino acid release. *Br. J. Pharmacol* **1988**, *94*, 871–881, doi:10.1111/j.1476-5381.1988.tb11599.x.

5. Cataldi, M. Veratridine☆. *Ref. Modul. Biomed. Sci.* **2016**, 1–9, doi:10.1016/b978-0-12-801238-3.99386-3.

6. Del Valle, E.M.M. Cyclodextrins and their uses: A review. *Process Biochem.* **2004**, *39*, 1033–1046, doi:10.1016/S0032-9592(03)00258-9.

7. Szente, L.; Szejtli, J. Highly soluble cyclodextrin derivatives: chemistry, properties, and trends in development. *Adv. Drug Deliv. Rev.* **1999**, *36*, 17–28.

8. Loftsson, T.; Fridhriksdottir, H.; Olafsdottir, B.J.; Gudhmundsson, O. Solubilization and stabilization of drugs through cyclodextrin complexation. *Acta Pharm. Nord.* **1991**, *3*, 215–217.

9. Ho, S.; Thoo, Y.; Young, D.J.; Fong Siow, L. Cyclodextrin encapsulated catechin: Effect of pH, relative humidity and various food models on antioxidant stability. *LWT* **2017**, *85*, 232–239, doi:10.1016/j.lwt.2017.07.028.

10. Mori, T.; Tsuchiya, R.; Doi, M.; Nagatani, N.; Tanaka, T.

Solubilization of ultraviolet absorbers by cyclodextrin and their potential application in cosmetics. *J. Incl. Phenom. Macrocycl. Chem.* **2019**, *93*, 91–96, doi:10.1007/s10847-018-0846-5.

11. Kfoury, M.; Landy, D.; Ruellan, S.; Auezova, L.; Greige-Gerges, H.; Fourmentin, S. Determination of formation constants and structural characterization of cyclodextrin inclusion complexes with two phenolic isomers: carvacrol and thymol. *Beilstein J. Org. Chem* **2016**, *12*, 29–42, doi:10.3762/bjoc.12.5.

12. Villalonga, R.; Cao, R.; Fragoso, A. Supramolecular chemistry of cyclodextrins in enzyme technology. *Chem. Rev.* **2007**, *107*, 3088–3116, doi:10.1021/cr050253g.

13. Landy, D.; Mallard, I.; Ponchel, A.; Monflier, E.; Fourmentin, S. Remediation technologies using cyclodextrins: An overview. *Environ. Chem. Lett.* **2012**, *10*, 225–237, doi:10.1007/s10311-011-0351-1.

14. Loftsson, T.; Duchêne, D. Historical Perspectives Cyclodextrins and their pharmaceutical applications. *Int. J. Pharm.* **2007**, *329*, 1–11, doi:10.1016/j.ijpharm.2006.10.044.

15. Fliszár-Nyúl, E.; Lemli, B.; Kunsági-Máté, S.; Szente, L.; Poór, M. Interactions of Mycotoxin Alternariol with Cyclodextrins and Its Removal from Aqueous Solution by Beta-Cyclodextrin Bead Polymer. *Biomolecules* **2019**, *9*, doi:10.3390/biom9090428.

16. Ventrella, A.; Verrone, R.; Pinalysa Cosma; Fini, P.; Longobardi, F.; Lippolis, V.; Pascale, M.; Catucci, L. Physico-Chemical Investigation on the Interaction Between Ochratoxin A and Heptakis-2,6-di-O-Methyl-b-Cyclodextrin. *J Solut. Chem* **2014**, *43*, 1436–1447, doi:10.1007/s10953-014-0214-z.

17. Amadasi, A.; Dall'Asta, C.; Ingletto, G.; Pela, R.; Marchelli, R.; Cozzini, P. Explaining cyclodextrin-mycotoxin interactions using a "natural" force field. *Bioorganic Med. Chem.* **2007**, *15*, 4585–4594, doi:10.1016/j.bmc.2007.04.006.

18. Faisal, Z.; Kunsági-Máté, S.; Lemli, B.; Szente, L.; Bergmann, D.; Humpf, H.U.; Poór, M. Interaction of dihydrocitrinone with native and chemically modified cyclodextrins. *Molecules* **2019**, *24*, doi:10.3390/molecules24071328.

19. Poór, M.; Matisz, G.; Kunsági-Máté, S.; Derdák, D.; Szente, L.; Lemli, B. Fluorescence spectroscopic investigation of the interaction of citrinin with native and chemically modified cyclodextrins. *J. Lumin.* **2015**, *172*, 23–28, doi:10.1016/j.jlumin.2015.11.011.

20. Poór, M.; Zand, A.; Szente, L.; Lemli, B.; Kunsági-Máté, S. Interaction of α-and β-zearalenols with β-cyclodextrins. *Molecules* **2017**, *22*, doi:10.3390/molecules22111910.

21. Dernaika, H.; Chong, S. V; Artur, C.G.; Tallon, J.L. Spectroscopic Identification of Neurotoxin Tetramethylenedisulfotetramine (TETS) Captured by Supramolecular Receptor beta-Cyclodextrin Immobilized on Nanostructured Gold Surfaces. *J. Nanomater.* **2014**, doi:10.1155/2014/207258.

22. Masurier, N.; Estour, F.; Froment, M.-T.; Lefèvre, B.; Debouzy, J.-C.; Brasme, B.; Masson, P.; Lafont, O. Synthesis of 2-substituted b-cyclodextrin derivatives with a hydrolytic activity against the organophosphorylester paraoxon. *Eur. J. Med. Chem.* **2005**, *40*, 615–623, doi:10.1016/j.ejmech.2005.02.008.

23. Campàs, M.; Rambla-Alegre, M.; Wirén, C.; Alcaraz, C.; Rey, M.;

Safont, A.; Diogène, J.; Torréns, M.; Fragoso, A. Cyclodextrin polymers as passive sampling materials for lipophilic marine toxins in Prorocentrum lima cultures and a Dinophysis sacculus bloom in the NW Mediterranean Sea. *Chemosphere* **2021**, *285*, doi:10.1016/j.chemosphere.2021.131464.

24. Ryzhakov, A.; Do Thi, T.; Stappaerts, J.; Bertoletti, L.; Kimpe, K.; S A Couto, R.; Saokham, P.; Van Den Mooter, G.; Augustijns, P.; Somsen, G.W.; et al. Self-Assembly of Cyclodextrins and Their Complexes in Aqueous Solutions. **2016**, doi:10.1016/j.xphs.2016.01.019.

25. Do, T.T.; Van Hooghten, R.; Van den Mooter, G. A study of the aggregation of cyclodextrins: Determination of the critical aggregation concentration, size of aggregates and thermodynamics using isodesmic and K2–K models. *Int. J. Pharm.* **2017**, *521*, 318–326, doi:10.1016/j.ijpharm.2017.02.037.

26. Jain, A.S.; Date, A.A.; Pissurlenkar, R.R.S.; Coutinho, E.C.; Nagarsenker, M.S. Sulfobutyl Ether7 β-Cyclodextrin (SBE7 β-CD) Carbamazepine Complex: Preparation, Characterization, Molecular Modeling, and Evaluation of In Vivo Anti-epileptic Activity. *AAPS PharmSciTech* **2011**, *12*, 1163–1175, doi:10.1208/s12249-011-9685-z.

27. Shityakov, S.; Puskás, I.; Pápai, K.; Salvador, E.; Roewer, N.; Förster, C.; Broscheit, J.A. Sevoflurane-sulfobutylether-β-cyclodextrin complex: Preparation, characterization, cellular toxicity, molecular modeling and blood-brain barrier transport studies. *Molecules* **2015**, *20*, 10264–10279, doi:10.3390/molecules200610264.

28. Harder, E.; Damm, W.; Maple, J.; Wu, C.; Reboul, M.; Yu Xiang, J.;

Wang, L.; Lupyan, D.; K. Dahlgren, M.; L. Knight, J.; et al. OPLS3: A Force Field Providing Broad Coverage of Drug-like Small Molecules and Proteins. *J. Chem. Theory Comput.* **2015**, *12*, 281–296, doi:10.1021/acs.jctc.5b00864.

29. Codding, P.W. Structural Studies of Sodium Channel Neurotoxins. 2. Crystal Structure and Absolute Configuration of Veratridine Perchlorate. *J. Am. Chem. Soc.* **1983**, *105*, 3172–3176, doi:10.1021/ja00348a035.

30. A. Friesner, R.; L. Banks, J.; B. Murphy, R.; A. Halgren, T.; J. Klicic, J.; T. Mainz, D.; P. Repasky, M.; H. Knoll, E.; Shelley, M.; K. Perry, J.; et al. Glide: A New Approach for Rapid, Accurate Docking and Scoring. 1. Method and Assessment of Docking Accuracy. *J. Med. Chem.* **2004**, *47*, 1739–1749, doi:10.1021/jm0306430.

31. A. Halgren, T.; B. Murphy, R.; A. Friesner, R.; S. Beard, H.; L. Frye, L.; Thomas Pollard, W.; L. Banks, J. Glide: A New Approach for Rapid, Accurate Docking and Scoring. 2. Enrichment Factors in Database Screening. *J. Med. Chem.* **2004**, *47*, 1750–1759, doi:10.1021/jm030644s.

32. A. Friesner, R.; B. Murphy, R.; P. Repasky, M.; L. Frye, L.; R. Greenwood, J.; A. Halgren, T.; C. Sanschagrin, P.; T. Mainz, D. Extra Precision Glide: Docking and Scoring Incorporating a Model of Hydrophobic Enclosure for Protein−Ligand Complexes. *J. Med. Chem.* **2006**, *49*, 6177–6196, doi:10.1021/jm051256o.

33. Pantsar, T.; Poso, A. Binding affinity via docking: Fact and fiction. *Molecules* **2018**, *23*, 1899, doi:10.3390/molecules23081899.

34. Genheden, S.; Ryde, U. The MM/PBSA and MM/GBSA methods to

estimate ligand-binding affinities. *Expert Opin. Drug Discov.* **2015**, *10*, 449–461, doi:10.1517/17460441.2015.1032936.

35. Weiner, P.K.; Kollman, P.A. AMBER: Assisted model building with energy refinement. A general program for modeling molecules and their interactions. *J. Comput. Chem.* **1981**, *2*, 287–303, doi:10.1002/jcc.540020311.

36. Wang, J.; Wolf, R.M.; Caldwell, J.W.; Kollman, P.A.; Case, D.A. Development and testing of a general Amber force field. *J. Comput. Chem.* **2004**, *25*, 1157–1174, doi:10.1002/jcc.20035.

37. Allouche, A. Software News and Updates Gabedit — A Graphical User Interface for Computational Chemistry Softwares. *J. Comput. Chem.* **2012**, *32*, 174–182, doi:10.1002/jcc.

38. Jorgensen, W.L.; Chandrasekhar, J.; Madura, J.D.; Impey, R.W.; Klein, M.L. Comparison of simple potential functions for simulating liquid water. *J. Chem. Phys.* **1983**, *79*, 926–935, doi:10.1063/1.445869.

39. Wu, X.; Brooks, B.R. Self-guided Langevin dynamics simulation method. *Chem. Phys. Lett.* **2003**, *381*, 512–518, doi:10.1016/j.cplett.2003.10.013.

40. Berendsen, H.J.C.; Postma, J.P.M.; Van Gunsteren, W.F.; Dinola, A.; Haak, J.R. Molecular dynamics with coupling to an external bath. *J. Chem. Phys.* **1984**, *81*, 3684–3690, doi:10.1063/1.448118.

41. Cañete, E.; Diogène, J. Comparative study of the use of neuroblastoma cells (Neuro-2a) and neuroblastoma × glioma hybrid cells (NG108-15) for the toxic effect quantification of marine toxins.

Toxicon **2008**, *52*, 541–550, doi:10.1016/j.toxicon.2008.06.028.

42. Mosmann, T. Rapid colorimetric assay for cellular growth and survival: Application to proliferation and cytotoxicity assays. *J. Immunol. Methods* **1983**, *65*, 55–63, doi:10.1016/0022-1759(83)90303-4.

43. Waldvogel, S. *Book Review Cyclodextrins and Their Complexes: Chemistry, Analytical Methods, Applications (Helena Dodziuk, Ed.)*; 2007; Vol. 2007; ISBN 9783527312801.

44. Loftsson, T.; Saokham, P.; Sá Couto, A.R. Self-association of cyclodextrins and cyclodextrin complexes in aqueous solutions. *Int. J. Pharm.* **2019**, *560*, 228–234, doi:10.1016/j.ijpharm.2019.02.004.

45. Mazzaferro, S.; Bouchemal, K.; Gallard, J.F.; Iorga, B.I.; Cheron, M.; Gueutin, C.; Steinmesse, C.; Ponchel, G. Bivalent sequential binding of docetaxel to methyl-β-cyclodextrin. *Int. J. Pharm.* **2011**, *416*, 171–180, doi:10.1016/j.ijpharm.2011.06.034.

46. Bouchemal, K.; Mazzaferro, S. How to conduct and interpret ITC experiments accurately for cyclodextrin-guest interactions. *Drug Discov. Today* **2012**, *17*, 623–629, doi:10.1016/j.drudis.2012.01.023.

47. Zheng, P.J.; Wang, C.; Hu, X.; Tam, K.C.; Li, L. Supramolecular complexes of azocellulose and α-cyclodextrin: Isothermal titration calorimetric and spectroscopic studies. *Macromolecules* **2005**, *38*, 2859–2864, doi:10.1021/ma0483241.

48. Sun, D.Z.; Li, L.; Qiu, X.M.; Liu, F.; Yin, B.L. Isothermal titration calorimetry and 1H NMR studies on host-guest interaction of paeonol and two of its isomers with β-cyclodextrin. *Int. J. Pharm.* **2006**, *316*,

7–13, doi:10.1016/j.ijpharm.2006.02.020.

49. Forces, A. Solubility, and pKa, of Veratridine. *Anal. Biochem.* **1986**, *153*, 33–38, doi:https://doi.org/10.1016/0003-2697(86)90056-4.

50. Veiga, F.J.B.; Fernandes, C.M.; Carvalho, R.A.; Geraldes, C.F.G.C. Molecular modelling and 1H-NMR: Ultimate tools for the investigation of tolbutamide: β-cyclodextrin and tolbutamide: Hydroxypropyl-β-cyclodextrin complexes. *Chem. Pharm. Bull.* **2001**, *49*, 1251–1256, doi:10.1248/cpb.49.1251.

51. Ganza-Gonzalez, A.; Vala-Jato, J.L.; Anguiano-Igea, S.; Otero-Espinar, F..; Blanco-Méndez, J. A proton nuclear magnetic resonance study of the inclusion complex of naproxen with beta-cyclodextrin. *Int. J. Pharm.* **1994**, *106*, 179–185.

52. Ma, D.Y.; Zhang, Y.M.; Xu, J.N. The synthesis and process optimization of sulfobutyl ether β-cyclodextrin derivatives. *Tetrahedron* **2016**, *72*, 3105–3112, doi:10.1016/j.tet.2016.04.039.

53. Li, T.; Guo, R.; Zong, Q.; Ling, G. Application of molecular docking in elaborating molecular mechanisms and interactions of supramolecular cyclodextrin. *Carbohydr. Polym.* **2022**, *276*, 118644, doi:10.1016/j.carbpol.2021.118644.

54. Kuntz, I.D.; Blaney, J.M.; Oatley, S.J.; Langridge, R.; Ferrin, T.E. A Geometric Approach to Macromolecule-Ligand Interactions. *J. Mol. Biol.* **1982**, *161*, 269–288.

55. Manger, R.L.; Leja, L.S.; Lee, S.Y.; Hungerforg, J.M.; Wekell, M.M. Tetrazolium-based cell bioassay for neurotoxins active on voltage-sensitive sodium channels: Semiautomated assay for saxitoxins,

brevetoxins, and ciguatoxins. *Anal. Biochem.* **1993**, *214*, 190–194, doi:10.1006/abio.1993.1476.

56. Lingrel, J.B.; Kuntzweiler, T. Na+,K(+)-ATPase. *J. Biol. Chem.* **1994**, *269*, 19659–19662, doi:10.1016/S0021-9258(17)32067-7.

57. Caillaud, A.; Cañete, E.; de la Iglesia, P.; Giménez, G.; Diogène, J. Cell-based assay coupled with chromatographic fractioning: A strategy for marine toxins detection in natural samples. *Toxicol. Vitr.* **2009**, *23*, 1591–1596, doi:10.1016/j.tiv.2009.08.013.

Chapter 4

Synthesis and characterization of insoluble cyclodextrin nanosponges with variable crosslinker-size for marine toxin capturing applications

4.1 Introduction

Harmful algal blooms (HAB), also known as red tides, are a phenomenon caused by microscopic algae of different types that can be non-toxic or toxic but with the common characteristic of having harmful effects like damages on marine ecosystems, human health, as well as economic and environmental impact [1]. Non-toxic HAB are usually produced by the biomass accumulation of algae and can cause damage in fisheries, recreational facilities and of course, ecosystems by affecting co-occurring organisms and altering food-web dynamics [2]. In the case of toxic HAB, the secretion of potent toxins leads to the transfer of the algae toxins through the food-chain [3] producing disease and death of animals such as fish, seabirds and marine mammals, among many others. In other cases, the toxins can also bioaccumulate in different sea animals such as shellfish, or marine vertebrates resulting in very high concentration of toxins that can be lethal for humans when ingesting the sea food [4].

This phenomenon has become an incrementing problem throughout the last decades resulting in an increasing trend of bloom incidence, larger areas affected and higher economic losses [3] (Figure 4.1). The causes for the increase in HAB range from climate change to man-lead eutrophication [5] and nowadays most coastal countries are threatened by one or more algae species [1,6].

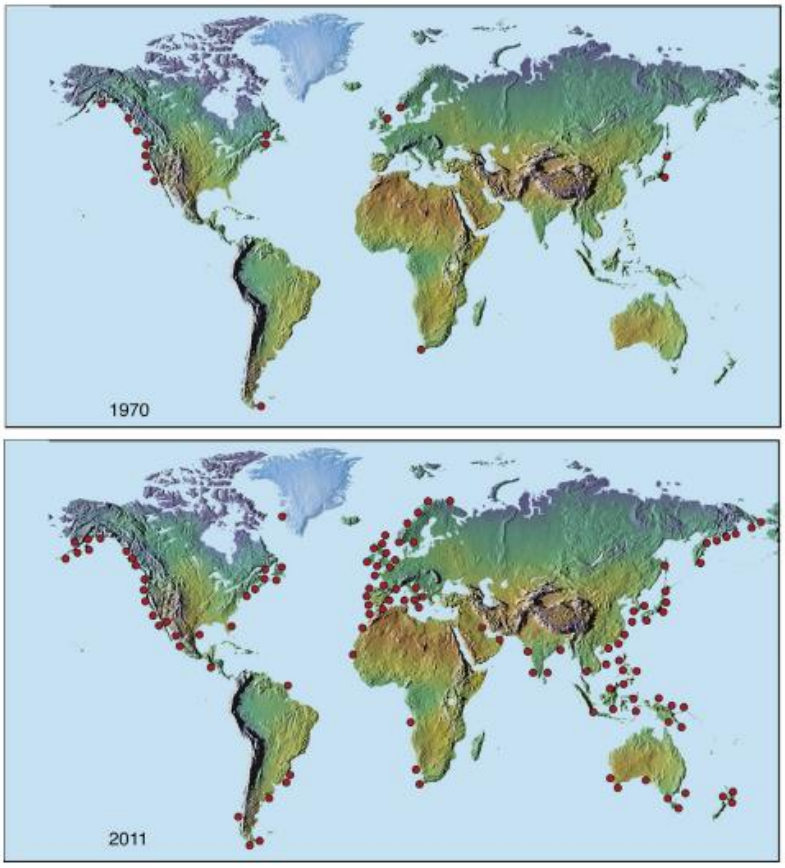

Figure 4.1. The expansion of global cases of Paralytic shellfish poisoning (PSP) from 1972 to 2011. Extracted from [7]

Methods for monitoring HAB can be divided in the ones focused on detecting the presence of algal cells such as microscopy or pigment analysis, satellite spectroscopy [8], or PCR-based approaches[9]; or the ones that focus on detecting the presence of marine toxins produced by the algae such as enzyme-linked immunosorbent assay (ELISA) [10], Solid-phase adsorption toxin tracking (SPATT) [11], or liquid chromatography mass spectrometry (LCMS) [12]. Monitoring the toxin's presence takes special relevance since there are many food-borne illnesses produced by many marine toxin molecules, see Table 5.1.

Table 5.1. Food-borne diseases produced by different marine toxins and their producing microorganisms [13]

	Disease or Condition					
	Ciguatera fish poisoning (CFP)	Neurotoxic shellfish poisoning (NSP)	Paralytic shellfish poisoning (PSP)	Amnesiac shellfish poisoning (ASP)	Diarrheic shellfish poisoning (DSP)	Azaspiracid shellfish poisoning (AZP)
Toxin-producing organism	Dinoflagellates: Gambierdiscus toxicus, possibly others	Dinoflagellates: Karenia brevis and other Karenia species	Dinoflagellates: Gymonodinium catenatum, Pyrodinium bahamense, Alexandrium species	Diatoms: Pseudo-nitzchia species	Dinoflagellates: Dinophysis species, Prorocentrum lima	Dinoflagellates: Properidiunium species
Toxin(s)	Ciguatoxins, Maitotoxin, Scaritoxin	Brevetoxin	Saxitoxin	Domoic Acid	Okadaic acid	Azaspiracid
Foods likely to be contaminated	Reef fish such as barracuda, grouper, red snapper, and amberjack	Shellfish, primarily mussels, oysters, scallops	Shellfish, primarily scallops, mussels, clams, oysters, and cockles, Some fish, and crabs	Shellfish, primarily scallops, mussels, clams, oysters, possibly some fish species	Shellfish, primarily scallops, mussels, clams, oysters	Shellfish
Short-term symptoms	Nausea, Vomiting, Diarrhea, Stomach pain	Nausea, Vomiting, diarrhea, Stomach pain, Numbness of lips, tongue, and throat, Dizziness	Nausea, Vomiting, Diarrhea, Shortness of breath, Irregular heartbeat, Numbness of mouth and lips, Weakness	Nausea, Vomiting, Diarrhea, Stomach pain, Shortness of breath, Irregular heartbeat, Seizures, Possibly coma,etc	Nausea, Vomiting, Diarrhea, Stomach pain, Possibly chills, Headache, Fever	Nausea, Vomiting, Diarrhea, Stomach pain
Long-term symptoms	Abnormal hot and cold sensations, Pain, Weakness, Low blood pressure	Unknown	Unknown	Possibly amnesia	Unknown	Unknown

Moreover, there is a consensus among HAB scientists that alongside traditional research there is a need for setting new courses of practices and research to deliver conceptual and quantitative advances for monitoring and forecasting future HAB trends [14].

In this sense, developing new materials that aide in the monitorization of marine toxins is a plausible strategy for controlling or minimizing the damaging effects of HAB. The use of passive samplers as a monitoring tool can be used as an early warning tool to forecast shellfish contamination, as well as geographical and temporal information of HABs, environmental persistence and toxin dynamics [15]. The technique consists in the passive adsorption of marine toxins on porous synthetic resins (such as the commercial resin Dianion HP-20) for the following extraction and analysis. Figure 4.2 shows the deployment of a SPATT device in a body of water. As Roué et al explain [16]: 'the SPATT unit is made of two layers of nylon mesh filled with a porous synthetic resin, and fixed between two PVC circular frames. The device is then inserted in plastic grids to prevent its damage and excessive grazing by fish and maintained in a vertical position in the water column using weights and floats' (Figure 4.2).

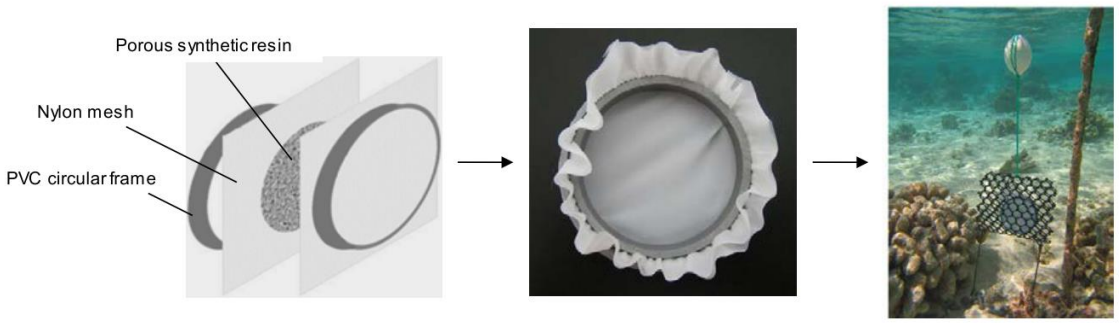

Figure 4.2. Example of one design used for the deployment of SPATT device in the field. Left: mode of assembly of SPATT device; Middle: SPATT device; Right: SPATT device deployed in the field. Extracted from [16]

As we have seen in the past chapters of this thesis, cyclodextrins (CDs) are cyclic oligosaccharides formed by 6, 7 or 8 glucopyranose units (α, β or γ-cyclodextrin, respectively) that have the ability to form host-guest inclusion complexes (ICs) with lipophilic molecules. Furthermore, cyclodextrin nanosponges (CD-NS) are a polymeric material formed by native CDs that can be cross-linked by different types of molecules, as it has been mentioned in this thesis introduction. The cross-linking reaction results in a web composed by different cavities, corresponding not only to the CD hydrophobic cavity, but also to the network of cavities formed between the outer part of CDs and the cross-linker. This forms a material with microscopically porous/sponge-like morphology.

CD-nanosponges as well as CD-polymers in general, have been widely studied for pharmaceutical applications as drug carriers [17] but there is little to no studies in the literature specifically using CD nanosponges as capturing agents for lipophilic marine toxins. Campàs et al [15] used insoluble β– and γ–CD polymers crosslinked with epichlorohydrin and hexamethylene diisocyanate which proved to be able to capture okadaic acid and pectenotoxins acting as passive sampling materials for marine toxins. This was a good starting point for the development of more CD-based polymeric materials with the potential to capture or preconcentrating different marine toxins.

In this research, we synthesized and characterized a new family of α–, β– and γ–CD-nanosponges using anhydride molecules of different length as cross-linkers. In addition, we used the different CD-NS in a proof-of-concept ELISA experiment as potential new materials for the monitorization of lipid-soluble marine toxins brevetoxin and okadaic acid (Figure 4.3)

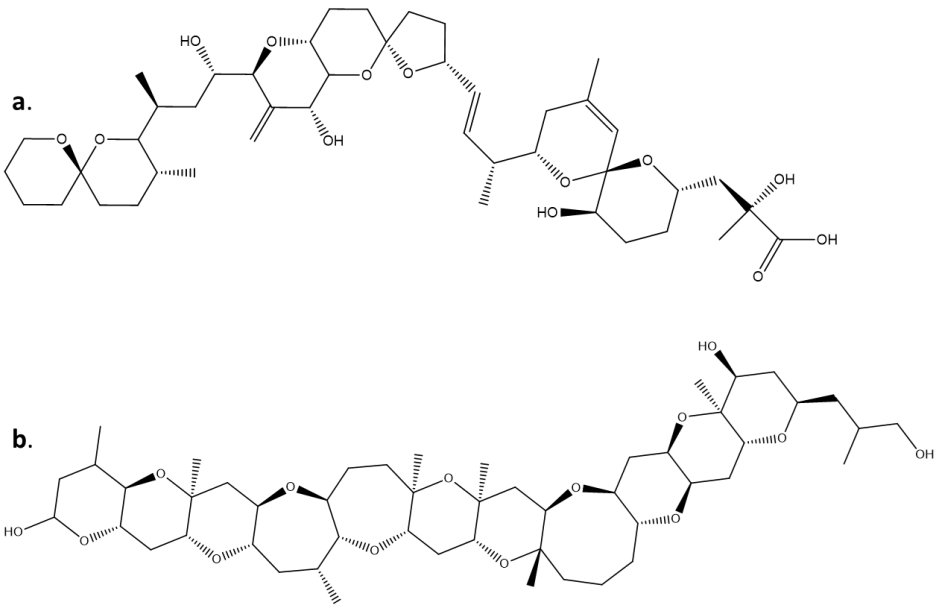

Figure 4.3. a. Brevetoxin molecule **b.** Okadaic acid molecule

4.2 Materials and Methods

All reagents were of analytical grade and used without further purification. α-CD, β-CD, and γ-CD were obtained from Wacker Chemie AG (Germany). Pyrromellitic dianhydride (PMDA) (97%), 3,3',4,4'-Biphenyltetracarboxylic dianhydride (BISPH) (97%), 4,4'-Oxydiphthalic anhydride (OXY) (97%), 4,4'-(4,4'-Isopropylidenediphenoxy) bis (phthalic anhydride) (ISO) (97%), Triethylamine (≥99.5%), Dimethyl sulfoxide (DMSO) (anhydrous, ≥99.9%) and Dimethyl sulfoxide-d6 deuteration degree min. 99.8% for NMR spectroscopy were purchased from Sigma Aldrich and used without further purification. Okadaic acid stock was a gift from Institute of Agrifood Research and Technology (IRTA, Sant Carles de la Ràpita, Spain), Brevetoxin PbTx-2 (CAS 79580-28-2) (≥95%), was purchased from Santa Cruz Biotechnology, EuroProxima okadaic acid ELISA kit, was obtained from R-BIOPHARM, Spain, Brevetoxin (NSP), ELISA, 96-test was

obtained from Eurofins Abraxis, Spain. All solutions were prepared with Milli-Q water (Millipore Inc., resistivity 18.2 MΩ·cm @ 25 °C).

4.2.1 Synthesis procedure

Cyclodextrin nanosponges (CD-NS) were prepared by modification of the synthetic procedures previously reported by Trotta et al. [18,19] for the classical PMDA nanosponges. We used a molar ratio of 1:6 (CD:anhydride) for the PMDA, OXY, and BISPH anhydrides. In the case of the ISO anhydride we always used a molar ratio of 1:4 (CD:anhydride). All three native CDs were dried overnight in a vacuum bell at 100°C to guarantee that the reaction was performed under anhydrous conditions. 51 mM α–CD, 44 mM β–CD and 38 mM γ– CD were each dissolved in 100 mL of anhydrous DMSO at room temperature under vigorous stirring. After obtaining a clear solution, 1.5 mL of TEA was added to the reaction flask. Finally, the corresponding molar equivalent of each anhydride was added, and the system vigorously stirred overnight at 70°C until obtaining a solid polymeric mass (Figure 4.4).

After the polymerization reaction was completed, the workup procedure consisted in breaking the polymeric mass into smaller pieces with the help of a spatula and transfer to a beaker containing 3 L of MiliQ water were the CD-NS were washed under magnetic stirring for 3 hours to dissolve possible unreacted CD. After centrifuging to separate the polymeric mas, the CD-NS were washed with acetone under stirring and centrifuged. In the final step the washing was performed with ethanol similarly to the procedure described above. The washing procedure was performed at least three times in each step. In the final step we performed a dialysis of the CD-NS in a 5 L beaker containing MiliQ water and changing the water multiple times.

4.2.2 Characterization of anhydride cyclodextrin polymers

The FTIR spectra were acquired on a Jasco FT/IR-6700 FTIR typeA Spectrometer, ATR PRO ONE as accessory. 32 scans at 4 cm-1 resolution were recorded. XRD patterns were recorded at room temperature obtained with a diffractometer Siemens EM-10110BU model D5000, operating with the Cu Kα line (λ=1.541 Å). TGA were recorded in a Mettler Toledo TGA/SDTA851 with a balance MT1 type. The measurements were carried out under N2 atmosphere, at 10 ºC/min, temperature range of 30 – 800 ºC. The results were analysed with STARe software. Field Emission Scanning Electron Microscope (FESEM) images were carried out in a Scios 2 equipment from FEI Company under high vacuum conditions and at 20 kV of voltage. Prior to taking the FESEM images, a gold sputtering process was performed for each of the CD-NS samples.

For obtaining the ^{1}H-NMR spectra of the CD-NS a basic hydrolysis reaction was performed at 90°C by adding 20 mg of each CD-NS in 1 mL of a solution containing 500 μL of DMSO-d6 and 500 μL of 0.5 mM NaOD under vigorous stirring. The reaction was followed until the complete solubilization of each CD-NS. Afterwards, 550 μL aliquots were put in NMR tubes and the spectra were measured at 400 MHz in a Varian NMR System 400 at 298 K.

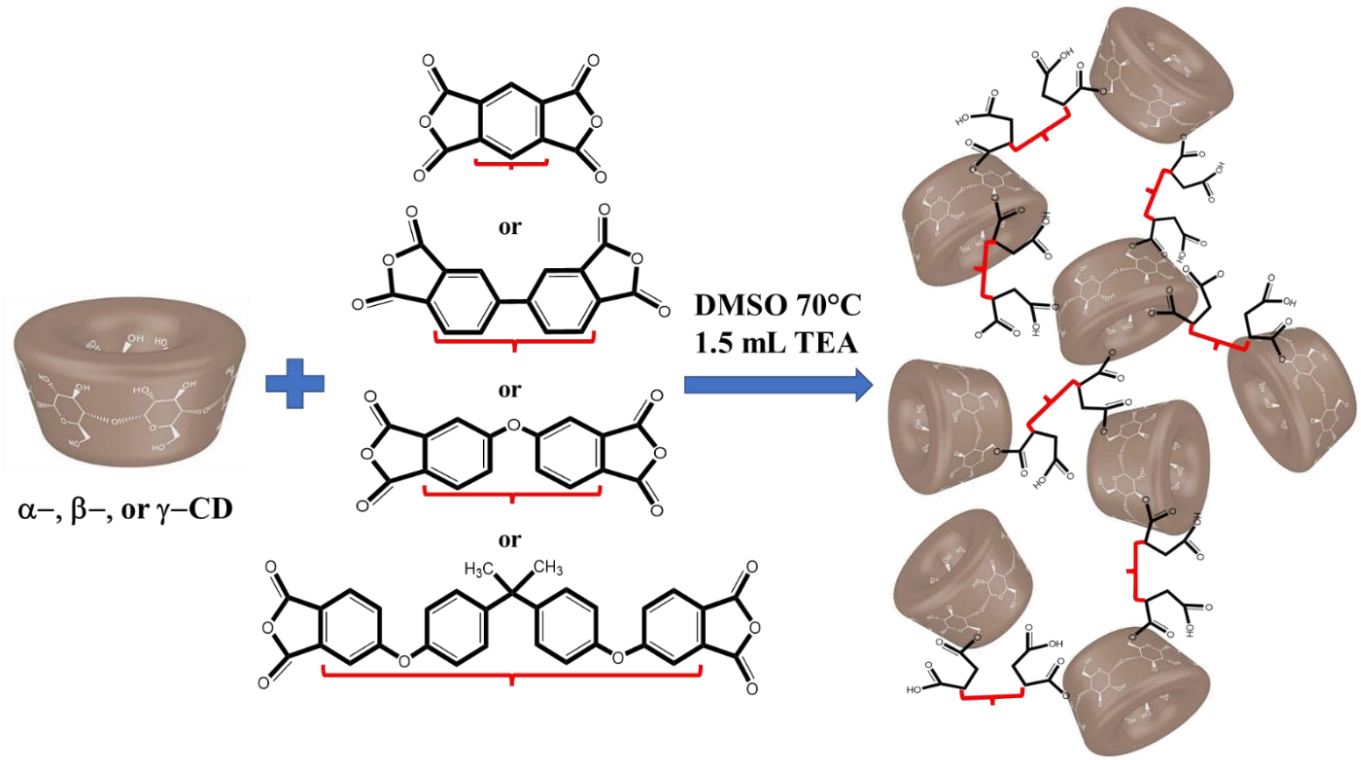

Figure 4.4. Synthesis preparation scheme of the CD-NS polymers

4.2.3 Toxin extraction estimation with ELISA experiments

Both okadaic acid and brevetoxin ELISA experiments are based on competitive enzyme immunoassays which were carried out following the procedure of the okadaic acid (OA) ELISA kit, from EuroProxima and the Brevetoxin (BRTX), ELISA, 96-test from Eurofins Abraxis. The microtiter plates coated with purified sheep antirabbit were used as received.

Previously, spiked solutions of the toxins at concentrations 5 ng/ml and 1 ng/mL (for OA and brevetoxin respectively) were prepared in MilliQ water. Afterwards, aliquots of 1.5 ml were added to 100 mg of the dried α–, β–, and γ– CD-NS (12 CD-NS plus three replicas for each of them) and three controls without polymers. All aliquots were vigorously stirred and subsequently centrifuged after 60 min, to isolate the supernatant and analyze the toxin concentration with the commercial ELISA kits.

The OA and brevetoxin calibration curves were prepared in the range from 2 to 10 ng/ml, and 0.2 to 2.5 ng/mL, respectively, by using the standard solutions available in each ELISA kit. The obtained absorbance of each sample was interpolated in the calibration curve to determine the remaining quantity of OA or brevetoxin in solution after the extraction with each CD-NS.

4.3 Results and Discussion

Twelve different insoluble CD-NS were synthesized using the three types of native CDs with four different types of anhydrides in order to have a complete set or family of polymeric materials that were tested as passive adsorbers for marine toxins.

4.3.1 Synthesis and characterization of CD-anhydride polymers

The reaction mechanism for the synthesis of CD-NS crosslinked with anhydrides has been described to be as a polycondensation reaction, where there is a nucleophilic attack mainly at the primary hydroxyl groups of the CDs, and the hydrogen atoms are substituted by the carbonyl ester bonds [20]. This type of crosslinking reaction typically produces insoluble CD-NS, although there are reports in the literature of this reaction producing a soluble polymeric material when using CD-derivatives instead of native CDs [21]. In this case the authors do not classify the material as a CD-NS but instead as a CD-polymer, precisely because of their water-soluble nature.

In this research, the main application that intended for the CD-NS, was as passive adsorbers for marine toxins. In this sense, it was important to obtain an insoluble material, to be able to separate it easily from water. The rigidity or stiffness of the synthesized CD-NS has been linked with the CD:crosslinker ratio used in the synthesis. Rossi et [22] performed a systematic characterization of the networking properties of PMDA CD-NS at different CD:PMDA ratios. Their findings show that the reticulation in CD-NS grows to a saturation level, after which there is no further crosslinking of the whole system, but rather some branching of CD units. The molar ratio for the maximum crosslinking in CD-NS was found to be 1:6 CD:PMDA.

Taking this into account, we performed the synthesis of the PMDA, OXY, and BISPH CD-NS using a 1:6 molar ratio. Nevertheless, for the case of the ISO CD-NS, when performing the synthesis at the aforementioned ratio, it was not possible to obtain a rigid polymeric mass with neither of the three native CDs. A possible rationale for this, is that since ISO is the longest anhydride molecule used, the effect of steric hindrance affects the crosslinking reaction at a lower CD:crosslinker ratio. It was possible to overcome this issue by using a lower CD:ISO ratio of 1:4 for which we were able to obtain the rigid polymeric mass we were aiming for.

4.3.2 Furier Transform infrared spectroscopy

FTIR analysis is a useful tool to determine structural information from the synthesized material by showing the presence of specific functional groups. The presence of a wide band at 1727 cm-1 in all the 12 synthesized CD-NS can be attributed to the ester carbonyl group (C=O). This is the most important peak since it demonstrates the successful crosslinking between the and the anhydride molecules [23]. Moreover, these peaks are not present in the spectra of the native α– β– or γ–CD (Figure 4.5).

Additionally, it can be observed a much smaller presence of bands at 3300 cm−1 attributed to O-H stretching in all the CD-NS in comparison to the native CD. 1474 cm−1 due to C-H bending, 1021 cm−1 due to C-O stretching [24].

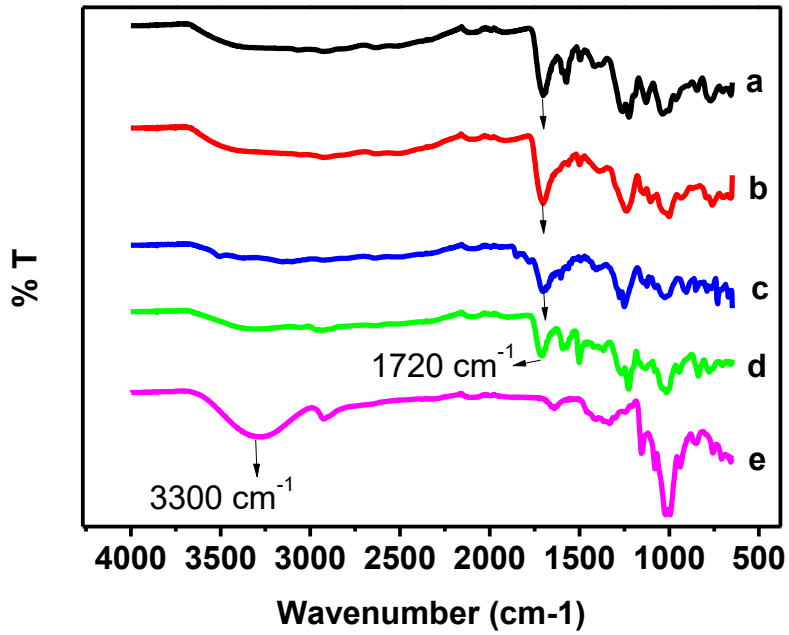

Figure 4.5 FTIR spectra of β-CD-NS crosslinked with a. OXY anhydride b. PMDA anhydride c. BISPH anhydride d. ISO anhydride and e. Native β-CD (The FTIR spectra of the α-CD-NS and γ-CD-NS can be found in the annex section)

4.3.3 Thermo gravimetric analysis (TGA)

The thermal stability of all the synthesized CD-NS was evaluated by following the weight loss during pyrolysis using the thermogravimetric analysis (TGA). The obtained thermograms (Figure 4.6) show similar three main stages of degradation for all the synthesized CD-NS. The first degradation stage corresponds to the evaporation of water and organic solvents present in the samples used to wash the CD-NS and occurs before reaching 100 °C. The second stage is the main degradation step where occurs the largest mass loss in the CD-NS and takes place between 250 °C and 450 °C. From these results we can conclude that all the synthesized CD-NS have a thermal stability up to ≈250°C. The last step occurs over 450 °C and has been

considered as a rearrangement of the char [25]. The obtained results are in agreement with previously reported studies for the PMDA CD-NS [25–27].

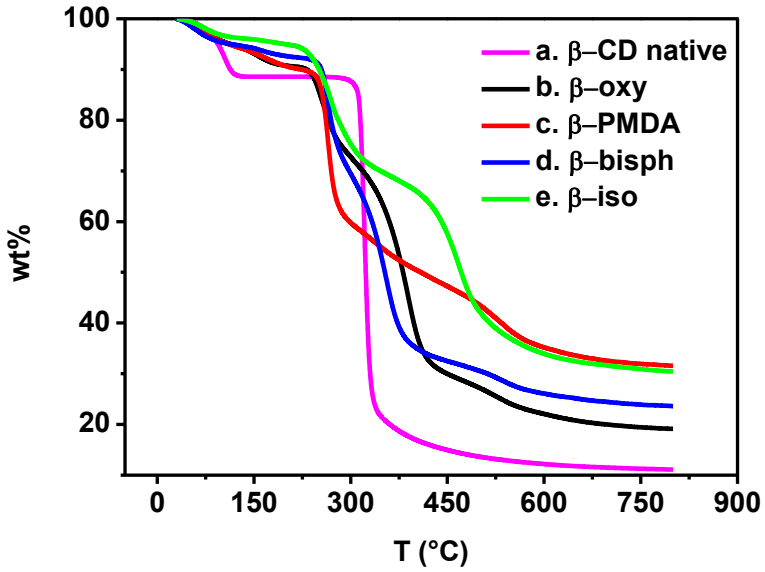

Figure 4.6 Thermograms of native β-CD (a) and β-CD-NS crosslinked with b. OXY anhydride c. PMDA anhydride d. BISPH anhydride and e. ISO anhydride. (The thermograms of the α-CD-NS and γ-CD-NS can be found in the annex section)

4.3.4 X-Ray Diffraction

XRD patterns of the CD-NS demonstrate the formation of a new amorphous material (Figure 4.7). This is observed in the absence of sharp Bragg peaks in the range from 5 to 40◦ as well as the presence of wider peaks in comparison to those of the native CDs which are crystalline materials. This is in agreement with previously reported data from the classic PMDA-NS [28].

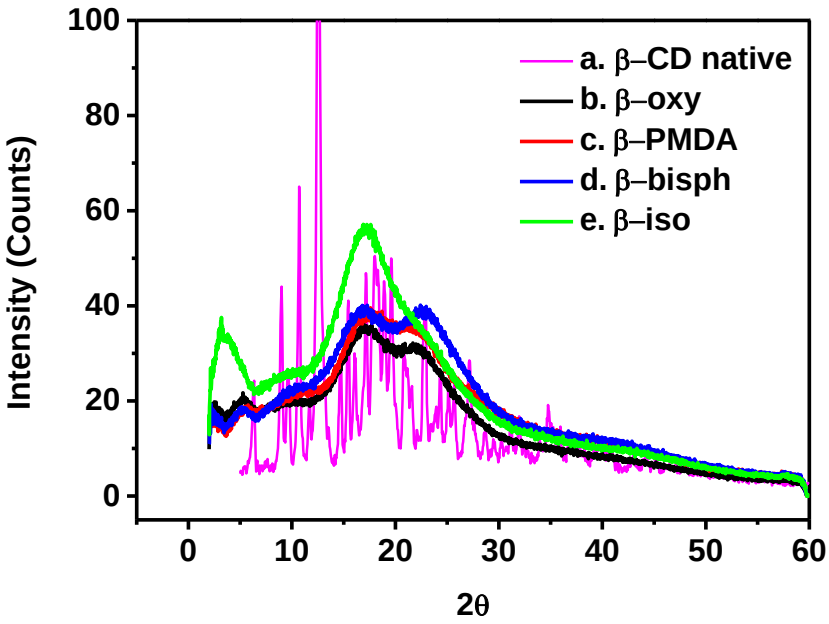

Figure 4.7 XRD patterns of β-CD-NS crosslinked with a. Native β-CD b. OXY anhydride c. PMDA anhydride d. BISPH anhydride and e. ISO anhydride. (The XRD patterns of the α-CD-NS and γ-CD-NS can be found in the annex section)

Moreover, the presence of a big and wider peak between 10-30° in the XRD patterns corresponding to the ISO CD-NS (green lines in Figure4.7) indicates that the CD units lie further apart between each other [29] in the polymeric material. This is expected because those particular CD-NS are crosslinked by the ISO anhydride which is the longest anhydride molecule used in the synthesis.

4.3.5 ^{1}H-NMR Spectroscopy

In order to further study the synthesized CD-NS, it was important to estimate the amount of ester bridges formed between the anhydrides crosslinkers and each of the CDs during the polymerization reaction. Since the obtained CD-NS are insoluble in water and organic solvents, we performed ester hydrolysis experiments at 90ºC in DMSO and basic medium to solubilize the polymers and subsequently characterized them with proton ^{1}H-NMR. Several reports in the literature have shown that the use of dimethyl sulfoxide (DMSO) as a solvent in ester hydrolysis results in a great increase of the hydrolysis reaction rate in comparison with water as a solvent [30] [31]. This has been attributed to the fact that DMSO is a polar aprotic solvent which effectively results in a lower activation energy barrier (ΔG) for the hydrolysis reaction due to a lower enthalpy of activation [32].

Figure 4.8 shows the proton ^{1}H-NMR spectra performed on the polymers once they were hydrolyzed and thus, dissolved in the DMSO-d6/NaOD solution. The value of the anomeric carbon in each one of the CDs was set fixed according to the amount of glucopyranose units (6, 7 or 8 for α, β or γ-CD, respectively). After integrating the peaks corresponding to the anhydride protons and dividing by the number of protons in each anhydride molecule, it was possible to estimate the real number of crosslinking units per CD unit (which could also be understood as the ‘degree of substitution’ of the monomer unit), as shown in Table 4.2. Having this information, it is also possible to estimate the molecular weight of the monomer unit.

Table 4.2 Number of anhydride molecules linked per CD unit and molar weight estimation for the monomer units

Polymer / Characteristics	≈Anhydride moieties per CD (NMR)	Number of protons in anhydride molecule	≈Mw monomer unit
α-PMDA	7.4	2.0	2545.1
β-PMDA	8.0	2.0	2884.3
γ-PMDA	6.6	2.0	2725.8
α-oxy	5.8	6.0	3094.2
β-oxy	7.0	6.0	3302.3
γ-oxy	6.0	6.0	3158.4
α-bisphe	5.1	6.0	2806.8
β-bisphe	5.8	6.0	2831.5
γ-bisphe	7.2	6.0	3418.8
α-iso	3.8	6.0	3261.9
β-iso	3.9	6.0	3173.6
γ-iso	3.8	6.0	3283.6

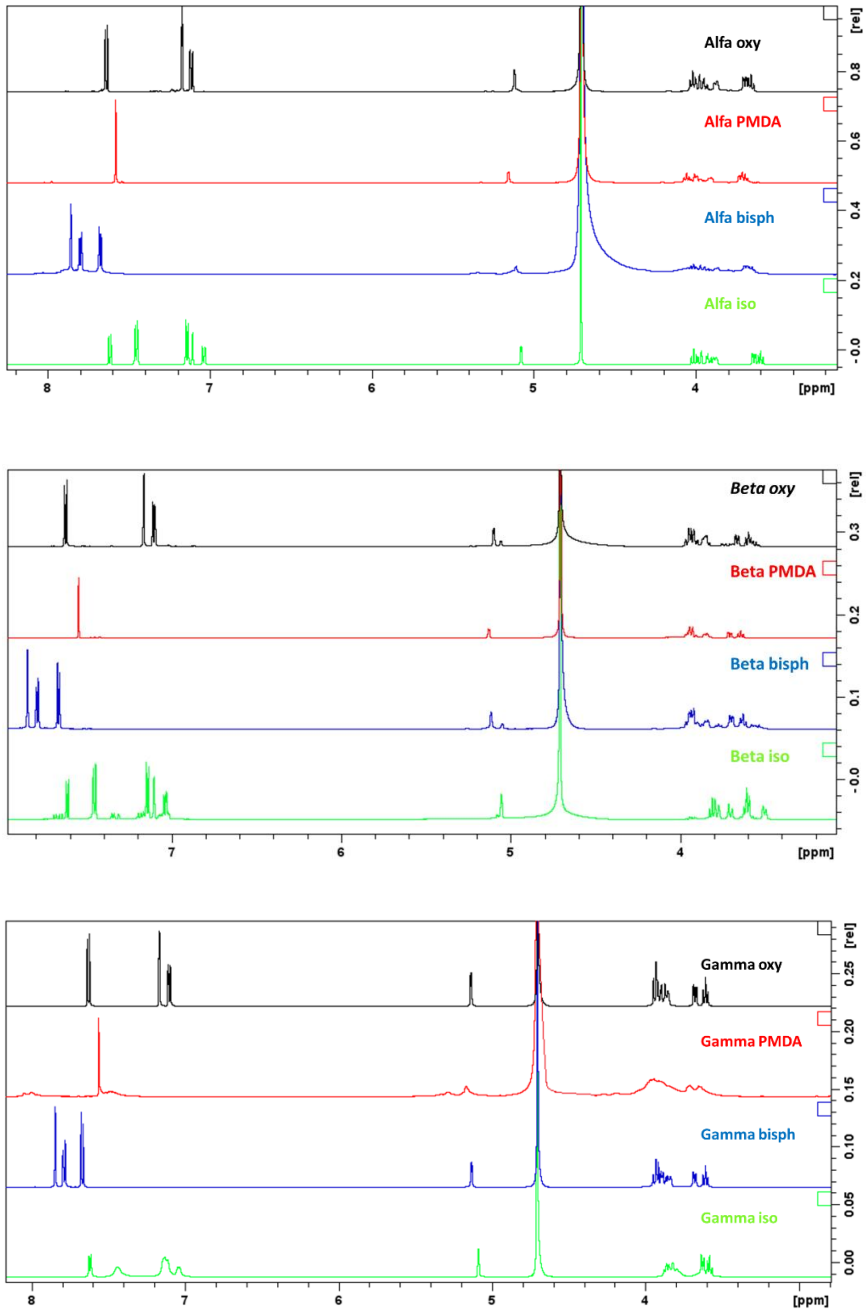

Figure 4.8 ^{1}H-NMR spectra of the hydrolyzed a. α-cyclodextrin-based anhydride NS b. β-cyclodextrin-based anhydride NS and c. γ-cyclodextrin-based anhydride NS

In general, the hydrolysis experiments show that the number of anhydride molecules that are effectively crosslinked per CD unit does not always correspond to the same CD:anhydride ratio initially used in the synthesis. This means that for some of the CD-NS there is some unreacted CD and for other cases there is unreacted anhydride. This is possibly due to …

4.3.6 FESEM and TEM

FESEM and TEM microscopy images were taken to visualize the morphology of the materials. Prior to be introduced in the FESEM microscope, the CD-NS were sputter-coated with gold to avoid charge accumulation and enhance the image quality. In the FESEM images (Figure 4.9), it can be observed that all the CD-NS have a similar morphology; the materials exhibit a sort of corrugation or stretch mark-like morphology which has also been observed in previously synthesized PMDA CD-NS [25,27]. The formation of any pores or cavities in the material was not observed in the micro scale. For the case of TEM microscopy (Figure 4.10), it was possible to observe the CD-NS particles at different sizes. Interestingly, all the PMDA-NS form a gel-like film which makes it difficult to observe in their particle form. This can be attributed to the very high degree of swelling of these types of CD-NS. Another interesting observation was obtained for the β-OXY-NS, which showed the formation of elongated nanometric structures which seem to be stacking among each other. This was only observed for this specific CD-NS.

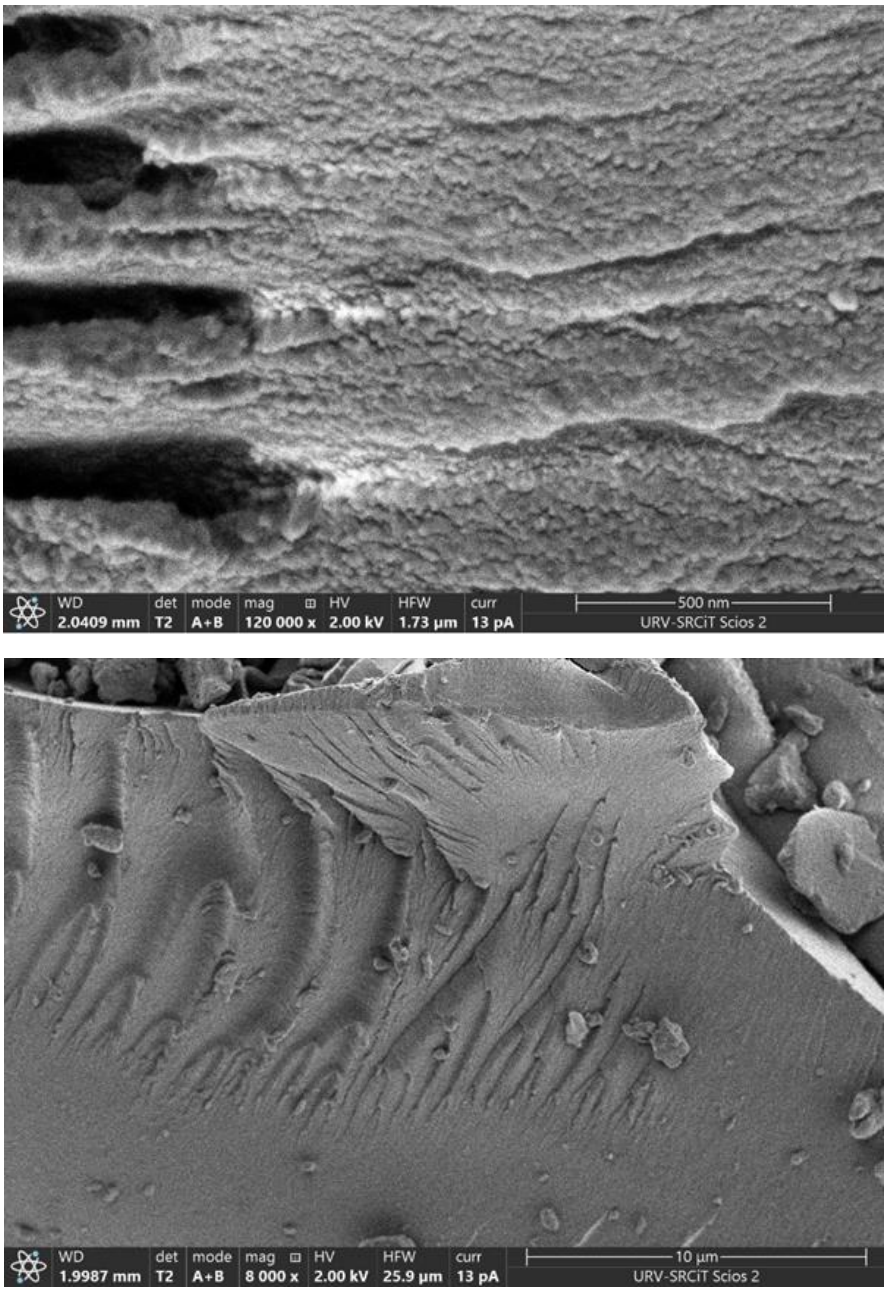

Figure 4.9 FESEM images of BISPH-β-CD-NS seen at a magnification of 120000 x (top) and 8000 x (bottom). The FESEM images for all the rest of CD-NS can be found in the annex section

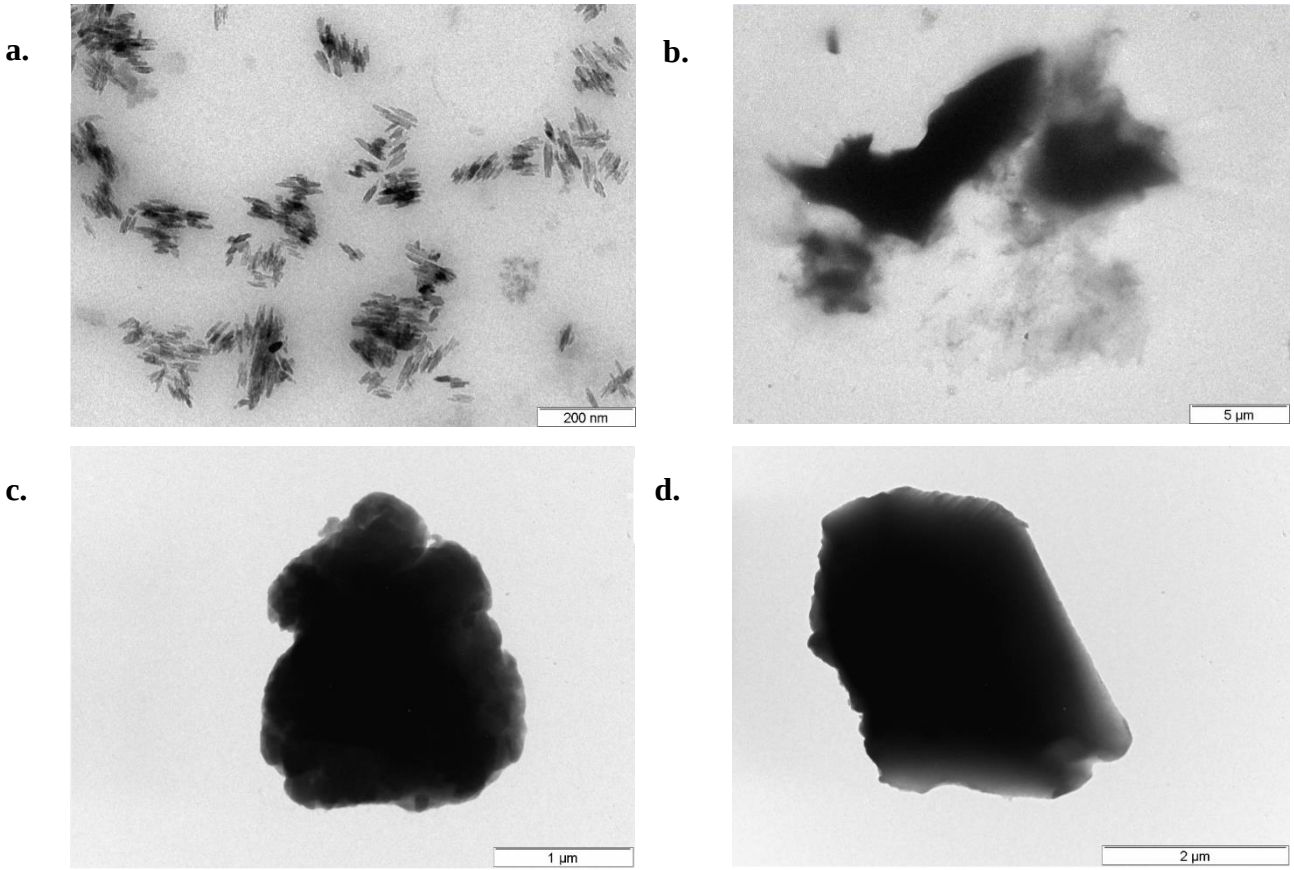

Figure 4.10 TEM images of β-CD-NS crosslinked with a. OXY anhydride b. PMDA anhydride c. BISH anhydride and d. ISO anhydride at different magnifications. The TEM images for the α- and γ-CD-NS and can be found in the annex section

4.3.7 Enzyme linked immuno assay (ELISA) experiments

The final evaluation performed on the synthesized materials consisted in developing a proof-of-concept experiment to test the capacity of the CD-NS to extract marine toxins at a fixed concentration of 5 ng/mL for okadaic acid and 1 ng/mL for brevetoxin in a time of 60 min. We performed competitive ELISA experiments in triplicate to verify the final concentration of marine toxin in solution after the extraction with each CD-NS.

In each of the competitive ELISA assays, either the okadaic acid or the brevetoxin present in the sample compete with a horse radish peroxidase (HRP) enzyme modified and covalently linked with either of the two toxins (OA-HRP or BVTX-HRP) to bind the anti-OA or anti-BVTX antibodies. Each toxin has a higher affinity for their specific antibodies, thus, if present in the sample the toxins will be bind by the specific antibodies. The OA-HRP or BVTX-HPR will bind to the remaining free antibodies. The process is visualized by using TMB as substrate and the absorbance is measured spectrophotometrically. The absorbance value is inversely proportional to the toxin concentration in the sample [33].

The okadaic acid and brevetoxin are long polyether molecules (Figure 4.2) that affect the human health by inhibiting protein phosphatases (in the case of the okadaic acid) [34], or by blocking the voltage gated sodium channels of cells (in the case of brevetoxin) [35]. The toxin ingestion produces the diseases neurotoxic shellfish poisoning (NSP) and diarrhetic shellfish poisoning (DSP) (Table 4.1). Our initial hypothesis was that given the big size of the marine toxin molecules, the CD that would best host them would be γ-CD given its bigger inner cavity size. Moreover, we hypothesized that CD-NS with a longer crosslinker and the biggest CD cavity (i.e., the ISO-γ-CD-NS)

would perform in a better way by capturing more amount of marine toxins. Figures 4.11 and 4.12 show the final concentrations of okadaic acid and brevetoxin, respectively, which remains in solutions after CD-NS extraction. The PMDA-CD-NS were unsuccessful to capture any of the two marine toxins, this is possibly due to the high swelling of these type of CD-NS in water which also made it very difficult to separate them from the solution. The other CD-NS synthesized with anhydride crosslinkers OXY, BISPH and ISO were successful to capture the marine toxins in solution at different extents, except for the case of the OXY-β-CD-NS. As we could see with TEM microscopy, this particular CD-NS has a different morphology to the rest of CD-NS, showing some stacked particles, and we can speculate that this is affecting the adsorption capacity for this CD-NS.

Interestingly, our initial hypothesis was proved to be incorrect since the ISO-γ-CD-NS captured much less quantity of either OA or BRTX.

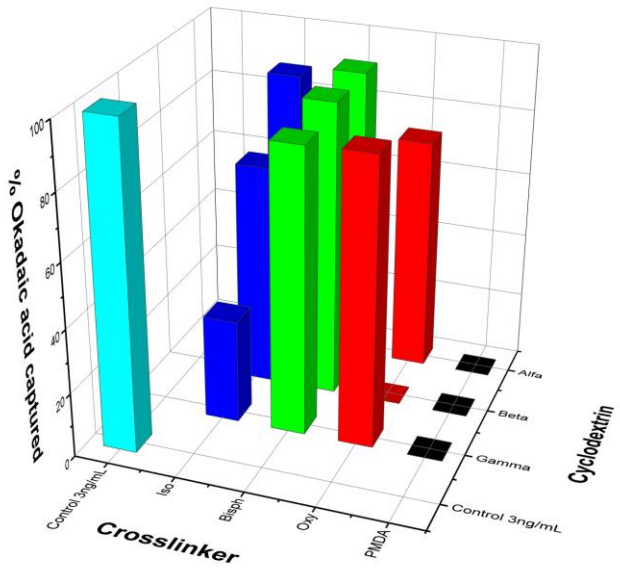

Figure 4.11 Concentration of okadaic acid remaining in solution after the extraction with CD-NS.

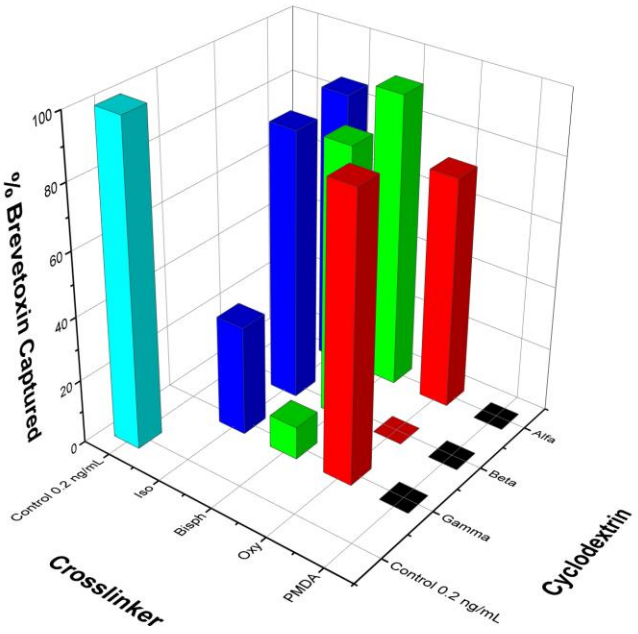

Figure 4.12 Concentration of brevetoxin remaining in solution after the extraction with CD-NS.

4.4 Conclusions

We have successfully synthesized a complete battery of 12 different types of CD-NS by using 4 types of anhydrides crosslinkers of different length and the 3 types of native CDs. From the obtained CD-NS, only the classical PMDA-CD-NS had been previously synthesized and characterized in the literature. The materials were characterized with different techniques that corroborated the formation of an insoluble polymeric material. Finally, proof-of-concept ELISA experiments confirmed the trapping of marine toxins okadaic acid and brevetoxin by all CD-NS with exception of the ones crosslinked with PMDA. This work is the first report of an application for CD-NS in marine toxin capture and becomes a potential application as a SPATT material for monitoring and forecasting future HAB trends.

4.5 References

1. Hallegraeff, G.; Enevoldsen, H.; Zingone, A. Global harmful algal bloom status reporting. *Harmful Algae* **2021**, *102*, doi:10.1016/j.hal.2021.101992.

2. Pal, M.; Yesankar, P.J.; Dwivedi, A.; Qureshi, A. Biotic control of harmful algal blooms (HABs): A brief review. *J. Environ. Manage.* **2020**, *268*, 110687, doi:10.1016/j.jenvman.2020.110687.

3. Anderson, D.M. Approaches to monitoring, control and management of harmful algal blooms (HABs). **2009**, doi:10.1016/j.ocecoaman.2009.04.006.

4. Paul, V.J.; Arthur, K.E.; Ritson-Williams, R.; Ross, C.; Sharp, K. Chemical defenses: From compounds to communities. *Biol. Bull.*

2007, *213*, 226–251, doi:10.2307/25066642.

5. Heisler, J.; Glibert, P.M.; Burkholder, J.M.; Anderson, D.M.; Cochlan, W.; Dennison, W.C.; Dortch, Q.; Gobler, C.J.; Heil, C.A.; Humphries, E.; et al. Eutrophication and harmful algal blooms: A scientific consensus. *Harmful Algae* **2008**, *8*, 3–13, doi:10.1016/j.hal.2008.08.006.

6. Hallegraeff, G.M. Harmful algal blooms in the Australian region. *Mar. Pollut. Bull.* **1992**, *25*, 186–190, doi:10.1016/0025-326X(92)90223-S.

7. Anderson, C.R.; Moore, S.K.; Tomlinson, M.C.; Silke, J.; Cusack, C.K. *Living with Harmful Algal Blooms in a Changing World: Strategies for Modeling and Mitigating Their Effects in Coastal Marine Ecosystems*; Elsevier Inc., 2015; ISBN 9780123965387.

8. Petterson, L.H.; Pozdnyakov, D. *Monitoring of harmful algal blooms*; Springer, 2013; ISBN 9783540228929.

9. Medlin, L.K.; Orozco, J. Molecular Techniques for the Detection of Organisms in Aquatic Environments, with Emphasis on Harmful Algal Bloom Species. **2017**, doi:10.3390/s17051184.

10. Zhang, C.; Zhang, J. Current Techniques for Detecting and Monitoring Algal Toxins and Causative Harmful Algal Blooms. *J. Environ. Anal. Chem.* **2014**, *02*, 1–12, doi:10.4172/2380-2391.1000123.

11. MacKenzie, L.; Beuzenberg, V.; Holland, P.; McNabb, P.; Selwood, A. Solid phase adsorption toxin tracking (SPATT): A new monitoring tool that simulates the biotoxin contamination of filter feeding

bivalves. *Toxicon* **2004**, *44*, 901–918, doi:10.1016/j.toxicon.2004.08.020.

12. Gaysinski Marc, Ortalo-Magné Annick, P.T.O. and C.G. *Springer Protocols, Natural Products from Marine Algae*; 2015; Vol. 2; ISBN 9781493926831.

13. Knap, A.; Dewailly, É.; Furgal, C.; Galvin, J.; Baden, D.; Bowen, R.E.; Depledge, M.; Duguay, L.; Fleming, L.E.; Ford, T.; et al. Indicators of ocean health and human health: Developing a research and monitoring framework. *Environ. Health Perspect.* **2002**, *110*, 839–845, doi:10.1289/ehp.02110839.

14. Wells, M.L.; Karlson, B.; Wulff, A.; Kudela, R.; Trick, C.; Asnaghi, V.; Berdalet, E.; Cochlan, W.; Davidson, K.; De Rijcke, M.; et al. Future HAB science: Directions and challenges in a changing climate. *Harmful Algae* **2020**, *91*, doi:10.1016/J.HAL.2019.101632.

15. Campàs, M.; Rambla-Alegre, M.; Wirén, C.; Alcaraz, C.; Rey, M.; Safont, A.; Diogène, J.; Torréns, M.; Fragoso, A. Cyclodextrin polymers as passive sampling materials for lipophilic marine toxins in Prorocentrum lima cultures and a Dinophysis sacculus bloom in the NW Mediterranean Sea. *Chemosphere* **2021**, *285*, doi:10.1016/j.chemosphere.2021.131464.

16. Roué, M.; Taiana Darius, H.; Chinain, M. Solid Phase Adsorption Toxin Tracking (SPATT) Technology for the Monitoring of Aquatic Toxins: A Review. *Toxins (Basel).* **2018**, doi:10.3390/toxins10040167.

17. Trotta, F.; Zanetti, M.; Cavalli, R. Cyclodextrin-based nanosponges as drug carriers. *Beilstein J. Org. Chem.* **2012**, *8*, 2091–2099,

doi:10.3762/bjoc.8.235.

18. Trotta, F.; Tumiatti, W. Patent Application Publication Pub. No.: US 2005/0154198A1 2005, *1*.

19. Trotta, F. Cyclodextrin Nanosponges and their Applications. *Cyclodextrins Pharm. Cosmet. Biomed. Curr. Futur. Ind. Appl.* **2011**, 323–342, doi:10.1002/9780470926819.ch17.

20. Castiglione, F.; Crupi, • V; Majolino, • D; Mele, • A; Panzeri, • W; Rossi, • B; Trotta, • F; Venuti, • V Vibrational dynamics and hydrogen bond properties of b-CD nanosponges: an FTIR-ATR, Raman and solid-state NMR spectroscopic study., doi:10.1007/s10847-012-0106-z.

21. Adeoye, O.; Bártolo, I.; Conceição, J.; Bento Da Silva, A.; Duarte, N.; Francisco, A.P.; Taveira, N.; Cabral-Marques, H. Pyromellitic dianhydride crosslinked soluble cyclodextrin polymers: Synthesis, lopinavir release from sub-micron sized particles and anti-HIV-1 activity. **2020**, doi:10.1016/j.ijpharm.2020.119356.

22. Rossi, B.; Caponi, S.; Castiglione, F.; Corezzi, S.; Fontana, A.; Giarola, M.; Mariotto, G.; Mele, A.; Petrillo, C.; Trotta, F.; et al. Networking properties of cyclodextrin-based cross-linked polymers probed by inelastic light-scattering experiments. *J. Phys. Chem. B* **2012**, *116*, 5323–5327, doi:10.1021/jp302047u.

23. Berto, S.; Bruzzoniti, A.M.C.; Cavalli, A.R.; Perrachon, A.D.; Prenesti, A.E.; Sarzanini, A.C.; Trotta, A.F.; Tumiatti, A.W. Synthesis of new ionic b-cyclodextrin polymers and characterization of their heavy metals retention., doi:10.1007/s10847-006-9273-0.

24. Gabr, M.M.; Mortada, S.M.; Sallam, M.A. Carboxylate cross-linked cyclodextrin: A nanoporous scaffold for enhancement of rosuvastatin oral bioavailability. **2017**, doi:10.1016/j.ejps.2017.09.026.

25. Varan, C.; Anceschi, A.; Sevli, S.; Bruni, N.; Giraudo, L.; Bilgiç, E.; Korkusuz, P.; İskit, A.B.; Trotta, F.; Bilensoy, E. Preparation and characterization of cyclodextrin nanosponges for organic toxic molecule removal. *Int. J. Pharm.* **2020**, *585*, doi:10.1016/j.ijpharm.2020.119485.

26. Zanetti, M.; Anceschi, A.; Magnacca, G.; Spezzati, G.; Caldera, F.; Rosi, G.P.; Trotta, F. Micro porous carbon spheres from cyclodextrin nanosponges. *Microporous Mesoporous Mater.* **2016**, *235*, 178–184, doi:10.1016/j.micromeso.2016.08.012.

27. Rafati, N.; Zarrabi, A.; Caldera, F.; Trotta, F.; Ghias, N. Pyromellitic dianhydride crosslinked cyclodextrin nanosponges for curcumin controlled release; formulation, physicochemical characterization and cytotoxicity investigations. *J. Microencapsul.* **2019**, *36*, 715–727, doi:10.1080/02652048.2019.1669728.

28. Mele, A.; Castiglione, F.; Malpezzi, L.; Ganazzoli, F.; Raffaini, G.; Trotta, F.; Rossi, B.; Fontana, A.; Giunchi, G. HR MAS NMR, powder XRD and Raman spectroscopy study of inclusion phenomena in bCD nanosponges., doi:10.1007/s10847-010-9772-x.

29. Storsberg, J.; Ritter, H. Cyclodextrins in polymer synthesis: A “green” route to fluorinated polymers via cyclodextrin complexes in aqueous solution. *Macromol. Chem. Phys.* **2002**, *203*, 812–818, doi:10.1002/1521-3935(20020401)203:5/6<812::AID-MACP812>3.0.CO;2-6.

30. Vinson, J.A. Hydrolysis of latex paint in dimethyl sulfoxide: An organic laboratory experiment. *J. Chem. Educ.* **1969**, *46*, 877, doi:10.1021/ed046p877.

31. Kojo, I.; Shoji, A.; Hanano, M. Solvent Effect of Dimethyl Sulfoxide on Alkaline Hydrolysis of Amide. *Chem. Pharm. Bull.* **1974**, *22*, 864–870.

32. Sorensen-Stowell, K.; Hengge, A.C. *Thermodynamic Origin of the Increased Rate of Hydrolysis of Phosphate and Phosphorothioate Esters in DMSO/Water Mixtures*;

33. Kreuzer, M.P.; O'Sullivan, C.K.; Guilbault, G.G. Development of an ultrasensitive immunoassay for rapid measurement of okadaic acid and its isomers. *Anal. Chem.* **1999**, *71*, 4198–4202, doi:10.1021/ac9901642.

34. Bialojan, C.; Takai, A. Inhibitory effect of a marine-sponge toxin, okadaic acid, on protein phosphatases. Specificity and kinetics. *Biochem. J.* **1988**, *256*, 283–290, doi:10.1042/bj2560283.

35. Baden, D.G. Brevetoxins: unique polyether dinoflagellate toxins; Brevetoxins: unique polyether dinoflagellate toxins. *FASEB J.* **1989**, *3*, 1807–1817, doi:10.1096/fasebj.3.7.2565840.

4.6 Annex

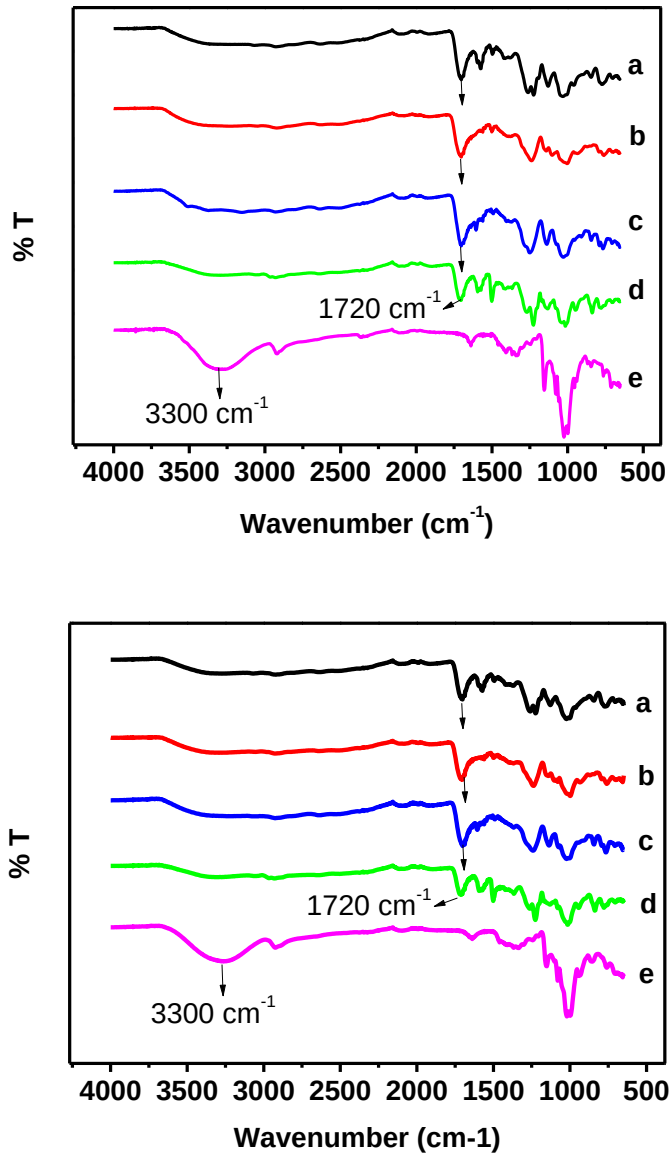

Annex 4.1 Top figure: FTIR spectra of α–CD-NS crosslinked with a. OXY anhydride b. PMDA anhydride c. BISPH anhydride d. ISO anhydride and e. Native α–CD **Bottom figure:** FTIR spectra of γ–CD-NS crosslinked with a. OXY anhydride b. PMDA anhydride c. BISPH anhydride d. ISO anhydride and e. Native γ–CD.

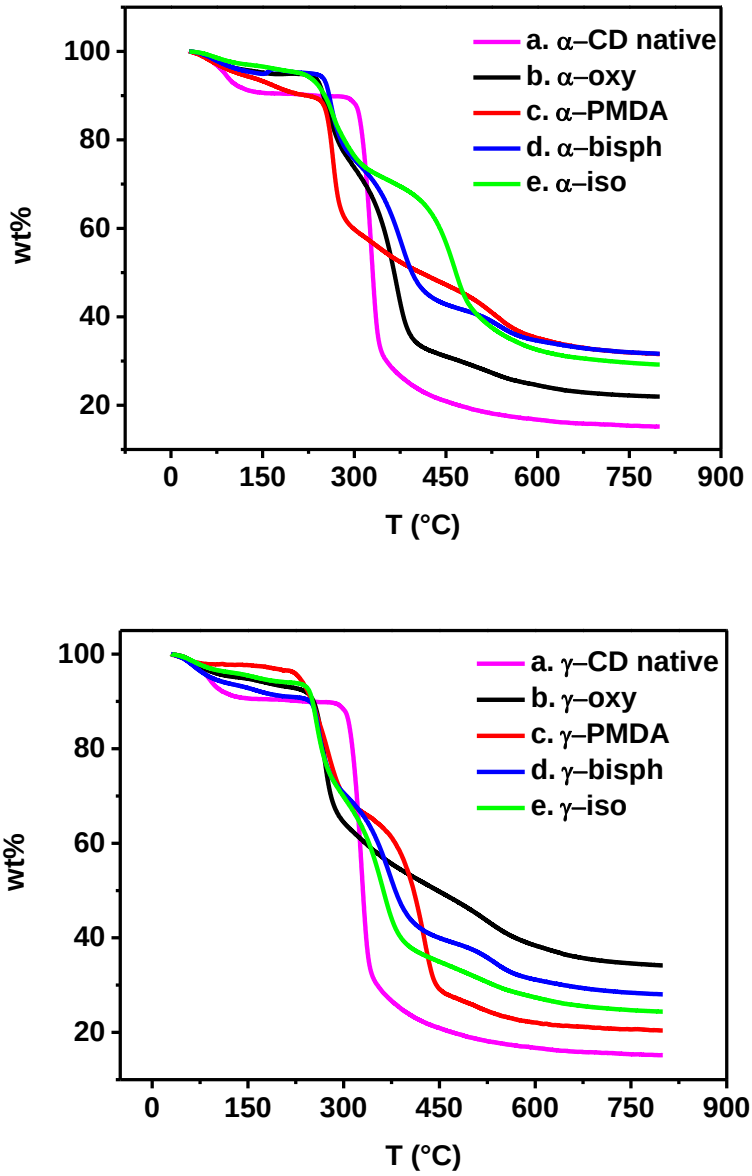

Annex 4.2 Top figure: Thermograms of native α–CD (a.) and α–CD-NS crosslinked with b. OXY anhydride c. PMDA anhydride d. BISPH anhydride and e. ISO anhydride. **Bottom figure:** Thermograms of native γ–CD (a.) and γ–CD-NS crosslinked with b. OXY anhydride c. PMDA anhydride d. BISPH anhydride and e. ISO anhydride.

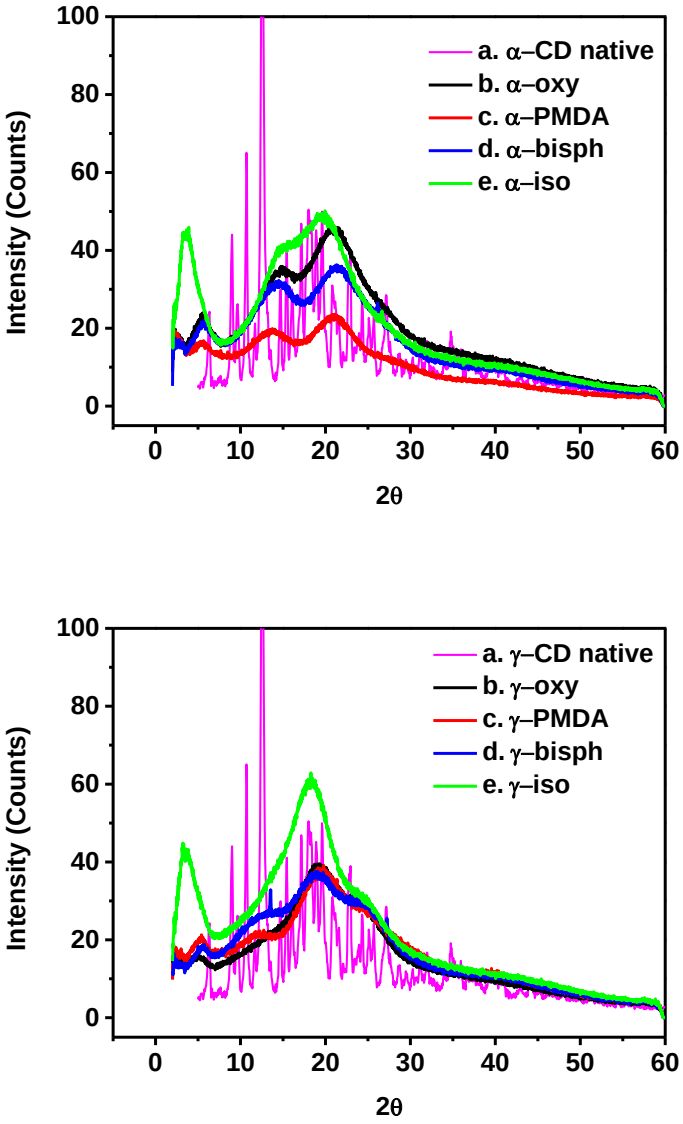

Annex 4.3 Top figure: XRD patterns of native α–CD (a.) and α–CD-NS crosslinked with b. OXY anhydride c. PMDA anhydride d. BISPH anhydride and e. ISO anhydride. **Bottom figure:** XRD patterns of native γ–CD (a.) and γ–CD-NS crosslinked with b. OXY anhydride c. PMDA anhydride d. BISPH anhydride and e. ISO anhydride.

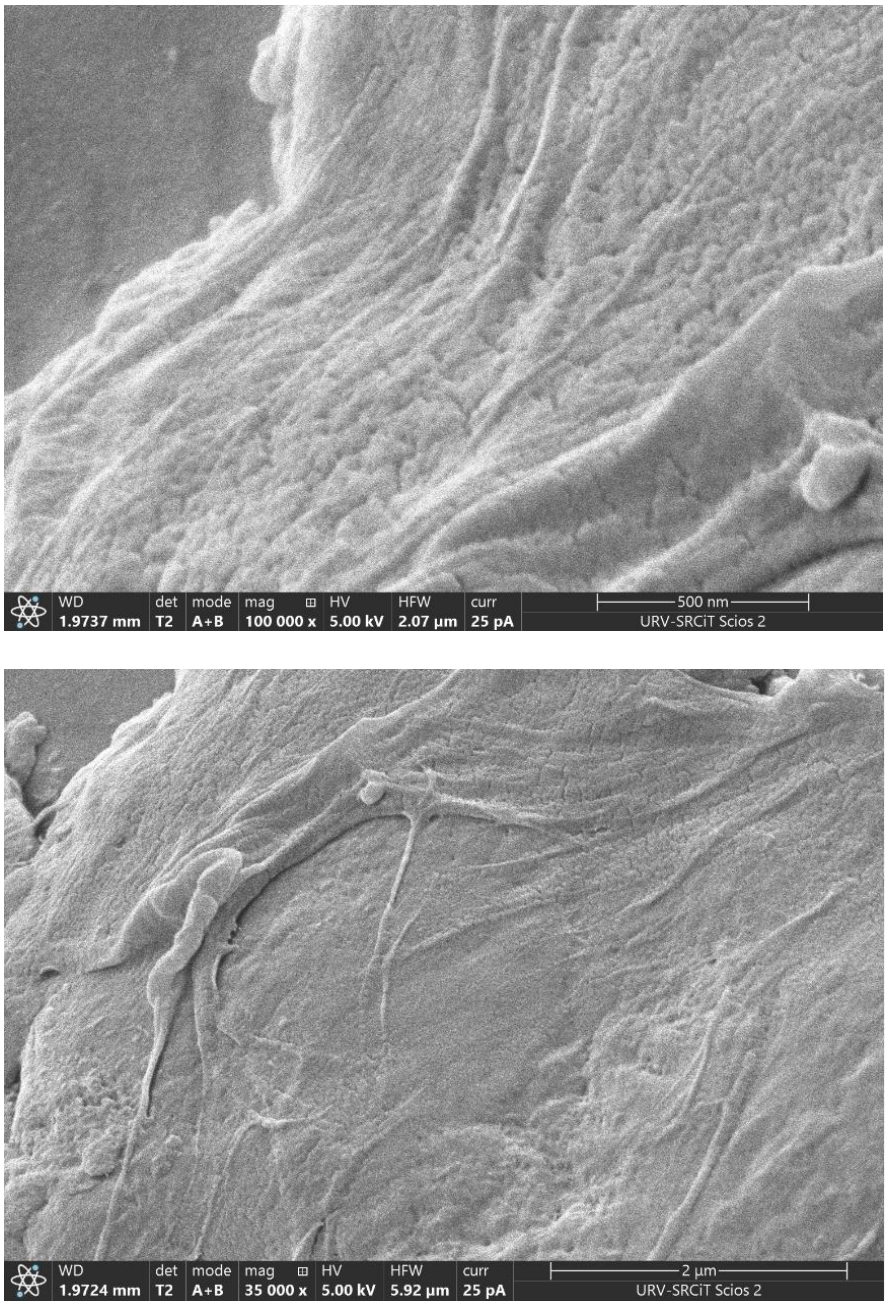

Annex 4.5 FESEM images of PMDA-α-CD-NS seen at a scale of 500 nm (top) and at lower magnification (bottom)

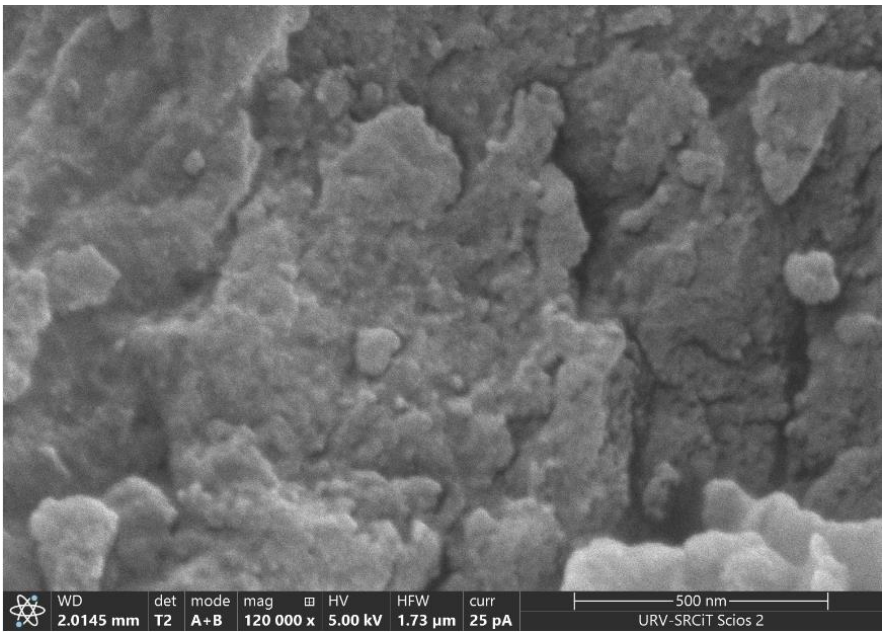

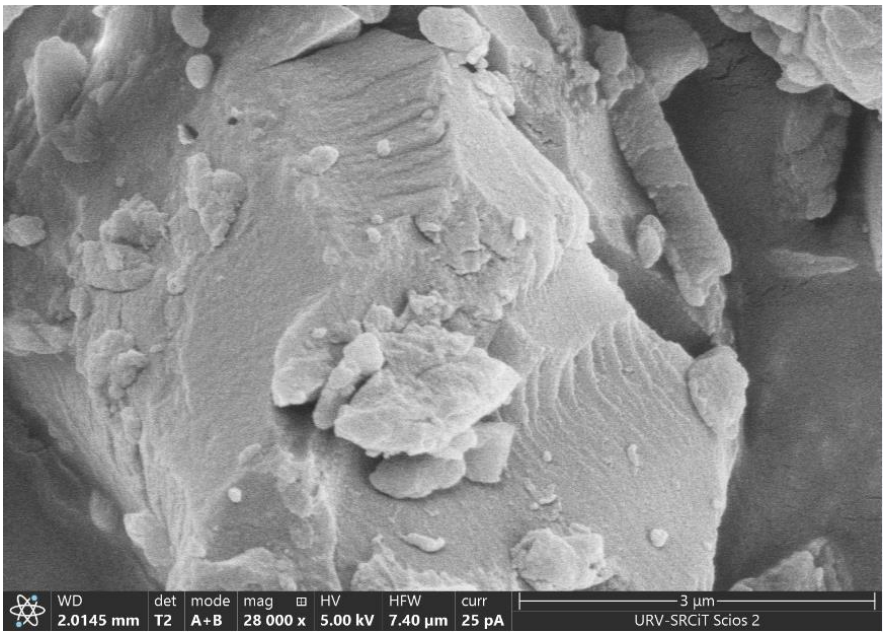

Annex 4.6 FESEM images of OXY-α-CD-NS seen at a scale of 500 nm (top) and at lower magnification (bottom)

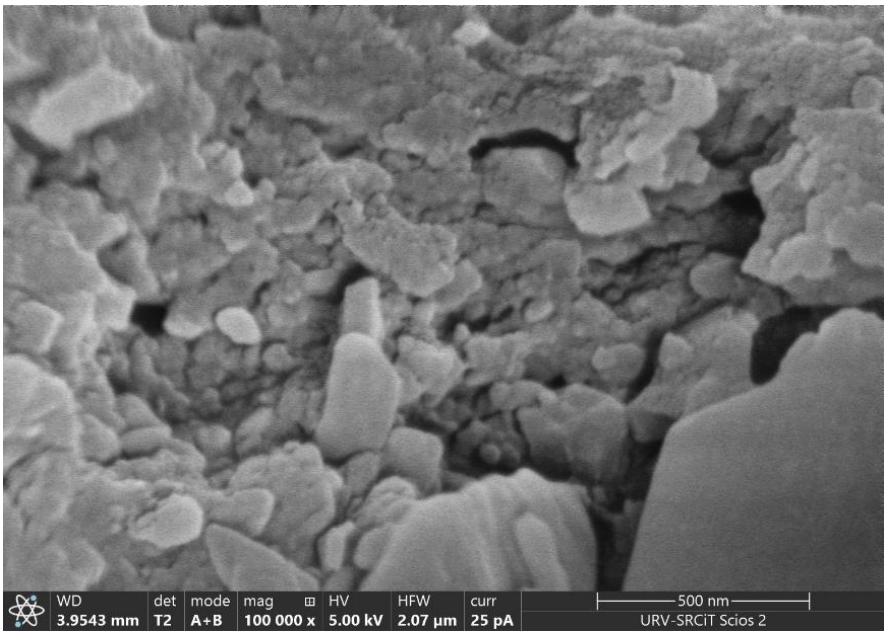

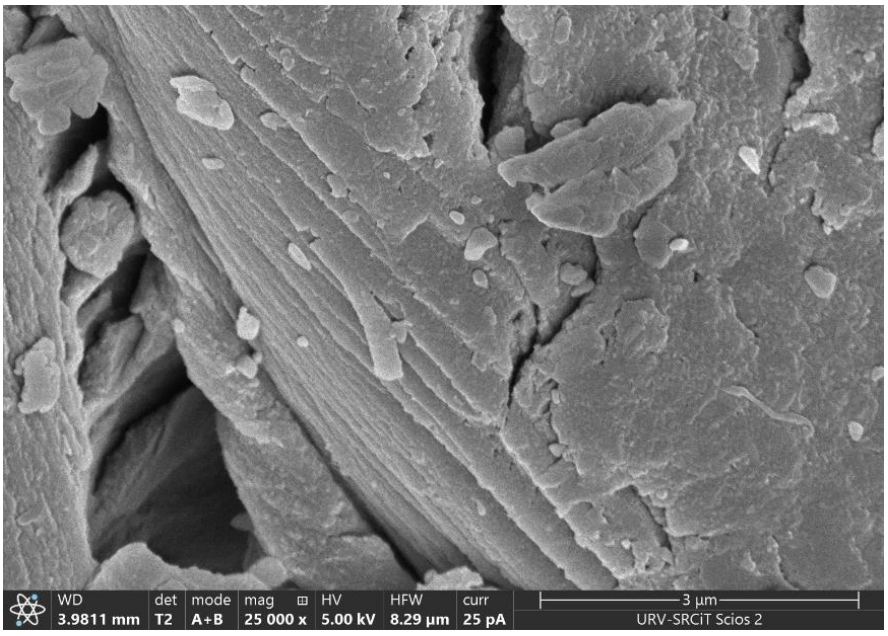

Annex 4.7 FESEM images of BISPH-α-CD-NS seen at a scale of 500 nm (top) and at lower magnification (bottom)

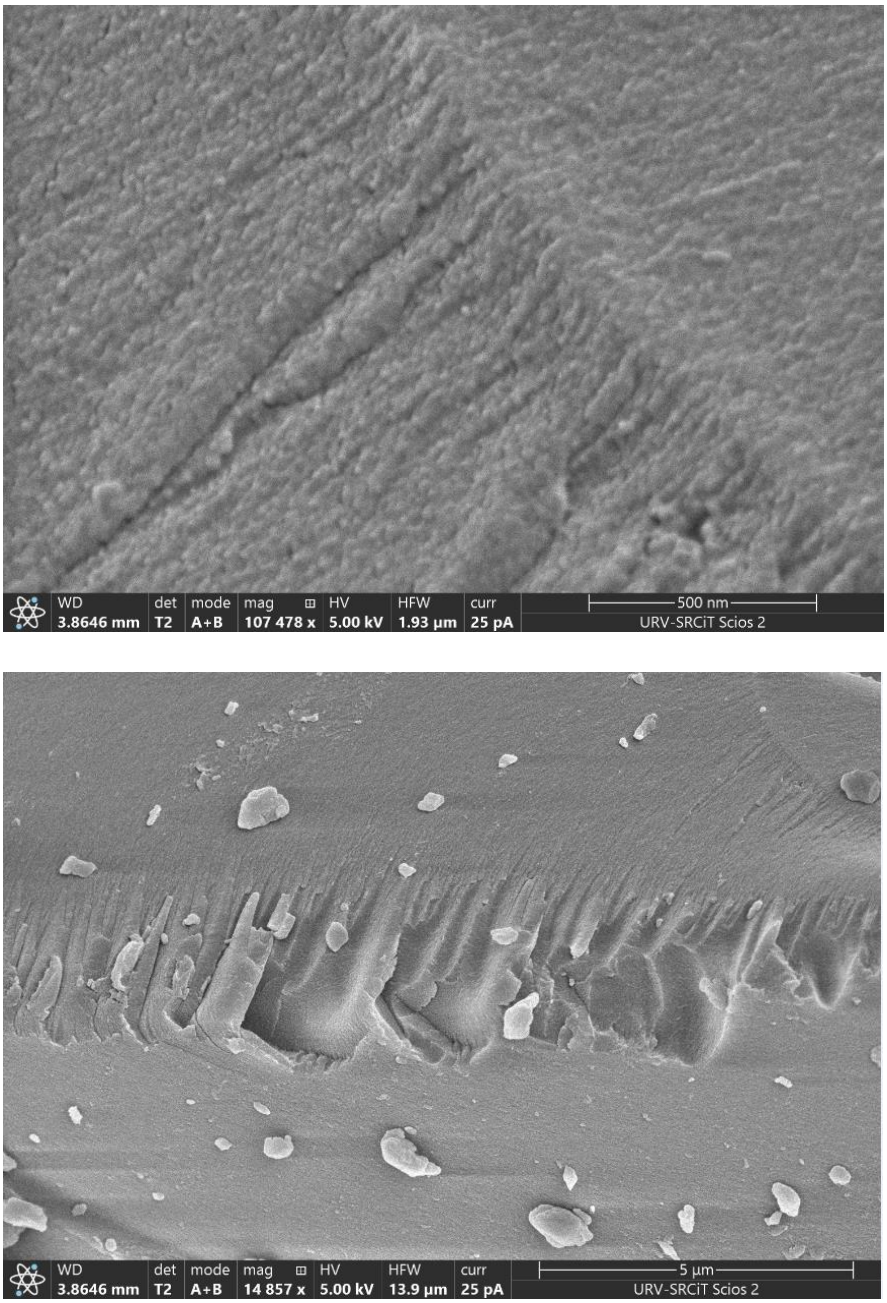

Annex 4.8 FESEM images of ISO-α-CD-NS seen at a scale of 500 nm (top) and at lower magnification (bottom)

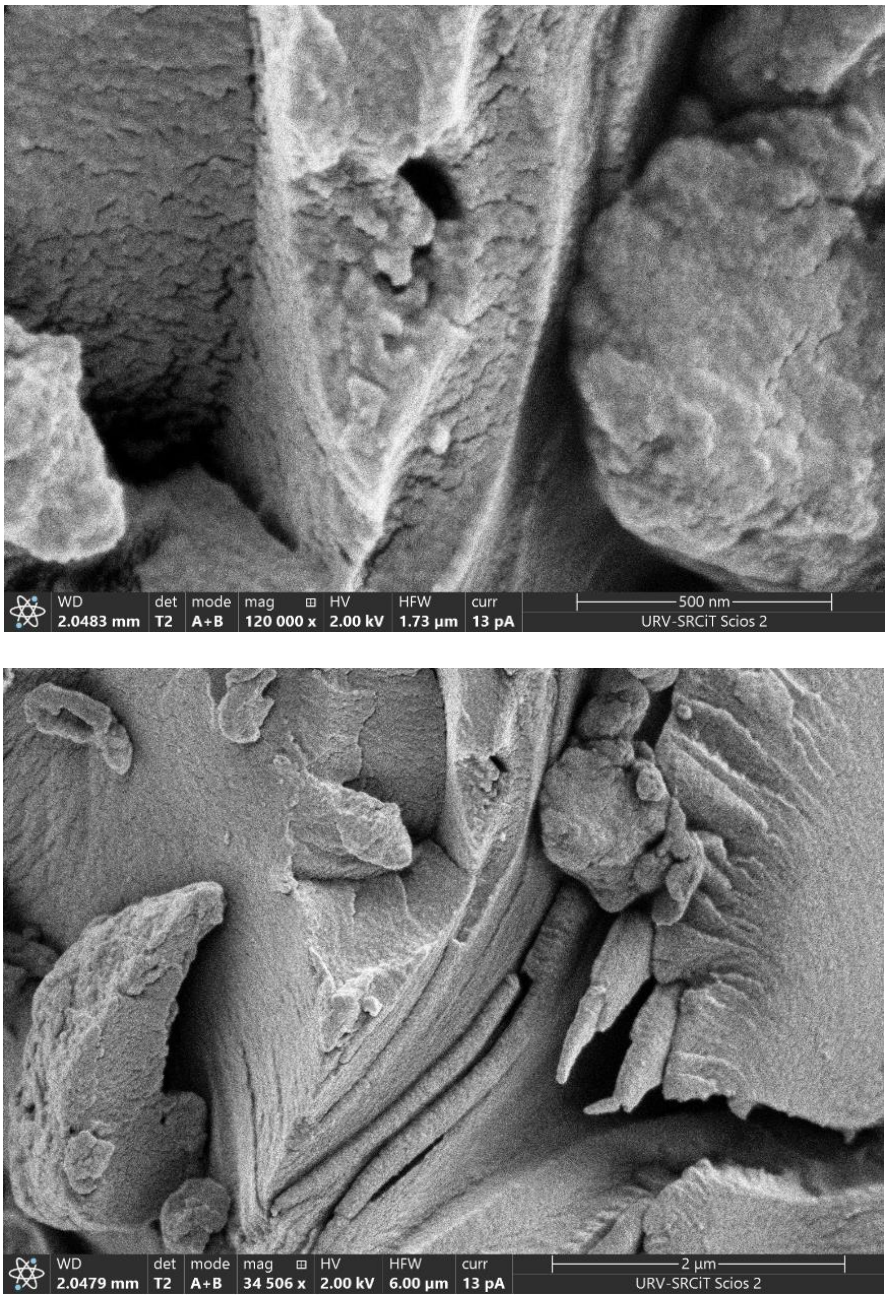

Annex 4.9 FESEM images of PMDA-β-CD-NS seen at a scale of 500 nm (top) and at lower magnification (bottom)

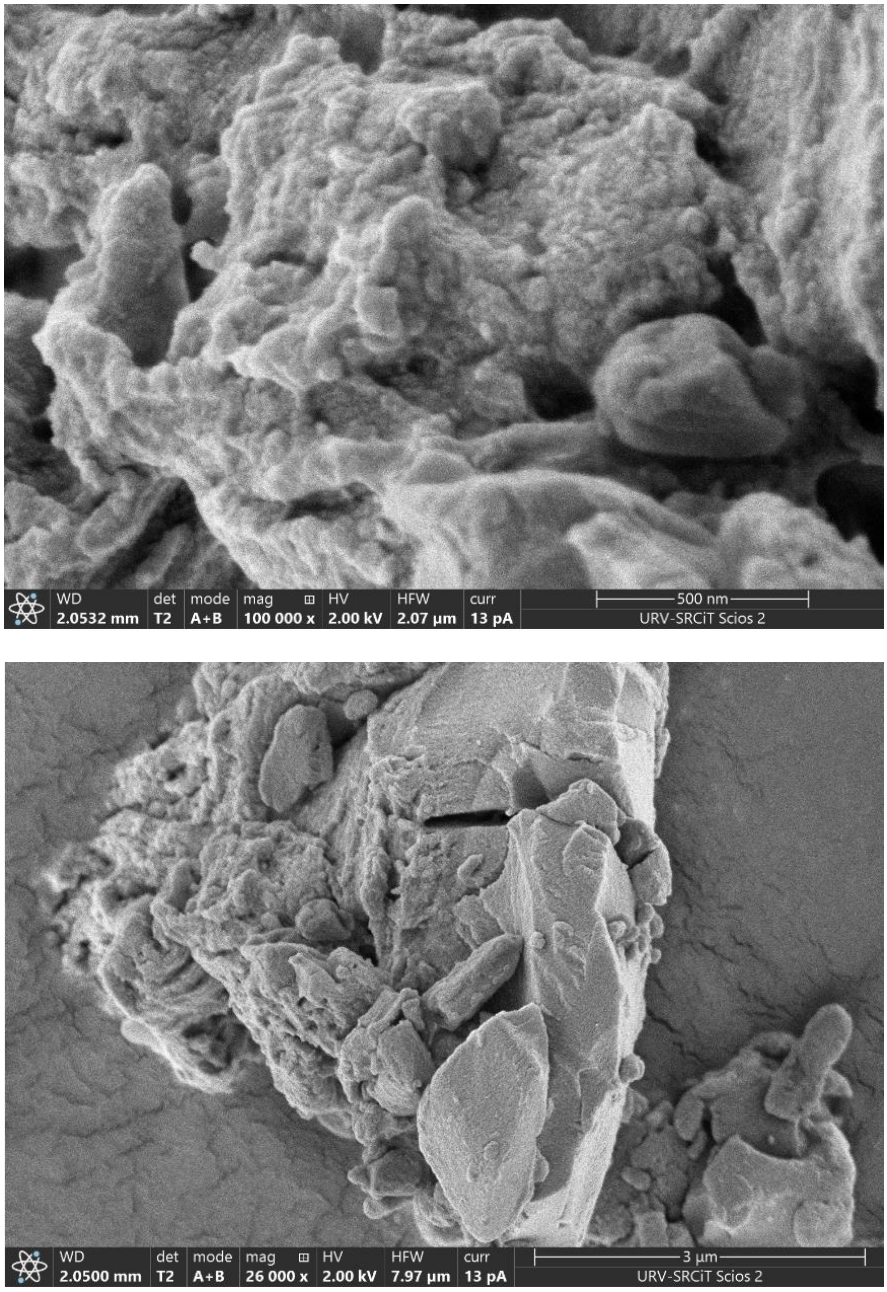

Annex 4.10 FESEM images of OXY-β-CD-NS seen at a scale of 500 nm (top) and at lower magnification (bottom)

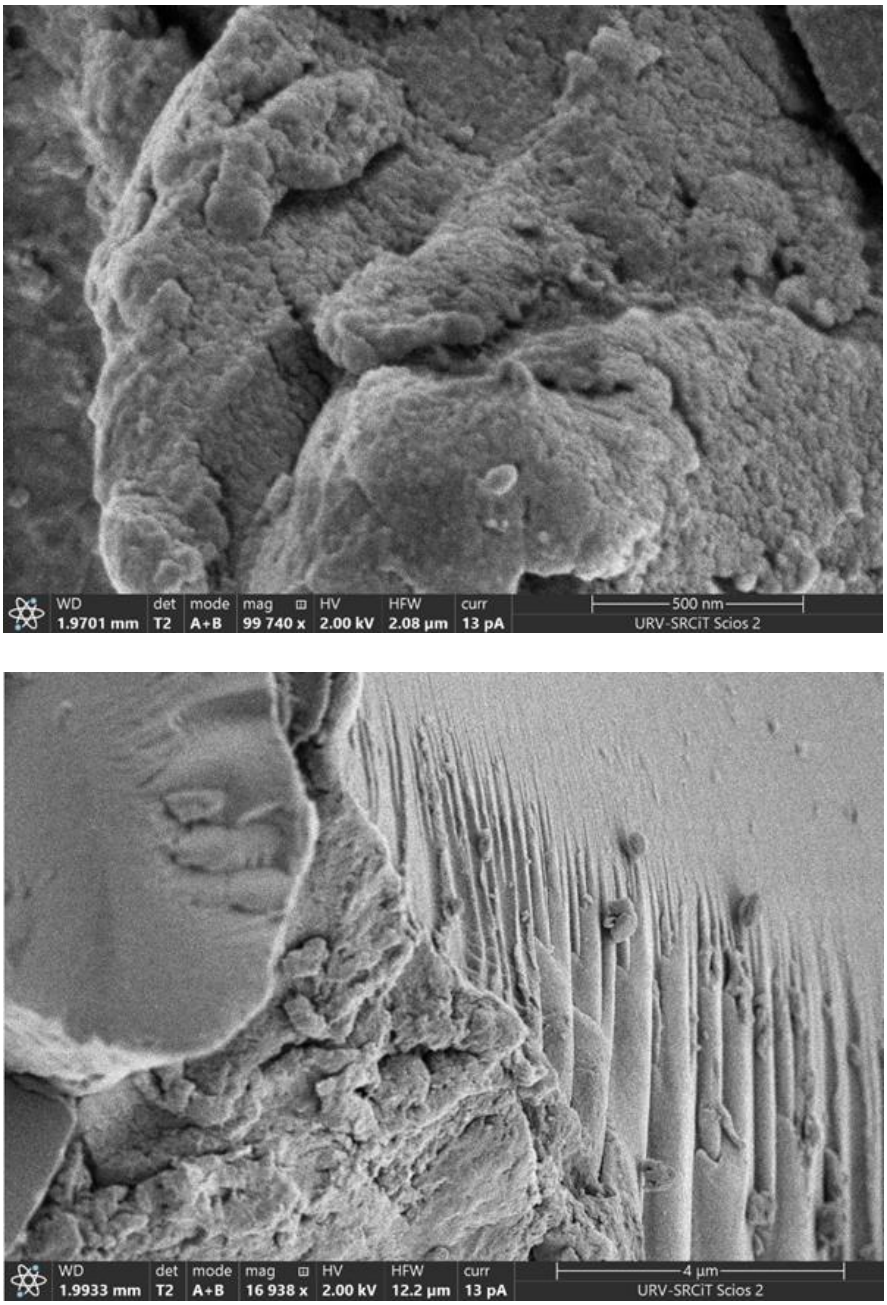

Annex 4.11 FESEM images of ISO-β-CD-NS seen at a scale of 500 nm (top) and at lower magnification (bottom)

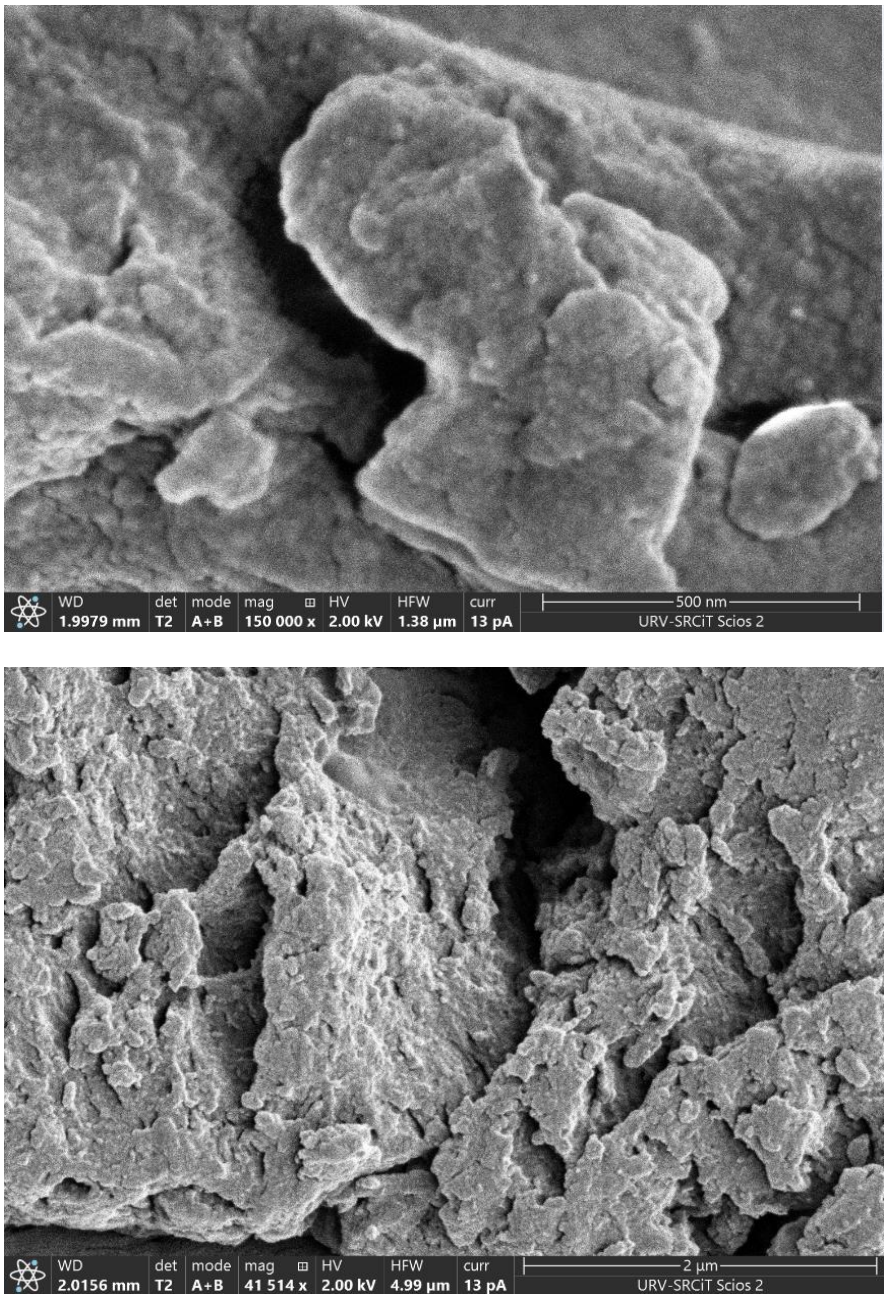

Annex 4.12 FESEM images of PMDA-γ-CD-NS seen at a scale of 500 nm (top) and at lower magnification (bottom)

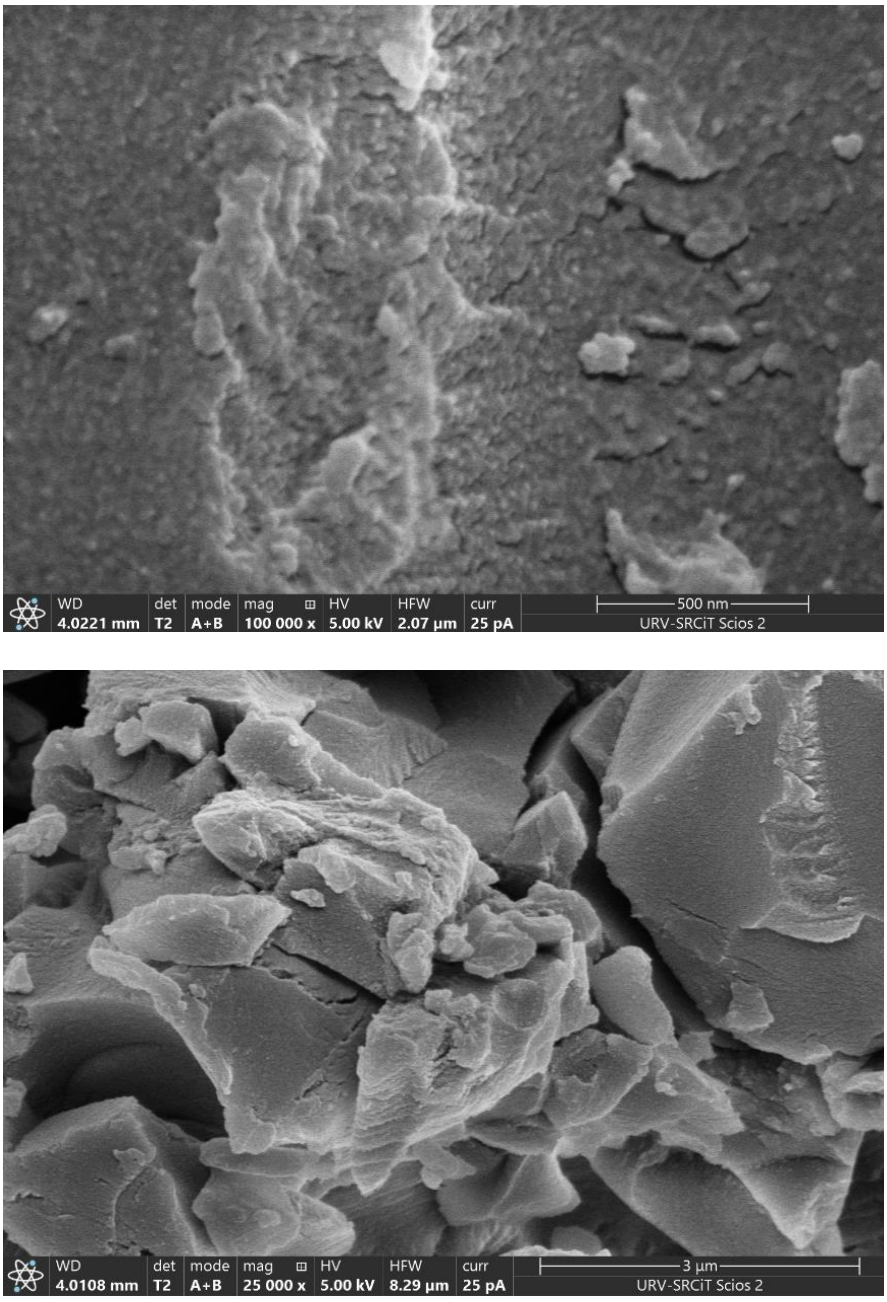

Annex 4.13 FESEM images of OXY-γ-CD-NS seen at a scale of 500 nm (top) and at lower magnification (bottom)

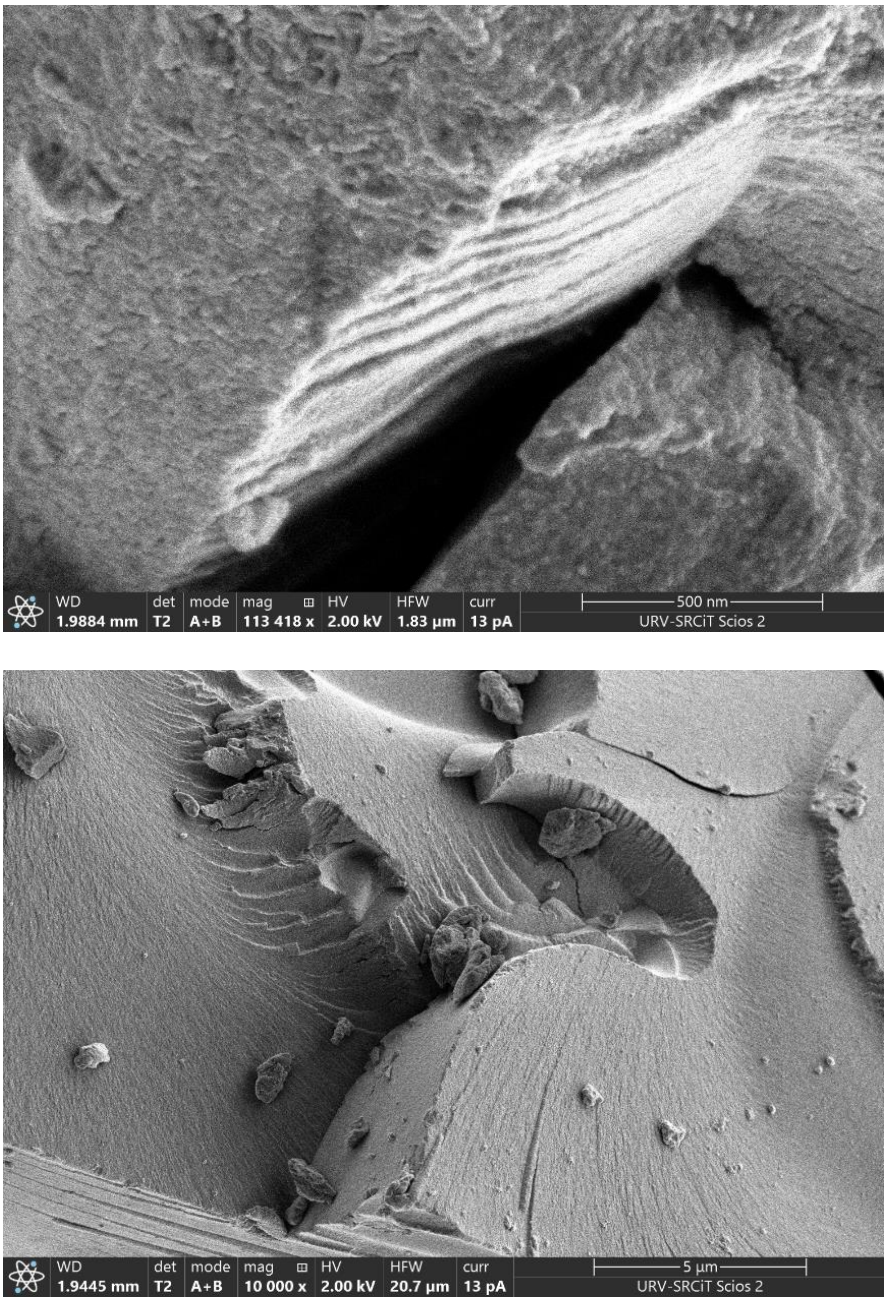

Annex 4.14 FESEM images of BISPH-γ-CD-NS seen at a scale of 500 nm (top) and at lower magnification (bottom)

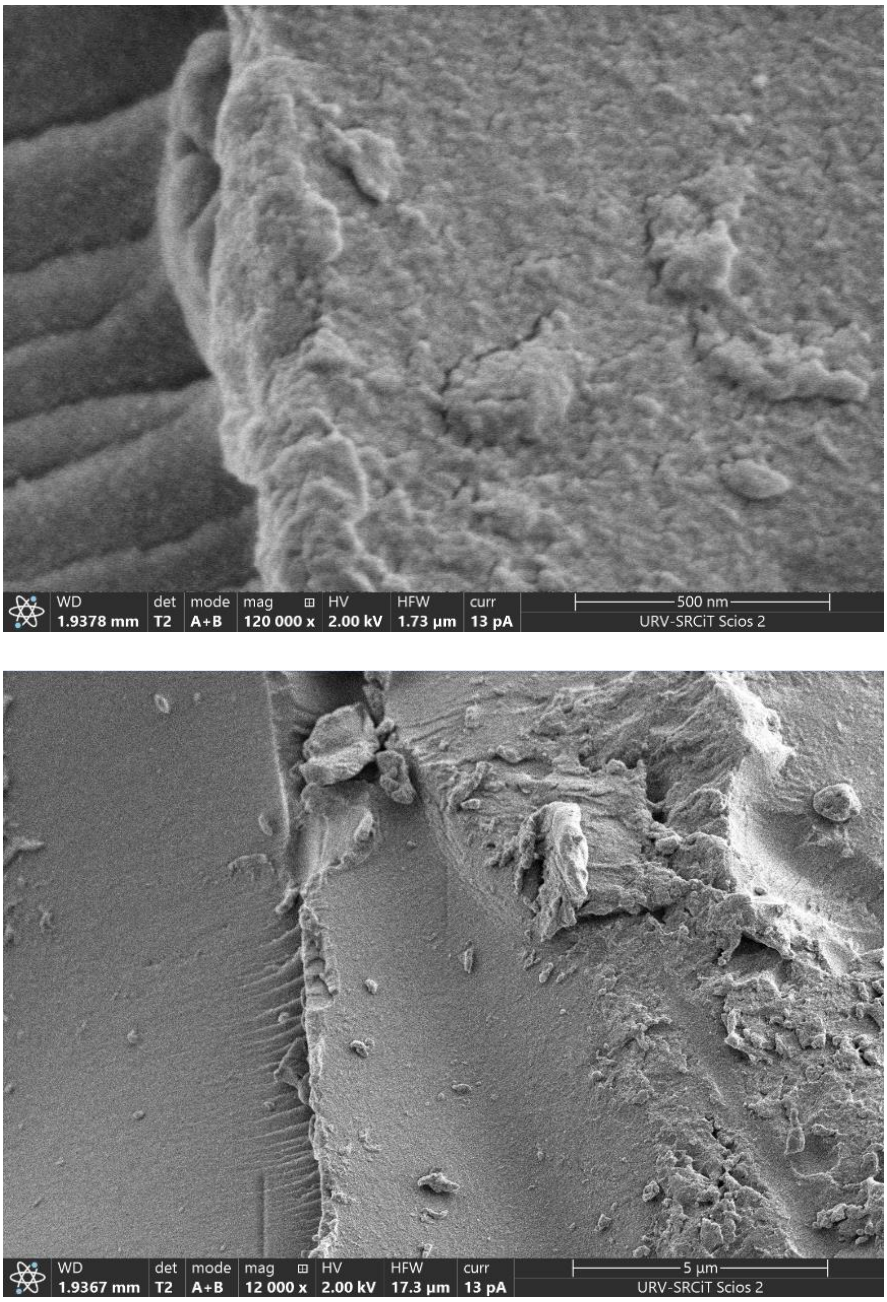

Annex 4.15 FESEM images of ISO-γ-CD-NS seen at a scale of 500 nm (top) and at lower magnification (bottom)

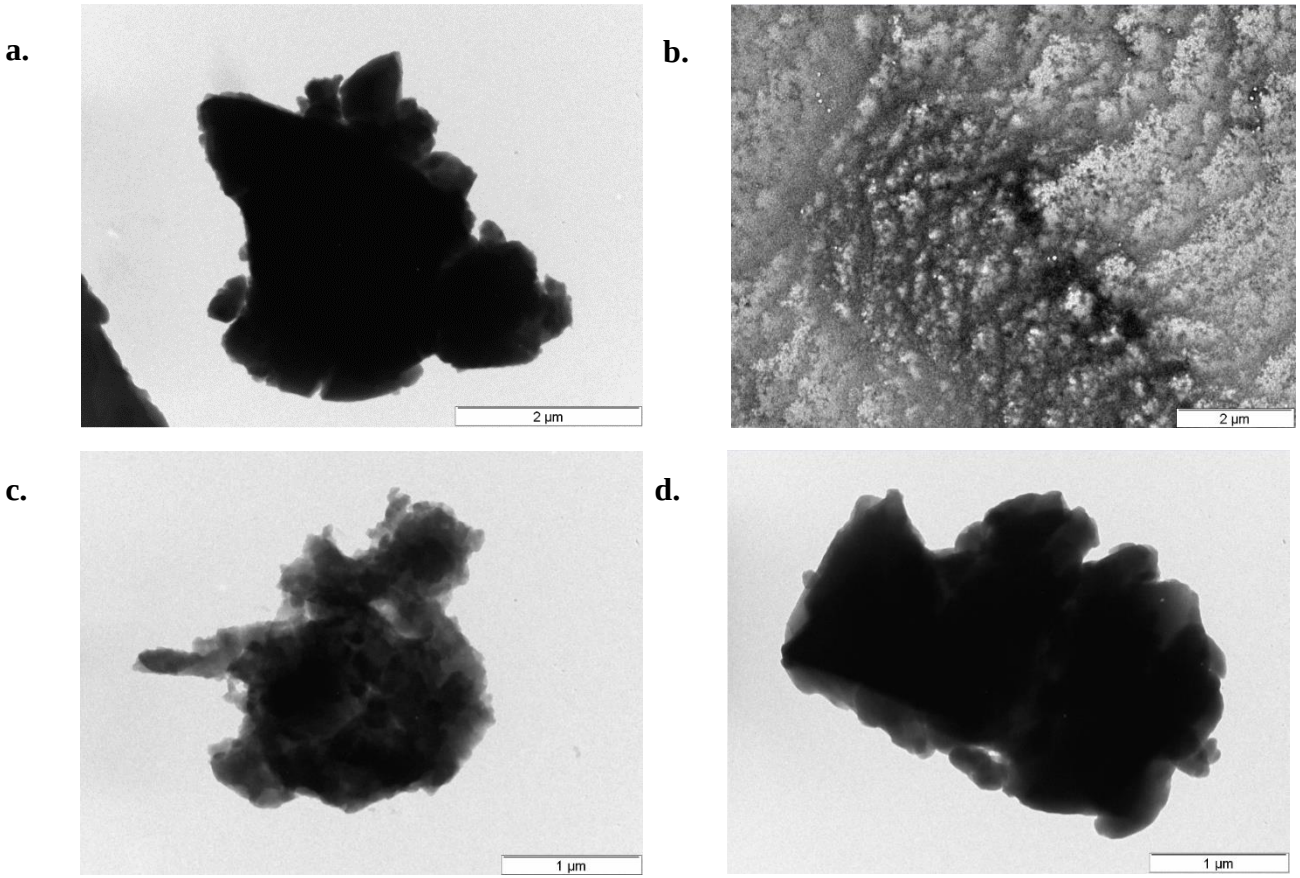

Annex 4.16 TEM images of α-CD-NS crosslinked with a. OXY anhydride b. PMDA anhydride c. BISH anhydride and d. ISO anhydride at different magnifications.

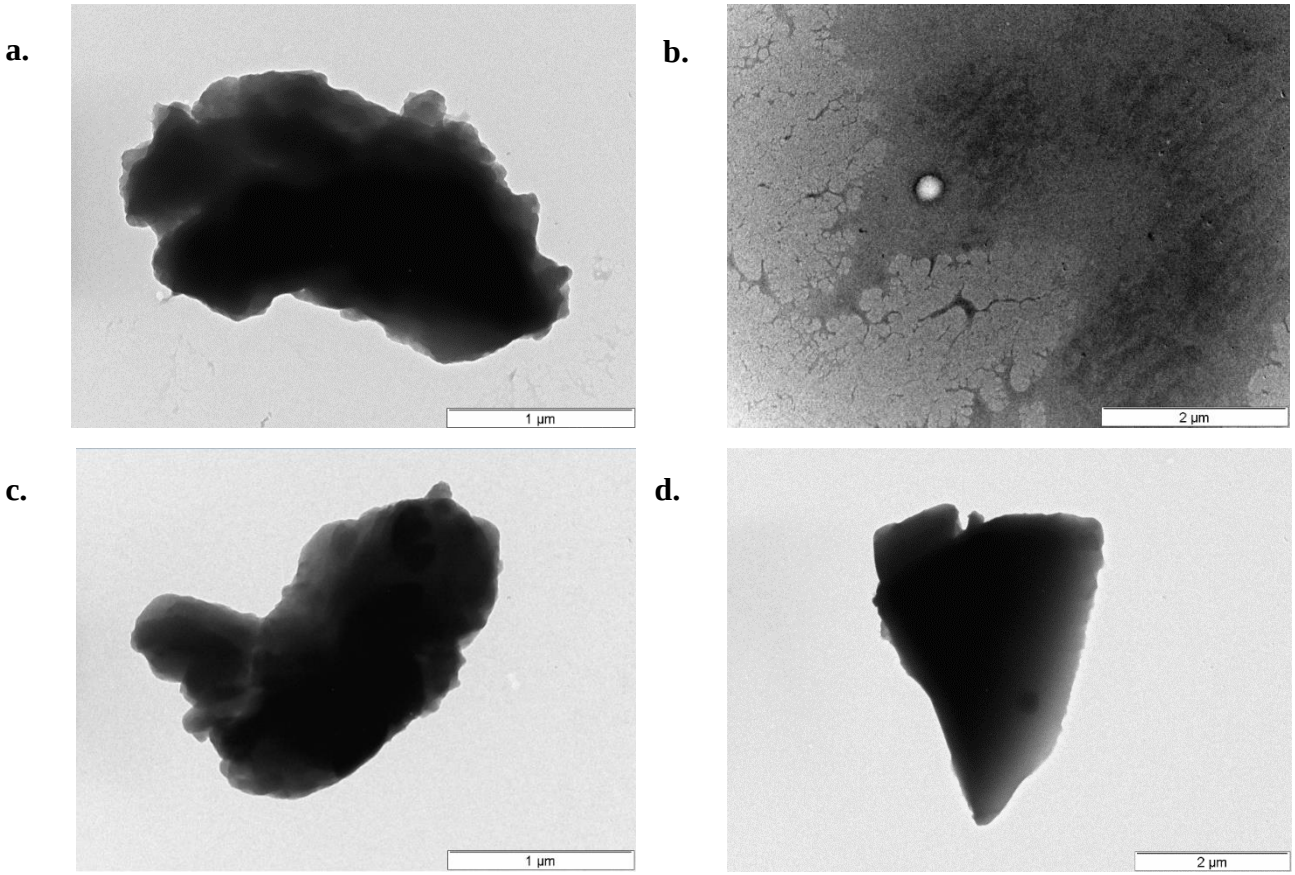

Annex 4.16 TEM images of γ-CD-NS crosslinked with a. OXY anhydride b. PMDA anhydride c. BISH anhydride and d. ISO anhydride at different magnifications.

Conclusions and Future Work

Cyclodextrins and their chemically modified derivatives, including appended CDs and CD-derived polymeric materials, constitute a large family of compounds with numerous relevant applications in many industries. Exploiting the potential of such materials is an ever-growing research field that lies inside the nanoscience and nanotechnology domain. The continuous growth in these applications pushes the frontier of fundamental knowledge further and ultimately leads to the progress in bioremediation, computer science, cosmetics, pharmacology, and medicine just among many more.

As Professor Richard Feynman famously stated in his Caltech lecture: “there is plenty of room at the bottom”. Indeed, more than 60 years after his statement we continue to find room, one grain of sand at a time, or I should say, one cyclodextrin at a time.

UNIVERSITAT
ROVIRA i VIRGILI

UNIVERSITAT · ROVIRA · I · VIRGILI
SAPIENTIAE · LIBERI · LIBERTATI · SAPIENTES